Design of a Cryogenic Turbine for a Hybrid Cryocooler

by

Thomas L. Fraser

A thesis submitted in partial fulfillment of

the requirements for the degree of

Master of Science

(Mechanical Engineering)

at the

UNIVERISTY OF WISCONSIN-MADISON

2006

Approved by

_____ _____

Professor Gregory F. Nellis Date

Abstract

The hybrid pulse tube-reverse Brayton cycle cryocooler has the potential for cooling to temperatures on the order of 10 K. By using the rectifying interface which converts the oscillating pulse tube flow to continuous flow, both vibrations and low temperature regenerator losses are overcome, making the hybrid an ideal candidate for cooling infrared focal plane arrays which demand low temperature and low vibration. However, the turboexpander within the reverse Brayton cycle is complex and its performance is highly dependent on the performance of its subcomponents, thus necessitating a model predicting the turboexpander performance.

A model was developed to predict the performance of the reverse Brayton cycle stage including the recuperative heat exchanger and turboexpander components. The turboexpander was numerically modeled in detail to include the sub-models of rotordynamics, the thermal and leakage performance of the seal, and the turboalternator. Where possible, the models were verified against either an analytical model or experimental data. A parametric analysis was carried out to determine the optimal design and conditions for the turboexpander.

Acknowledgements

First and foremost I would like to thank Greg Nellis. Besides being my advisor for this project he is also responsible for sparking an interest in energy science through his heat transfer courses I took as an undergrad. He also provided me with the opportunity to conduct this research, and provided guidance while dealing with the seemingly non-existent progress on my part. I must say that EES is to time to what a black hole is to light.

I would like to thank my parents for first putting me through college as an undergrad, making funds a non-issue. They provided me with endless support throughout the years; whenever I needed anything, be it some homemade cookies, a loan, or the occasional load of laundry, they have always been there.

I am grateful for all the knowledge imparted on me by my professors throughout the years: Sandy Klein, Tim Shedd, and John Pfotenhauer. Sandy's program, EES, has been invaluable to my project; I seriously doubt that I could have accomplished what I did without it.

My friends, though increasingly abandoning me here in Madison for other parts of the country, have been a source of release from the stress of computer modeling, though sometimes maybe too much so. Everyone in the SEL has been great.

Finally, I would like to thank Atlas Scientific for their financial support. Jim Maddocks and Jon Evans have been helpful in their laidback conduct.

Table of Contents

List of Figures

List of Tables

Nomenclature

Rotordynamics

A	response amplitude
a_n	normal acceleration
a_t	tangential acceleration
b	damping coefficient
c_{jb}	journal bearing clearance
C_{mo}	moment coefficient
E	modulus of elasticity
e	shaft center offset from bearing center
F	excitation force
F_{jb}	journal bearing force
F_n	normal force
F_t	tangential force
G	shear modulus
h	varying shaft clearance
I	area polar moment of inertia
I_x	polar mass moment of inertia
J	polar second area moment of inertia
k	stiffness
k_t	tangential stiffness
k_{jb}	journal bearing normal stiffness
L_{jb}	journal bearing length
L_{sh}	shaft length
m	mass
m_{eq}	equivalent mass supported by journal bearing
p	pressure
$\dot{Q}$	flow rate
R_{tb}	thrust bearing radius
R_{sh}	shaft radius
Re_{rot}	rotational Reynolds number
s	thrust bearing axial clearance
T_f	frictional torque
u	magnitude of shaft unbalance
v	velocity
v_t	tangential velocity
v_θ	tangential fluid velocity
$\dot{W}_f$	friction power

Symbols

ε	eccentricity ratio
ν	kinematic viscosity
ρ	density
μ	fluid viscosity
μ_{sh}	mass per length of the shaft
θ	angular position
Ω	angular velocity/frequency
Ω_{th}	whirl instability threshold speed
ω_s	whirl frequency

Turboalternator

A	flux path cross-sectional area
$\vec{B}$	flux density vector
B_m	flux density of magnet
$\bar{D}$	mean flux path through the magnet
D_{lip}	diameter of stator pole lip
D_{shl}	outer diameter of stator shell
D_{st}	stator pole diameter
D_{wire}	diameter of winding and lead wire
F_m	magnetomotive force
$\vec{H}$	magnetic field intensity
H_m	magnetic field strength of magnet
I_{rms}	root mean square electrical current
l	flux path length
L	equivalent electrical inductance
l_{lead}	length of leads
L_{shl}	length of stator shell
N	number of winds per layer
$\hat{n}$	unit vector parallel flux path
R_{eq}	equivalent electrical resistance
$R_{winding}$	resistance of the windings
R_{load}	resistance of the potentiometer
R_{lead}	resistance of the leads
t	time
T_0	room temperature
$T_{bearing}$,	temperature in bearings
th_{shl}	thickness of stator shell
V	voltage
$\dot{W}_{load}$	power dissipated by turboalternator
Z_R	resistive impedance
Z_L	inductive impedance

Symbols

λ	flux linkage
μ_0	magnetic permeability of free space
μ_f	magnetic permeability of ferrite
ϕ	magnetic flux
ϕ_{st}	stator flux
ϕ_{leak}	leakage flux
ρ	resistivity
$\Re$	reluctance
$\Re_{st}$	reluctance of stator
$\Re_{shl}$	reluctance of stator shell
$\Re_{eq}$	equivalent reluctance of magnetic circuit

Seal

$A_{c,land}$	cross-sectional area for flow in the lands
A_{seal}	effective cross sectional area for conduction through the seal
A_{sh}	effective cross sectional area for conduction through the shaft
c_{land}	seal clearance
c_p	specific heat capacity
d_{groove}	depth of seal grooves
$D_{h,land}$	hydraulic diameter of the flow passage
E	modulus of elasticity
$f_{land,i}$	apparent friction factor
$\dot{g}$	heat generation due to fluid friction
h	enthalpy
hf_{LHS}	enthalpy flow from the left of the control volume
hf_{RHS}	enthalpy flow to the right of the control volume
i	index position within seal
j	index of land number
K_c	sudden contraction coefficient
K_e	sudden expansion coefficient
$k_{sh,}$	thermal conductivity of the shaft material
k_{seal}	thermal conductivity of the seal material
L_{seal}	seal length
n	number of control volumes
N_{groove}	number of labyrinth grooves
$\dot{m}_{leak}$	seal mass flow leakage rate
P_{turb}	purbine pressure
$\dot{q}_{cond,turb}$	conductive heat leak to turbine
$\dot{q}_{RHS,i}$	conduction from the right side of the control volume

$\dot{q}_{LHS,i}$	conduction from the left side of the control volume
Re_{land}	Reynolds number within land
T	seal temperature
T_{cold}	turbine operating temperature
T_{land}	temperature at center of land
T_{hot}	bearing cartridge temperature
th_{seal}	seal thickness
v	fluid velocity
w_{groove}	width of the labyrinth grooves
w_{land}	width of the seal lands
$w^{+}_{land,i}$	dimensionless length with respect to hydrodynamic flow development
x	axial position
x_{groove}	axial position of center of groove
x_{land}	axial position of center of land
$\overline{x}$	dimensionless axial position

Symbols

α	dimensionless heat transfer to the turbine
Δc_{land}	change in seal clearance
ΔP	pressure drop
Δx	axial length of the control volume
ε	strain
γ	Graetz number
μ	fluid viscosity
θ	dimensionless temperature
ρ	density
σ_{hoop}	tangential hoop stress in seal

Supplementary Models and Integration

Turbine

v_{isen}	isentropic nozzle velocity
v_{tip}	blade tip velocity
Δh_s	isentropic enthalpy drop
η_s	aerodynamic efficiency
λ	velocity ratio

Recuperator

$\dot{C}$	capacitance rate
i	index within recuperator

$\dot{m}_{turb,in}$	turbine mass flow rate
P_c	cold stream pressure
P_w	warm stream pressure
$h_{w,out,ac}$	exit enthalpy of the warm stream including axial conduction
$h_{c,out,ac}$	exit enthalpies of the cold stream including axial conduction
N	number of control volumes
NTU	number of transfer units
$\dot{q}_{max,i}$	maximum heat transfer within control volume
$\dot{q}$	heat transfer of control volume
$\dot{q}_{ac}$	conduction penalty
$\dot{q}_{total}$	total stream-to-stream heat transfer in the recuperator.
$T_{c,in}$	cold stream inlet temperature
$T_{w,in}$	warm stream inlet temperature
UA	area-heat transfer product
UA_{total}	overall recuperator area-heat transfer product
ε	effectiveness

Journal Bearings

E	shaft offset
F	resultant journal bearing force
k_{jb}	journal bearing stiffness
$\dot{m}_{jb}$	journal bearing mass flow consumption
$\Delta P_{bearing}$	pressure drop through journal bearings

1 Introduction

1.1 Applications

Small cryogenic refrigerators, or cryocoolers, serve a multitude of functions ranging from liquefying helium for magnetic resonant imaging (MRI) machines to cryosurgical apparatuses to cooling superconductors for physics experiments. These different uses each have different requirements. The main use of the cryocooler considered in this thesis the cooling of space-based infrared (IR) sensors, though it is quite possible that the concept could be expanded to include other applications.

Space-based IR sensors can be used for several purposes. The military uses these sensors for missile defense systems such as the Space Based Infrared System (SBIRS) and the Defense Support Program (DSP) which SBIRS is replacing, as well as real-time battlefield characterization and technical intelligence. Atmospheric science applications of IR sensors range from daily weather forecasting to gathering data for the development of more accurate weather models. Various space telescopes such as the Hubble Space Telescope (HST), Infrared Astronomical Satellite (IRAS), and the newest and currently operating Spitzer Space Telescope (SST), all take images of distant galaxies in the IR band in order to increase our knowledge of distant stellar formations and the history of the cosmos.

All of these space based IR sensor applications benefit from high spatial and wavelength resolution. For example, a missile detection system must detect the relatively small heat signatures of intercontinental ballistic missiles as well distinguish that heat signature from its background. High resolution infrared images of clouds are required to investigate the different layers and temperatures of clouds, which show up more clearly in the IR band, as well as distinguish the clouds from the ground. In the case of IR space telescopes, a higher resolution results in more information gained from the images.

In order for infrared sensors to operate accurately (i.e. have high wavelength and spatial resolution) two main requirements must be met: the sensor must be cooled to very low temperatures, and the vibrations, or jitter, must be extremely low. Cooling IR sensors can be done passively through either a cryoradiator or liquid cryogen, or actively by a mechanical cryocooler. A cryoradiator is limited with regard to the lowest temperature that it can reach, and any substantial refrigeration load will require a very large cryoradiator. Liquid cryogens such as liquid helium are used by evaporating the cryogen thus absorbing the latent heat of vaporization. Though simple and effective, the use of a liquid cryogen places an absolute limit on the lifespan of the sensor, and any unforeseen parasitic load may drastically reduce the anticipated life and compromise the mission's objectives. Prolonging the active life of the sensor would require additional cryogen taking more space and posing an additional payload for launch. Superfluid helium is often used on space telescopes; for example the Spitzer telescope, contained 360 liters of superfluid helium weighing 50.4 kg when it was launched in 2003 and is expected to be functional for approximately 3 years (SSC, 2006). For IR sensors that require a long

usable life, mechanical cryocoolers are both lighter and more compact than the use of a liquid cryogen. The cryocooler considered in this thesis is intended to operate for a period of at least 5 to 10 years at 10 K with a refrigeration load of 1 W.

1.2 Two-stage, Hybrid Cryocooler

There are several mechanical cryocooler options that can meet the refrigeration requirements (approximately 1 W at 10 K) and low on-focal plane array (FPA) vibration specifications associated with space based IR sensors. However, in order to achieve high efficiency at cryogenic temperatures the *de facto* standard is the pulse tube refrigerator. The pulse tube is a variation of the regenerative Stirling refrigeration cycle which uses a linear compressor in order to produce an oscillating fluid flow. However, because the pulse tube uses oscillating flow and, due to the rigid attachment of the cold head to the compressor, it can transfer a substantial amount of mechanical vibrations to the FPA that is being cooled. Also, at low temperatures common regenerator materials exhibit a large reduction in specific heat whereas helium, the working fluid, exhibits a large increase in specific heat, as illustrated in Figure 1-1. This mismatch in specific heats leads to a reduction in performance and limits the efficiency of the pulse-tube. Increasing the regenerator size to account for the lowered effectiveness results in higher void volume and axial conduction losses; thus it is not possible to improve the performance by making an arbitrarily large regenerator. The use of a regenerator that is composed of multiple layers of regenerator materials, each with locally high heat capacity can partially overcome this problem; however, these rare earth metals are expensive and such a complex regenerator requires careful design and construction.

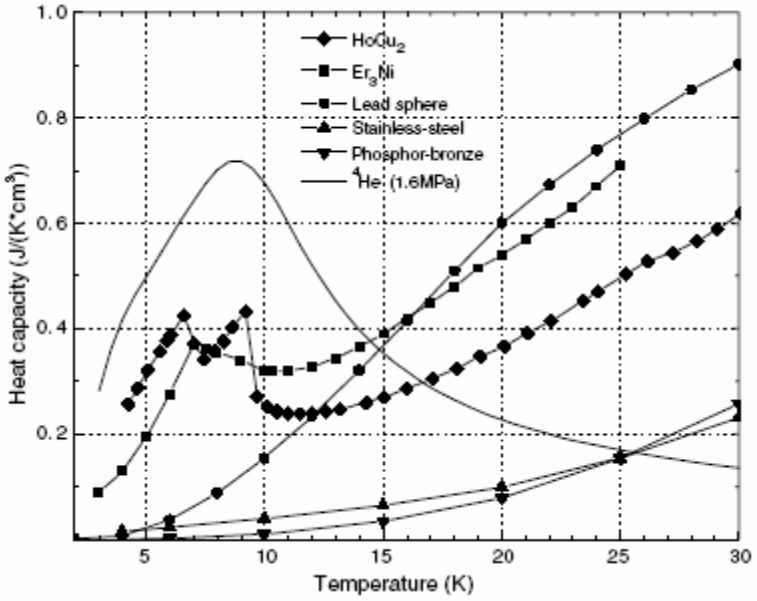

Figure 1-1: Specific heat capacity of several common regenerator materials and helium at low temperatures (Qui *et. al.*, 2005)

To avoid the difficulties associated with a regenerative cycle at low temperatures as well as to provide vibration isolation from the compressor, a recuperative lower stage cycle is coupled directly to the pulse tube upper stage. The steady-flow associated with the recuperative cycle will also be beneficial for integration with multiple or distributed loads. A rectifying interface is used as a direct thermo-fluid link between the recuperative and regenerative stages. The rectifying interface consists of check valves that allow flow in one direction to and from the cold heat exchanger of the pulse tube, as shown in Figure 1-2. Buffer volumes are used to maintain near-constant high and low pressures for the recuperative cycle.

At the anticipated temperature of 10 K and moderate pressures (e.g. 1.8 MPa to 1.3 MPa) it is necessary to use an isentropic as opposed to isenthalpic expansion in the recuperative cycle. The isenthalpic, or Joule-Thompson (JT), expansion of helium under these conditions will result in a temperature rise that is nominally 30% of that produced by an isentropic expansion. Additionally, the inversion temperature of helium is approximately 40 K; the use of a JT cycle above the inversion temperature is not thermodynamically possible and therefore the upper pulse tube stage would have to operate substantially lower than the anticipated 60 K in order to use a lower stage JT cycle.

Therefore, the reverse Brayton cycle was chosen as the lower stage because it produces a near-isentropic expansion by expanding the gas through a turbine. The gas expands while imparting energy to turbine blades and producing mechanical power (as opposed to a JT expansion in which the gas can be thought of as only doing work on itself). The schematic of the complete hybrid cryocooler is illustrated in Figure 1-2.

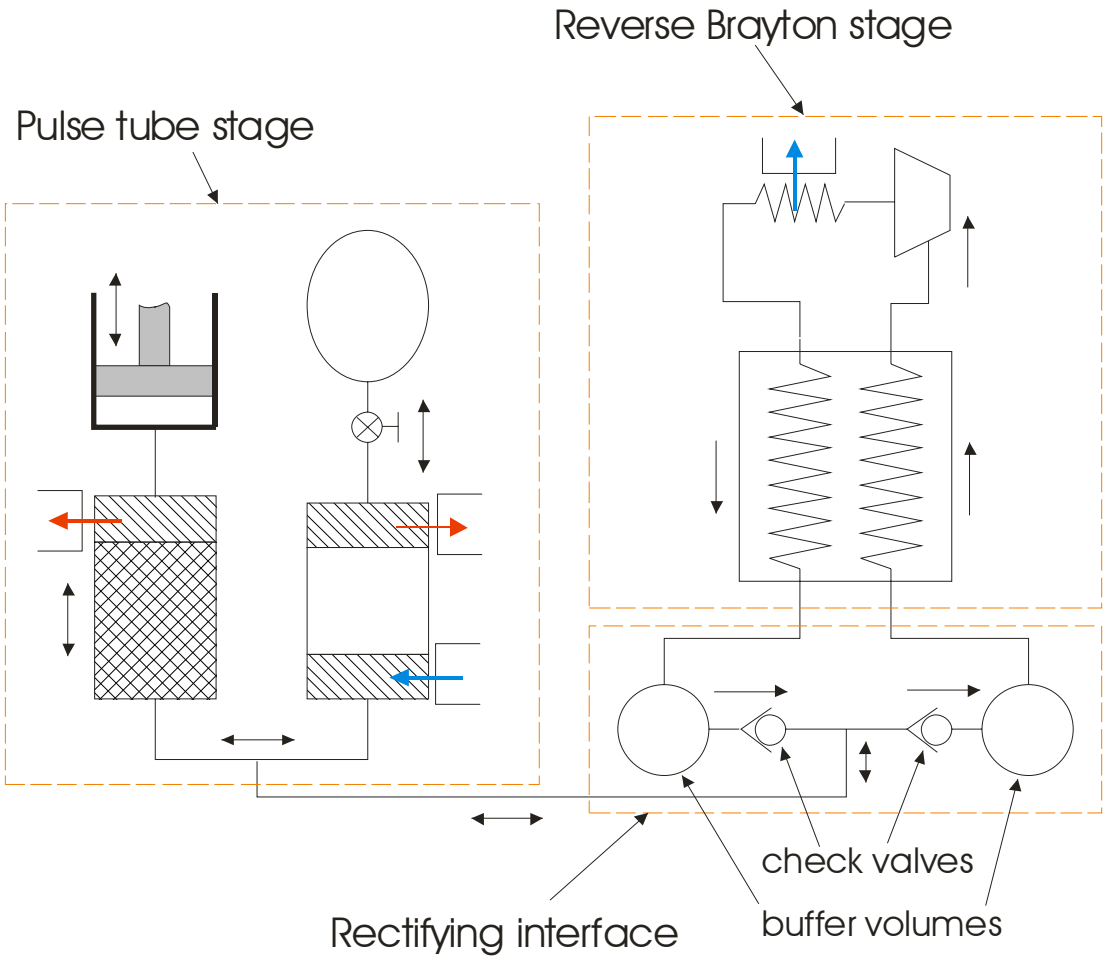

Figure 1-2: Hybrid schematic

1.3 Reverse Brayton Cycle

The reverse Brayton cycle consists of the low and high pressure buffer volume (LPBV and HPBV), a recuperative heat exchanger, the turboexpander, and the load heat exchanger as illustrated in Figure 1-3. Because it is a continuous flow cycle, the refrigerant may be directed across multiple loads in order to cool several IR sensors.

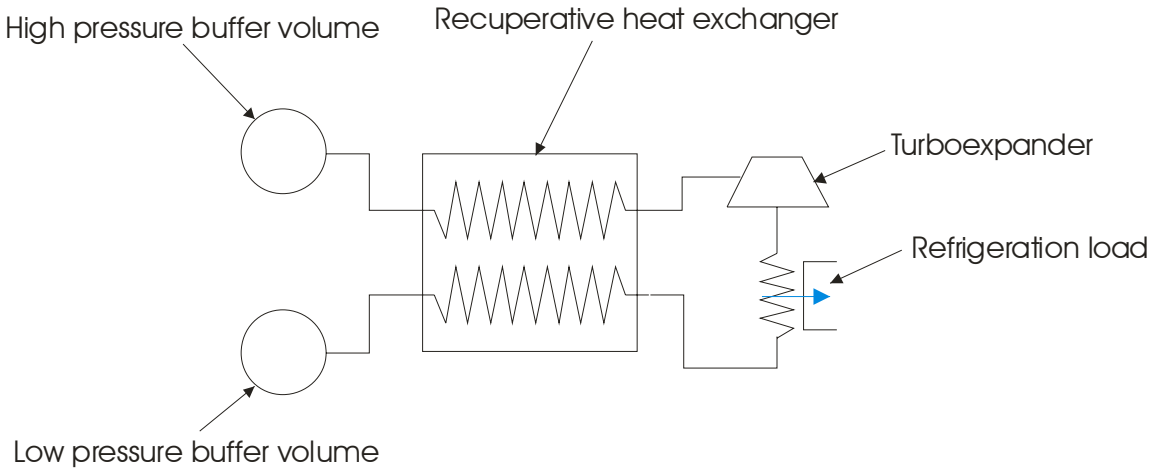

Figure 1-3: Reverse Brayton cycle schematic

This thesis focuses primarily on the turboexpander that is used in the reverse Brayton cycle. The turboexpander has several sub-components: the shaft, hydrostatic journal bearings, hydrostatic thrust bearing, turboalternator, and turbine and nozzles, as shown schematically in Figure 1-4. The performance of these different components interact to a high degree and affect the turboexpander performance.

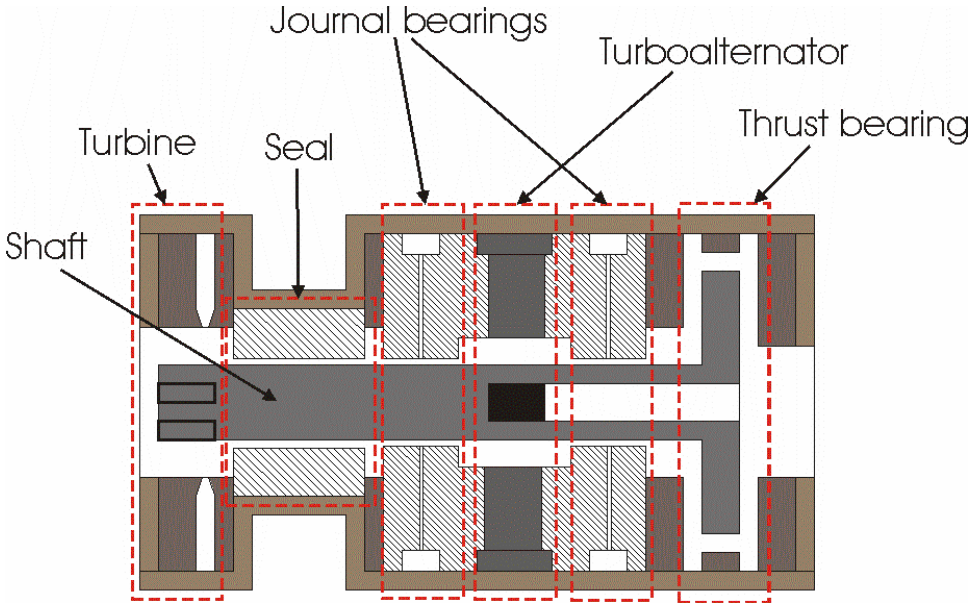

Figure 1-4: Schematic of turboexpander components

1.4 Objectives

The objective of this thesis is to develop a predictive model of the low temperature, reverse Brayton cycle. This model focuses on the complex interaction within the turboexpander which is the most complex sub-component in the cycle. The model is developed in the form of several detailed sub-models that address rotordynamics, seal performance, and turboalternator performance, as well as less detailed supplementary sub-models of the recuperator, turbine aerodynamic efficiency, and journal bearings. These sub-models interact in order to determine the complete cycle performance given the pulse tube performance and turboexpander geometry. The optimal turboexpander design is determined by performing a parametric analysis and varying the turboexpander geometry.

2. Rotor Dynamics

To operate effectively, the turboexpander must operate at speeds as high as 2500 rev/s with running clearances as low as 0.0005 inch (13 μm). These high-speed, close-clearance conditions can lead to rotor dynamic effects that drastically limit the turboexpander operating speed and can cause irreparable damage to the shaft and bearings unless the effects are adequately modeled and considered during design. These rotor dynamic effects are addressed in this chapter and include shaft natural frequencies (both flexible and rigid body), whirl instability, and frictional drag.

2.1 Natural Frequencies

While the shaft assembly will rotate about a definite axis, the center of mass of the shaft will inevitably lie some radial distance (u) away from the axis of rotation, as illustrated in Figure 2-1(a). This offset, or unbalance, will give rise to a centripetal force, F, acting in the radial, or normal, direction due to the center of mass having a nonzero tangential velocity, v. The force in a given direction (for example, the x-direction) will be sinusoidal with the same frequency as the shaft rotational speed, as illustrated in Figure 2-1(b).

This centripetal force is the excitation force; the system's response to the excitation force will be forced vibrations with the amplitude, $|A|$, given by Sandor *et. al.* (1999):

$$|A| = \frac{|F|}{\sqrt{\left(k - m\Omega^2\right)^2 + \left(b\Omega\right)^2}} \tag{2.1}$$

where $|F|$ is the magnitude of the excitation force, k is the system stiffness, m is the system mass, Ω is the excitation frequency which is equal to the rotational speed, and b is the damping coefficient. From Eq. (2.1) it is apparent that the amplitude of the vibrations will be maximum at a certain excitation frequency that is known as the resonant frequency of the system (ω_{res}):

$$\omega_{res} = \sqrt{\frac{k}{m} - \left(\frac{b}{m}\right)^2} \tag{2.2}$$

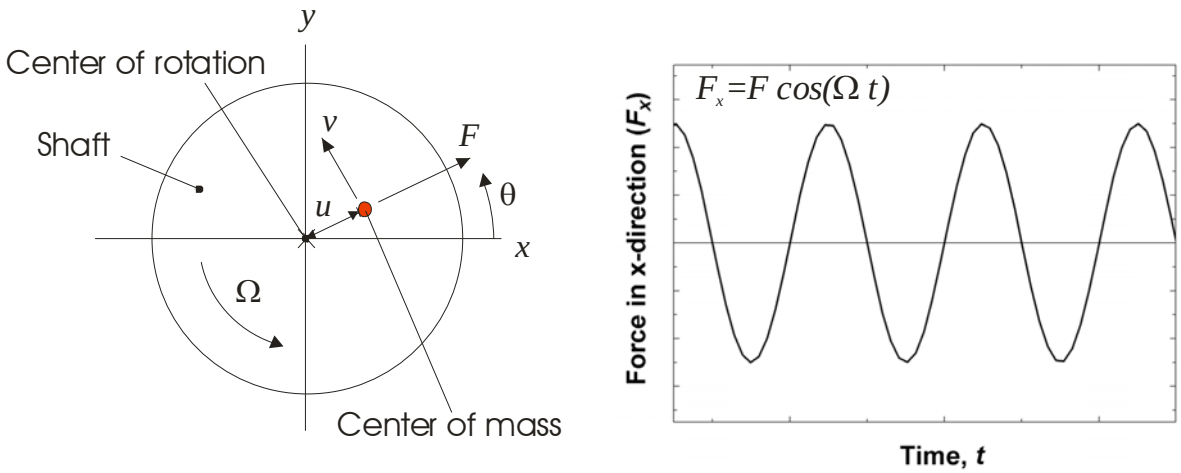

(a) (b)

Figure 2-1: Schematic of the force acting on an unbalanced shaft (a) and the force in the *x*-direction on an unbalanced shaft (b)

A common simplification is to approximate the resonant frequency as the undamped natural frequency, ω_n:

$$\omega_n = \sqrt{\frac{k}{m}} \tag{2.3}$$

Equation (2.3) is generally a reasonable simplification of Eq. (2.2) due to the relatively low damping term as compared to the stiffness term; this simplification is especially useful for systems in which the damping coefficient is not known.

For the turboexpander shaft assembly, the stiffness used in Eq. (2.3) can be evaluated in several ways. It is possible to focus on the shaft assembly itself and its stiffness while ignoring the stiffness of the bearings. The result of this analysis leads to the non-rigid, or flexible body natural frequency. It is also possible to assume that the shaft assembly is completely rigid and evaluate Eq. (2.3) using the stiffness of the bearings. The result of this analysis is the rigid body natural frequency.

2.1.1 Flexible Body Frequencies

When rotating at speeds coincident with the flexible body natural frequency, the shaft assembly will distort to its maximum value and therefore almost certainly contact the bearings. For this reason, it is not possible to run the turboexpander at speeds in excess of the first flexible body frequency (or even to speeds that are very close to this value). The lowest flexible body frequency is an upper limit on the shaft speed and therefore must be evaluated carefully during the design process.

There are multiple modes of deformation for the shaft which arise from the ability to examine the shaft stiffness relative to the axial, tangential (i.e. torsional), or longitudinal (i.e. bending) directions. Because the excitation force caused by shaft unbalance is acting

radially, the bending stiffness should be most relevant and also the lowest for a typical shaft geometry; the excitation forces in the axial and tangential directions should be negligible and the stiffness of the shaft relative to distortions in these directions should be much higher.

2.1.1.1 Finite Element Frequency Analysis of Shaft with Thrust Bearing

The shaft assembly is composite with a complex geometry and therefore finite element modeling was employed to determine the natural frequency of the assembly; this analysis was verified analytically in the limit of a simple shaft. SolidWorks (SolidWorks 2005) was used to generate a solid model of a shaft geometry that is representative of the nominal design, illustrated in Figure 2-2. The dimensions of the nominal design are summarized in Table 2-1 and the material properties used for this analysis are provided in Table 2-2. SolidWorks is integrated with the finite element (FE) analysis package COSMOS (SRAC, 2006), which was subsequently used to perform a frequency analysis on the model.

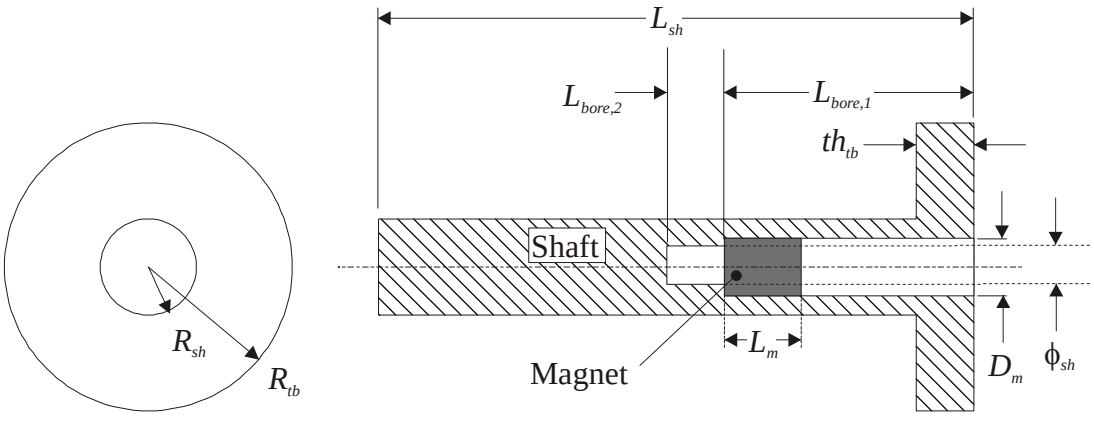

Figure 2-2: Schematic of shaft and thrust bearing

The mesh size was varied from 0.010 inch to 0.085 inch which corresponds to 1523 to 479136 mesh elements for the geometry listed in Table 2-1. Figure 2-1 illustrates the first bending natural frequency as a function of mesh size and shows that the solution has converged to within 3 Hz for a mesh size less than 0.05 inch. Therefore to produce accurate results while maintaining a reasonable calculation time, a mesh size of 0.04 inch was chosen for subsequent frequency analyses. Figure 2-4 illustrates the first three mode types and their associated frequencies predicted by COSMOS.

Table 2-1: Nominal shaft dimensions used for initial frequency analysis

Dimension	**Symbol**	[in]	[cm]
Shaft radius	R_{sh}	0.10	0.25
Shaft length	L_{sh}	2.00	5.08
Thrust bearing diameter	D_{tb}	0.25	0.64
Magnet diameter	D_m	0.12	0.30
Shaft extended bore	$\phi_{bore,2}$	0.10	0.25
Shaft initial bore length	$L_{bore,1}$	1.00	2.54
Shaft extended bore length	$L_{bore,2}$	0.20	0.51

Table 2-2: Material properties used in frequency analyses

Property	**Symbol**	**Titanium Alloy**[1]	**Neodymium Iron Boron**[2]
Modulus of Elasticity [GPa]	E	110	157
Shear Modulus [GPa]	G	42.0	63.3
Poisson's Ratio	ν	0.33	0.24
Density [kg/m^3]	ρ	4700	7400

[1] Properties from www.matweb.com
[2] Properties from www.hitachimetals.com

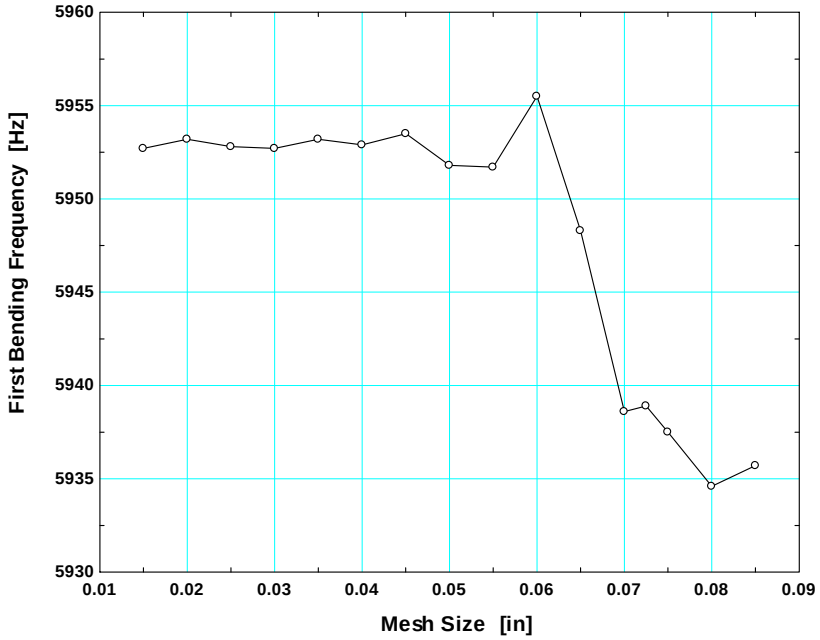

Figure 2-3: The first bending frequency as it varies with mesh size for a shaft with dimension listed in Table 2-1

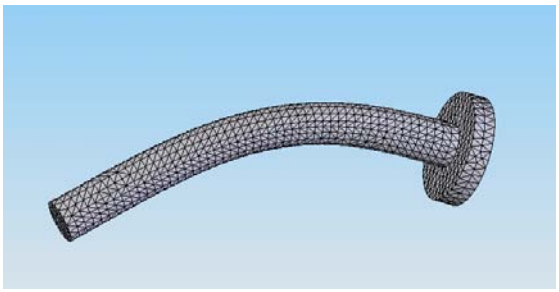

a) First Bending Mode, 6054 Hz

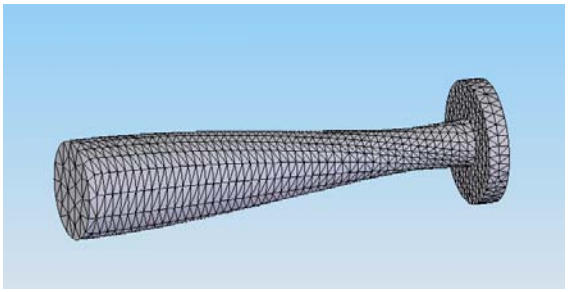

b) First Torsional Mode, 16263 Hz

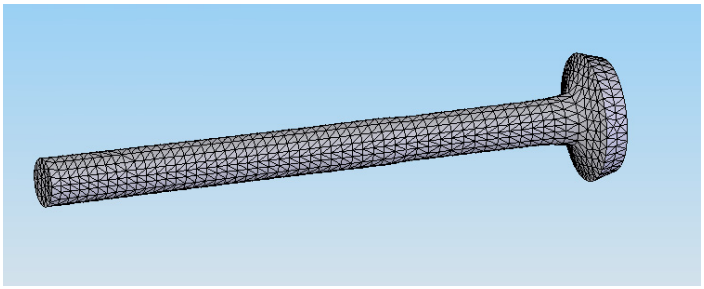

c) First Axial Mode, 33930 Hz

Figure 2-4: The first 3 natural frequency modes predicted by COSMOS including (a) the first bending, (b) the first axial, and (c) the first torsional modes for the shaft geometry summarized in Table 2-1.

Table 2-3 lists the frequencies associated with the first 15 modes of the turbine with the nominal dimensions and material properties summarized in Tables 2-1 and 2-2. Note that the first 6 modes occur at a frequency of 0 Hz because they are the rigid body modes which result from each of the 6 degrees of freedom associated with the model. These rigid body modes depend on the mass of shaft and the stiffness of the rotor dynamic support system, journal and thrust bearings; these quantities are not included in the solid model but will be analyzed in the next section. Also note that each of the bending frequencies is reported twice due to the presence of simultaneous bending in two planes.

Table 2-3: Natural frequencies calculated by COSMOS for the shaft geometry and material summarized in Table 2-1

Mode No.	Frequency *[Hz]*	Mode Type
1	0	Rigid Body
2	0	Rigid Body
3	0	Rigid Body
4	0	Rigid Body
5	0	Rigid Body
6	0	Rigid Body
7	6054	1st Bending
8	6055	1st Bending
9	16343	1st Torsional
10	16783	2nd Bending
11	16785	2nd Bending
12	28177	3rd Bending
13	28180	3rd Bending
14	33840	1st Axial
15	43335	2nd Torsional

For the purpose of design, the most important result reported in Table 2-3 is the 1st bending mode because it will always occur at the lowest frequency. Any practical shaft will have a large length-to-diameter ratio and therefore will be more susceptible to bending than axial vibrations; axial vibrations would be more important for a more disk-

shaped geometry. The torsional mode would be more of an issue for a thin shaft that has multiple, large masses attached.

2.1.1.2 Analytical Verification of Finite Element Analysis

The finite element results were verified in the limiting case of a simple shaft (i.e., one with no disks, holes, or magnets) using the analytical solution presented by Blevins (1995). The analytical solution was implemented using the Engineering Equation Solver (EES) software (Klein, 2005). The 1st harmonic frequencies in bending ($f_{n,bending}$), torsion ($f_{n,torsion}$), and axial vibration ($f_{n,axial}$) are:

$$f_{n,axial} = \frac{1}{2}\sqrt{\frac{E}{\mu_{sh}}} \tag{2.4}$$

$$f_{n,torsion} = \frac{1}{2\,L_{sh}}\sqrt{\frac{G\,J}{\mu_{sh}\,I_x}} \tag{2.5}$$

$$f_{n,bending} = \frac{1}{2\,\pi}\sqrt{\frac{E\,I}{L_{sh}\,\mu_{sh}}} \tag{2.6}$$

where

$$J = \frac{\pi\,R_{sh}^4}{2} \tag{2.7}$$

$$I = \frac{\pi\,R_{sh}^2}{4} \tag{2.8}$$

$$I_x = \frac{\mu_{sh}\,R_{sh}^2}{2} \tag{2.9}$$

E and G are the modulus of elasticity and shear modulus of the shaft material, J is the polar second area moment of inertia of the shaft, I is the area polar moment of inertia of the shaft, I_x is the polar mass moment of inertia of the shaft, L_{sh} and R_{sh} are the length and radius of the shaft, and μ_{sh} is the mass per length of shaft. Note that Eqs. (2.4), (2.5), and (2.6) are associated with Eq (2.3) modified for a plain shaft to represent axial, torsional, and bending stiffnesses. Higher order modes are integer multiples of these frequencies.

The frequencies calculated using the analytical solution are compared with the results obtained from a COSMOS analysis of a simple shaft that is equivalent to the nominal shaft assembly listed in Table 2-4 with the thrust bearing removed and without any bore or magnet. Figure 2-5 illustrates that decreasing the mesh size to 0.01 inches will cause the bending frequency predicted by the FE model to agree with the analytical solution to within 2.6 %, though it will always under-predict the frequency.

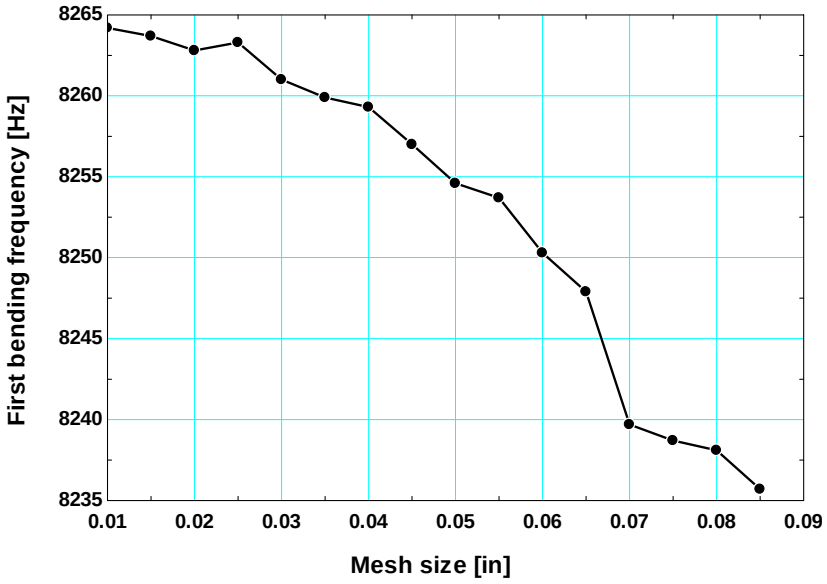

Figure 2-5: The first bending frequency predicted by COSMOS as it varies with mesh size for a plain shaft with dimensions summarized in Table 2-1

Table 2-4: Natural Frequency modes predicted by COMOS and calculated using Equations (2.4) through (2.6) for a simple shaft that is equivalent to the shaft summarized in Table 2-1 without a thrust bearing.

Mode No.	COSMOS	Analytical Model			Mode Type	Percent Difference
	Frequency [Hz]	*Frequency [Hz]*				
		N_bending	*N_axial[i]*	*N_torsion[i]*		
1	0				Rigid Body	
2	0				Rigid Body	
3	0				Rigid Body	
4	0				Rigid Body	
5	0				Rigid Body	
6	0				Rigid Body	
7	8262.8	8482.0			1st Bending	2.6 %
8	8263.6				1st Bending	
9	21817	23374			2nd Bending	6.7 %
10	21819				2nd Bending	
11	29112			29195	1st Torsional	0.3 %
12	40468	45812			3rd Bending	11.7 %
13	40469				3rd Bending	
14	47581		47616		1st Axial	0.07 %
15	58223			58391	2nd Torsional	0.3 %

2.1.1.3 Parametric Study of Turbine Dimensions

The finite element model was used to parametrically study the first bending frequency as the shaft length and thrust bearing radius were varied, with other dimensions given in Table 2-1. The mesh element size was set to 0.04 inch; note that varying the dimensions will change the number of mesh elements. The results of the parametric study are summarized in Table 2-5; this information is implemented as a lookup table in EES and can be used to find the first bending frequency of a shaft with a given length and thrust bearing radius through a two-dimensional interpolation process.

Note that the use of the interpolating table does not allow the examination of the relationship between the bending frequency and the other shaft dimensions; for example, the nominal shaft radius of 0.10 inch (2.54 mm) was used for all of the calculations in Table 2-5. The shaft radius was not varied due to the assumption that the radius would not be decreased during the design of the turboexpander and if it were increased then the first bending frequencies in Table 2-5 represent a viable limit. Note that if the radius does need to be decreased then the finite element analysis must be run again in order to verify that the operating speed is sufficiently below the first bending frequency. The solid models used in the finite element analyses as well as the material property library file are included on the CD attached to the thesis.

Table 2-5: The first bending frequencies for various thrust bearing radii and shaft lengths with all other dimensions as summarized in Table 2-1

Frequency [Hz]		Thrust Bearing Radius (R_{tb}) [in]			
		0.20	*0.25*	*0.30*	*0.35*
Shaft Length (L_{sh}) [in]	*1.6*	9551.8	8884.7	8228.1	7475.0
	1.7	8610.1	8026.7	7476.6	6864.0
	1.8	7806.2	7288.7	6820.5	6313.8
	1.9	7113.5	6649.4	6243.9	5820.0
	2.0	6509.2	6091.2	5735.6	5375.2
	2.1	5979.7	5600.2	5284.7	4974.6
	2.2	5512.6	5166.1	4882.7	4613.7
	2.3	5097.3	4779.9	4525.5	4287.7
	2.4	4727.5	4435.8	4204.3	3993.2
	2.5	4395.7	4127.1	3915.7	3726.9
	2.6	4098.9	3849.9	3655.4	3485.1
	2.7	3830.7	3599.2	3419.8	3265.0

2.1.2 Rigid Body Frequency

The natural frequency of the shaft in bending, as addressed in the previous section, is an important parameter that provides one upper limit to the operating speed. In addition, the rigid body natural frequency associated with the shaft supported on its bearings, assuming that the shaft assembly is treated as being completely rigid, must be considered. The rigid body natural frequency is the frequency that results when Eq. (2.3) is evaluated using the journal bearing stiffness and the mass of the shaft that is suspended by the journal bearing.

The equivalent mass supported on each bearing, $m_{eq,1}$ and $m_{eq,2}$, is computed according to:

$$m_{eq,1} = \frac{F_{jb,1}}{g}, \quad m_{eq,2} = \frac{F_{jb,2}}{g} \tag{2.10}$$

where $F_{jb,1}$ and $F_{jb,2}$ are the forces concentrated on journal bearings 1 and 2. The undamped natural frequency of each bearing is therefore:

$$\omega_{n,1} = \sqrt{\frac{k_{jb}}{m_{eq,1}}} \quad \omega_{n,2} = \sqrt{\frac{k_{jb}}{m_{eq,2}}} \tag{2.11}$$

where k_{jb} is the normal stiffness of the bearing.

The mass of the shaft that is concentrated on each bearing is based on the geometry of the shaft and the position of the bearings. The force provided by each bearing is assumed to be concentrated at a single point located in the axial center of each bearing, as illustrated in Figure 2-6.

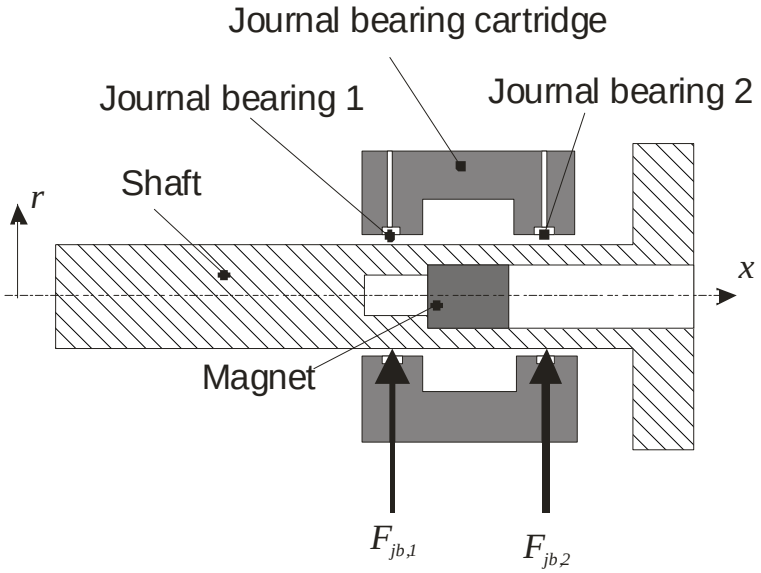

Figure 2-6: Schematic of shaft and journal bearing forces

The relatively complex geometry associated with the turbine shaft is considered by breaking it into sections of uniform axial cross-sectional area; if a journal bearing force is incident within a section then the section is further divided at the location where the force is applied, as shown in Figure 2-7. The journal bearing forces, $F_{jb,1}$ and $F_{jb,2}$, are found

by first performing a moment balance in the *x*-*r* plane taken about the center of journal bearing 1:

$$g\sum_{i=1}^{2} m_i \bar{x}_i + \bar{x}_{F_{jb,2}} F_{jb,2} = g\sum_{i=2}^{6} m_i \bar{x}_i \tag{2.12}$$

where $\bar{x}_i$ is the axial distance between the center of mass of section i (cm_i) and the location where the force $F_{jb,1}$ is applied (i.e. $\bar{x}_6$ in Figure 2-7; note that the spaces between sections are for illustration purposes only), g is the acceleration of gravity. The mass of each section is m_i and the section numbers are shown in Figure 2-7. A force balance on the shaft provides a second equation; Eqs. (2.12) and (2.13) together determine the unknown bearing forces:

$$F_{jb,1} + F_{jb,2} = g\sum_{i=1}^{8} m_i \tag{2.13}$$

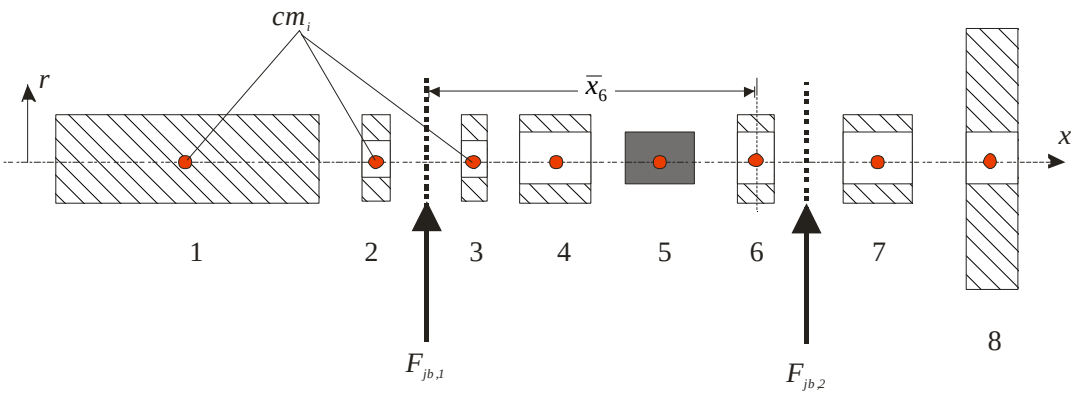

Figure 2-7: Schematic of sectioned shaft and journal bearing forces

Operating at the rigid body natural frequency of the shaft assembly will result in the maximum amplitude of the shaft motion in response to any unbalance force; the oscillation may be sufficiently large that contact with the bearing pad results. However, it may be possible to run the turboexpander through the rigid body natural frequency

provided that the shaft assembly is sufficiently balanced and the bearings provide adequate damping. The excitation force (F) on the shaft is the centripetal acceleration of the off-center mass:

$$F = mu\Omega^2 \tag{2.14}$$

where m is the mass of the shaft assembly, u is the magnitude of unbalance, and Ω is the operating speed. From Eq (2.1) it is evident that the amplitude of vibrations will be proportional to the excitation force. Figure 2-8 illustrates the amplitude of the response for various magnitudes of unbalance of a 3 gram shaft supported by a journal bearing with a stiffness of 200 kN/m and a damping coefficient of 1 kg/m-s. A shaft with a 10 μm unbalance will contact the bearings well before the undamped natural frequency of 1125 Hz; an unbalance of 1 μm will allow operation almost to the natural frequency, but will still result in contact with the bearings. However, an unbalance on the order of 0.1 μm will be able to surpass the natural frequency without contacting the bearings. Therefore, for a well-balanced shaft the natural frequency does not pose an absolute limitation on the operating speed.

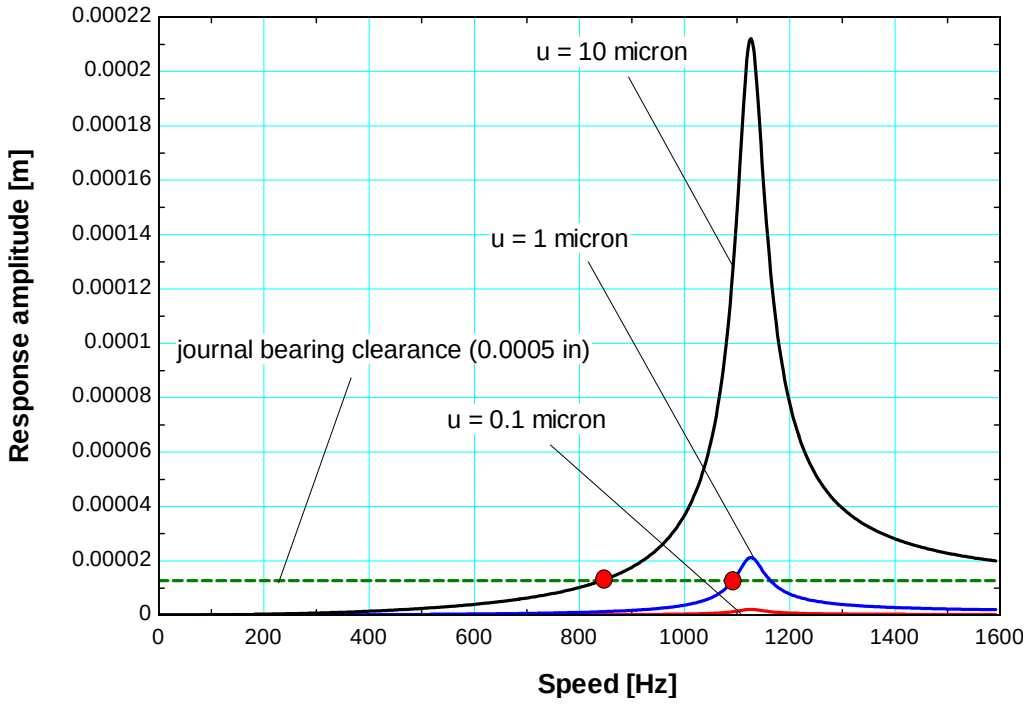

Figure 2-8: The response amplitude of a 3 gm shaft supported by journal bearings with a stiffness of 150 kN/m and damping coefficient of 1 kg/m-s for various magnitudes of unbalance.

2.2 Whirl Instability

When the shaft is moved off center a distance, e (not to be confused with u, the offset of the center of mass and center of rotation), the hydrostatic journal bearings apply a restorative normal force (F_n) related to the normal stiffness (k_n) of the bearing:

$$F_n = k_n e \tag{2.15}$$

However, the journal bearings, seal, and thrust bearing will also act as full hydrodynamic journal bearings and therefore each will possess an inherent tangential stiffness (k_t) which provides a tangential force (F_t) to the shaft as illustrated in Figure 2-9. Note that k_t is the cross-coupled stiffness; it relates an offset in the normal direction to the resulting force in the tangential direction; the negative sign denotes a destabilizing stiffness.

$$F_t = -k_t\, e \tag{2.16}$$

This tangential force gives rise to the phenomenon known as whirl instability. Whirl instability is characterized by an increasing shaft offset as the shaft orbits the center of its housing, causing the shaft to eventually contact the bearings.

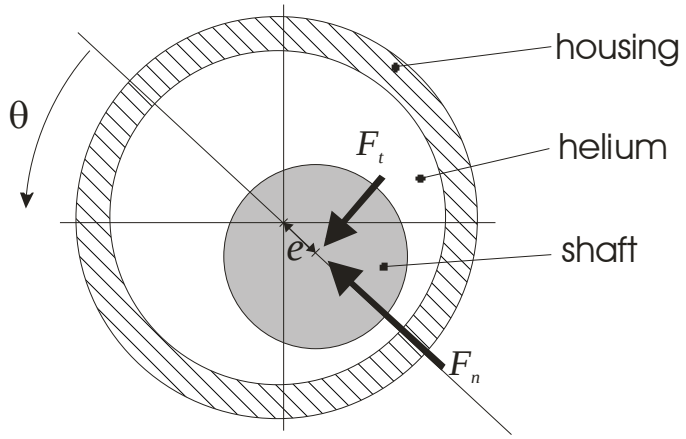

Figure 2-9: Schematic of the bearing forces incident on the shaft

2.2.1 Threshold Speed

Whirl instability can be best understood and quantified by examining the force-acceleration relationship for the shaft in the normal (radial) and tangential directions, as defined by Newton's second law:

$$F_n = m\, a_n \tag{2.17}$$

$$F_t = m\, a_t \tag{2.18}$$

where a_n and a_t are the tangential and normal accelerations, respectively (see Figure 2-10), and m is the mass of the shaft assembly. The normal acceleration for a perfectly balanced shaft can be written as:

$$a_n = \frac{d^2 e}{dt^2} - \omega_s^2 e \tag{2.19}$$

where t is time and ω_s is the rotational velocity at which the shaft orbits the center of the journal bearing. The first term in Eq (2.19) is the radial shaft acceleration which is negligible relative to the centripetal acceleration indicated by the second term under normal conditions associated with a circular whirl orbit. The centripetal acceleration will always be present for an orbiting shaft and can have a large impact on the shaft dynamics.

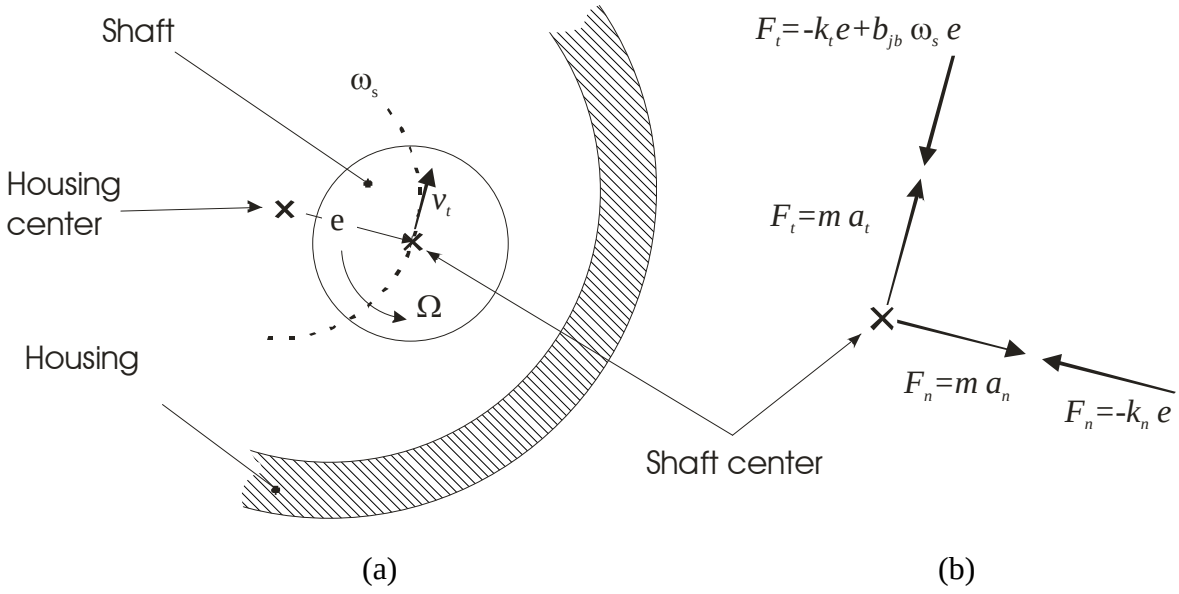

Figure 2-10: Schematic of (a) the shaft motion within the housing and (b) the forces acting on the shaft

Combining Eqs (2.15), (2.17), and (2.19) and neglecting insignificant normal acceleration leads to:

$$-k_n e = -m \omega_s^2 e \tag{2.20}$$

which simplifies to:

$$\omega_s = \sqrt{\frac{k_n}{m}} \tag{2.21}$$

Assuming the shaft assembly is axially centered on the journal bearings yields:

$$F_{jb,1} = F_{jb,2} = F_{jb} = \frac{F_n}{2} \tag{2.22}$$

$$k_n = 2k_{jb} \tag{2.23}$$

$$m_{eq,1} = m_{eq,2} = m_{eq} \tag{2.24}$$

which allows Eq (2.21) to be rewritten as:

$$\omega_s = \sqrt{\frac{k_{jb}}{m_{eq}}} \tag{2.25}$$

Therefore the axially centered shaft will orbit at a speed equal to the undamped rigid body natural frequency, ω_n, as defined in Eq (2.11).

The tangential acceleration can be written as the rate of change of the tangential velocity, v_t, with respect to time:

$$a_t = \frac{dv_t}{dt} \tag{2.26}$$

For small a small offset, the shaft can be assumed to be orbiting with an approximately circular path around the journal bearing center. This leads to the expression for the tangential velocity:

$$v_t = \omega_s e \tag{2.27}$$

Therefore the tangential acceleration can be rewritten as:

$$a_t = \frac{d(\omega_s e)}{dt} = \omega_s \frac{de}{dt} + e\frac{d\omega_s}{dt} \tag{2.28}$$

The whirl speed according to Eq (2.21) is only dependent on the bearing normal stiffness and the supported mass. Therefore, under steady state operating conditions only the first term of Eq (2.28) is nonzero.

The tangential force due to the stiffness in Eq (2.16) is only part of the total tangential force acting on the shaft. The orbiting motion of the shaft provides a damping force that opposes the whirling motion caused by the squeeze film effect. The total tangential force then becomes:

$$F_t = -k_t\, e + \omega_s\, b\, e \tag{2.29}$$

where b is the damping coefficient. Combining Eqs (2.18), (2.28), and (2.29) leads to:

$$-k_t\, e + \omega_s\, b\, e = m\, \omega_s\, \frac{de}{dt} \tag{2.30}$$

For the system to be stable the radial velocity, $\frac{de}{dt}$, must be either zero or negative (that is, the shaft will orbit inwards rather than outwards). This leads to the constraint for stable operation:

$$-k_t\, e + \omega_s\, b\, e \geq 0 \tag{2.31}$$

An excessive tangential stiffness force (i.e. one that is larger than the damping force) will result in a net force acting upon the shaft that is in the same direction as the whirl motion and therefore causes the shaft to accelerate tangentially; this causes the magnitude of the shaft offset to increase and it orbits outwards in a manner that is characteristic of whirl instability. The operating speed that causes Eq. (2.31) to be zero is the threshold speed, Ω_{th}, and is equal to the ratio of the tangential stiffness to the damping.

The tangential stiffness of the seal ($k_{t,s}$), journal bearing ($k_{t,jb}$), and thrust bearing ($k_{t,tb}$) are each a linear function of the rotational speed. Therefore, it is possible to define a new stiffness parameter for each component which is the stiffness normalized by the rotational speed (*k'*):

$$k'_{t,s} = \frac{k_{t,s}}{\Omega} \qquad k'_{t,jb} = \frac{k_{t,jb}}{\Omega} \qquad k'_{t,s} = \frac{k_{t,tb}}{\Omega} \tag{2.32}$$

This definition leads to the expression for the total tangential stiffness imposed on the shaft:

$$k_t = \left(k'_{t,jb} + k'_{t,tb} + k'_{t,s}\right)\Omega \tag{2.33}$$

The damping coefficient provided by the journal bearings, assuming the journal bearings can be approximated as infinitely long bearings, is given by:

$$b = \frac{12\,\pi\,L_{jb}\,\mu\,R_{sh}^3}{c_{jb}^3} \tag{2.34}$$

where L_{jb} is the combined length of both journal bearings, μ is the viscosity of the helium, Ω is the shaft operating speed, R_{sh} is the shaft radius, and c_{jb} is the journal bearing centered clearance.

Assuming that the only damping is provided by the journal bearings and applying Eqs (2.33) and (2.34) to Eq (2.31) at the threshold speed yields the expression for the threshold speed:

$$\Omega_{th} = \frac{12\,\pi\,L_{jb}\,\mu\,R_{sh}^3\,\omega_n}{c_{jb}^3\left(k_{t,jb}\text{`} + k_{t,tb}\text{`} + k_{t,s}\text{`}\right)} \tag{2.35}$$

This represents an absolute limit to the operating speed of the shaft. Operating above this speed is not possible and will certainly lead to contact between the shaft and bearings or seal.

2.2.2 Tangential Stiffness

The previous section showed that the threshold speed of the turbine depends strongly on the tangential stiffness of the close-clearance components. However, the stiffness calculation will depend on the ratio of the diameter of the shaft to the length of the bearing, or the *L/D* ratio. For a small *L/D*, such as in a labyrinth seal or thrust bearing edge, the short bearing approximation can be applied. For a large *L/D*, such as a plain seal, the long bearing approximation is more accurate. The general convention is that for an *L/D* less than 0.5 the short bearing approximation is used (Dubois, 1953) while for an *L/D* of greater than 2 the long bearing approximation is used (Fay, 1995). However, as the *L/D* for each journal bearing will most likely fall between 0.5 and 2 the method resulting in the larger stiffness, and thus a lower threshold speed, will be utilized; note that this is consistent with the long bearing approximation used to compute the damping coefficient. Figure 2-11 illustrates the geometry of a hydrostatic fluid bearing consisting of a bearing and a shaft separated by a helium film. Note that there is none of the elements of a hydrostatic bearing included in Figure 2-11; there are no orifices for the supply of high pressure gas. These elements are responsible for the bearing's normal stiffness but it is assumed that they have little effect on the damping coefficient or

tangential stiffness; these quantities are primarily related to the hydrodynamic aspects of the bearing.

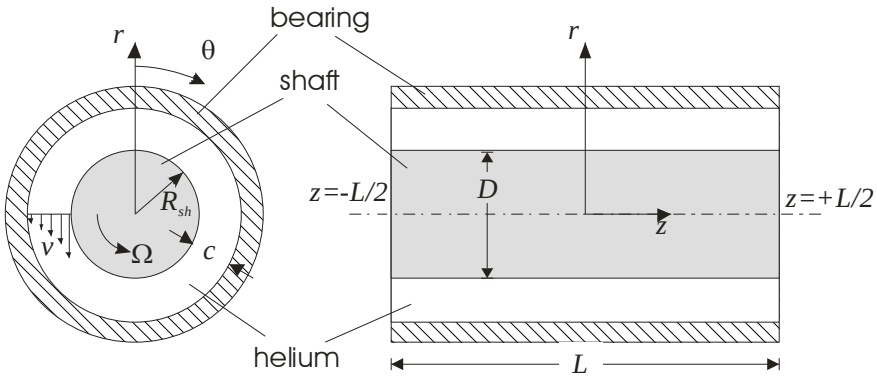

Figure 2-11: Schematic of a hydrodynamic bearing

When the shaft is centered, as shown in Figure 2-11, there is no net force. The bearing force, and thus the bearing stiffness, is the result of moving the shaft off of center by a distance *e*, illustrated in Figure 2-12. When the shaft is perturbed, the pressure distribution (*P*) becomes asymmetric, producing a net bearing force (F_b). The direction of this force does not align with the perturbation which is at the attitude angle (α) and will therefore have both normal and tangential components.

The clearance between the stator and off-center rotor, *h*, is defined as a function of angle θ, which is measured from the point of maximum clearance:

$$h = c\left(1 - \varepsilon\cos(\theta)\right) \tag{2.36}$$

where ε is the eccentricity ratio defined as the ratio of the offset to the centered clearance, *c*:

$$\varepsilon = \frac{e}{c} \tag{2.37}$$

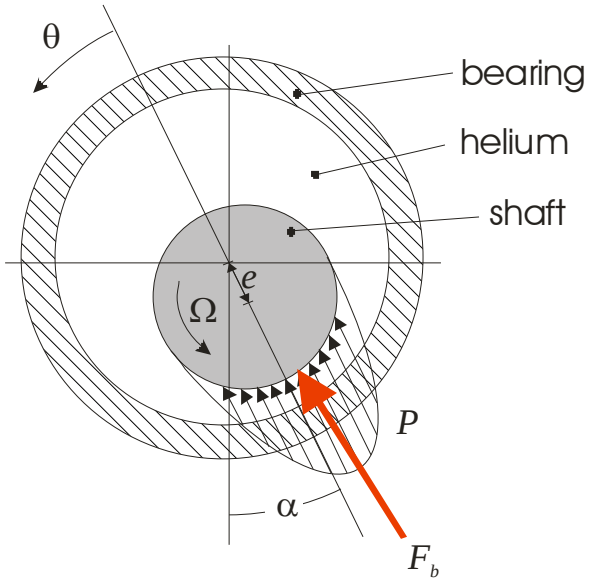

Figure 2-12: Schematic of the pressure distribution and resultant force of a rotor

Assuming that the helium behaves as an incompressible fluid (a reasonable assumption for the high pressures and low pressure differences expected in the cryogenic turbine), with constant viscosity, and neglecting fluid inertial forces it is possible to derive the Reynolds equation for a hydrodynamic bearing (Fay, 1995):

$$\frac{1}{R}\frac{\partial}{\partial\theta}\left(h^3\frac{1}{R}\frac{\partial p}{\partial\theta}\right)+\frac{\partial}{\partial z}\left(h^3\frac{\partial p}{\partial z}\right)=6\mu\Omega\frac{\partial h}{\partial\theta} \tag{2.38}$$

where R is the radius of the shaft, p is the pressure of the helium, μ is the helium viscosity, and Ω is the shaft rotational velocity.

2.2.2.1 Long Bearing Approximation

The long bearing approximation assumes that the pressure variation in the z-direction is negligible (i.e., side leakage is neglected), which simplifies Eq (2.38) to:

$$\frac{1}{R}\frac{\partial}{\partial\theta}\left(h^3\frac{1}{R}\frac{\partial p}{\partial\theta}\right)=6\mu\Omega\frac{\partial h}{\partial\theta} \tag{2.39}$$

Equation (2.39) is most easily solved indirectly by use of the Couette-Poisseulle flow equation for flow between cylinders, which also assumes no pressure gradient in the z-direction. The flow rate in the circumferential direction, $\dot{Q}$, is given by Fay (1994):

$$\dot{Q} = \frac{\Omega R L h}{2} + \frac{L h^3}{12 \mu}\left(-\frac{1}{R}\frac{dp}{d\theta}\right) \tag{2.40}$$

where L is the length of the bearing. Rearranging Eq. (2.40) in order to solve for the pressure gradient leads to:

$$\frac{dp}{d\theta} = \frac{6\Omega R^2 \mu}{h^3} - \frac{12 \mu R \dot{Q}}{L h^3} \tag{2.41}$$

Equation (2.36) for the height is substituted into Eq. (2.41) and the result is integrated about the rotor. The integral of the left hand side of Eq. (2.41) (the pressure term) around the shaft must be zero if the pressure is continuous. This results in an expression for the flow rate in terms of the eccentricity ratio:

$$\dot{Q} = \frac{c \Omega L R\left(1-\varepsilon^2\right)}{2+\varepsilon^2} \tag{2.42}$$

Substituting Eqs. (2.36) and (2.42) into Eq. (2.41) and rearranging yields:

$$dp = \left[\frac{6\Omega R^2 \mu}{c^3\left(1-\varepsilon\cos\left(\theta\right)\right)^3}\left(1-2c\frac{1-\varepsilon^2}{2+\varepsilon^2}\right)\right]d\theta \tag{2.43}$$

Integrating Eq. (2.43) around the shaft provides the pressure distribution around the rotor:

$$p = \pm\frac{6\Omega \mu R^2}{c^2}\frac{\varepsilon\sin(\theta)\left(2-\varepsilon\cos(\theta)\right)}{\left(2+\varepsilon^2\right)\left(1-\varepsilon\cos(\theta)\right)^2} + p_o \tag{2.44}$$

where p_o is the charge pressure, or the pressure of the helium when the rotor is motionless. Equation (2.44) is positive for θ from 0 and π and negative for θ from π and 2π. The force exerted on the shaft at any point around the rotor is given by:

$$F = p\,dA = p\,L\,R\,d\theta \tag{2.45}$$

The tangential component of the force is the component of the force that acts perpendicular to the direction of perturbation:

$$F_t = p\,L\,R\cos(\theta)\,d\theta \tag{2.46}$$

Combining Eqs (2.44) and (2.46) and integrating about the rotor results in the net tangential force:

$$F_t = 2\int_0^{\pi} \frac{6\Omega\mu R^2}{c^2}\frac{\varepsilon\sin(\theta)\left(2-\varepsilon\cos(\theta)\right)}{\left(2+\varepsilon^2\right)\left(1+\varepsilon\cos(\theta)\right)^2} L\,R\cos(\theta)\,d\theta \tag{2.47}$$

Note that the change in sign in Eq. (2.44) is negated by the cosine in equation (2.46) causing the force from 0 to π and π to 2π to be symmetric (i.e., both sides contribute to a positive tangential force on the shaft). The tangential stiffness (k_t) is defined as the ratio of the net force to the displacement:

$$k_t = \frac{1}{c}\frac{dF_t}{d\varepsilon} \tag{2.48}$$

Combining Eq (2.47) with Eq (2.48) in the limit of a small eccentricity yields the long bearing approximation for tangential stiffness:

$$k_t = \frac{6\pi\Omega\mu R_{sh}^3 L}{c^3} \tag{2.49}$$

2.2.2.2 Short Bearing Approximation

The short bearing approximation assumes a negligible pressure gradient in the tangential direction compared to the pressure gradient in the axial direction. Therefore Eq (2.38) is approximated by:

$$\frac{d^2 p}{dz^2} = \frac{6\mu\Omega}{h^3}\frac{dh}{d\theta} \tag{2.50}$$

Equation (2.50) can be integrated twice along the length of the rotor, which leads to:

$$p = \frac{6\mu\Omega}{h^3}\frac{dh}{d\theta}\frac{z^2}{2} + C_1 z + C_2 \tag{2.51}$$

where C_1 and C_2 are constants of integration. If $z = 0$ is chosen to be at the center of the bearing (see Figure 2-11) about which the flow in the z-direction is assumed to be symmetric, the pressure differential at that point is:

$$\frac{dp}{dz}\left(z = 0\right) = 0 \tag{2.52}$$

Either side of the bearing is assumed to be exposed to a pressure of p_o:

$$p\left(z = \pm L/2\right) = p_o \tag{2.53}$$

Applying the conditions associated with Eqs. (2.52) and (2.53) to Eq. (2.51) leads to the pressure distribution:

$$p = \frac{3\mu\Omega}{c^3}\frac{dh}{d\theta}\left(z^2 - \frac{L^2}{4}\right) + p_o \tag{2.54}$$

Substituting Eq. (2.54) into Eq. (2.46) and integrating about the rotor yields the tangential force acting on the rotor:

$$F_t = \frac{\mu \Omega R L^3}{4c^2} \frac{\pi \varepsilon}{\left(1-\varepsilon^2\right)^{3/2}} \tag{2.55}$$

Combining Eqs. (2.55) and (2.48) in the limit of small eccentricities produces the tangential stiffness of a short bearing:

$$k_t = \frac{\pi \mu \Omega R L^3}{4c^3} \tag{2.56}$$

Combining either of the estimates for the tangential stiffness with Eq. (2.35) provides an estimate of the threshold speed for whirl; this threshold speed becomes a critical design parameter and typically is the lowest limit on the shaft speed.

2.3 Friction Model

With the high operating speeds and close clearances of the bearings and seal it is likely that a substantial amount of power (relative to the shaft power) will be dissipated as heat by viscous friction. Due to the already warm temperature of the bearings compared to the turbine, the heat produced should not reflect any direct heat load on the turbine (except in the seal). However, in order to maintain adequate control of the turbine speed, the frictional power must be significantly less than the total turbine mechanical power. The mechanical power that is not dissipated by friction will be dissipated as electrical power that is generated by the turboalternator rotor/stator assembly. In order to design the turboexpander such that adequate control over the speed is maintained, it is necessary to estimate the amount of power that will be dissipated by fluid friction.

2.3.1 Radial Motion – Seal, Journal Bearings, and Thrust Bearing Edge

Within the radial space between the shaft and housing for the seal, journal bearings, and thrust bearing edge, the fluid motion is considered to be primarily circumferential; axial flow is assumed to be negligible. The shear stress at the wall of the rotor is given in polar coordinates by:

$$\tau_w = \mu \frac{\partial v_\theta}{\partial r} \tag{2.57}$$

where μ is the fluid viscosity and v_θ is the tangential fluid velocity. Here, it is assumed that there is inviscid flow with purely circumferential velocity so that the θ-momentum equation reduces to:

$$\frac{1}{r}\frac{d}{dr}\left(r\frac{dv_\theta}{dr}\right) - \frac{v_\theta}{r^2} = 0 \tag{2.58}$$

This is a second order ordinary differential equation with solution:

$$v_\theta = C_1 r + \frac{C_2}{r} \tag{2.59}$$

where C_1 and C_2 are constants. Applying the no slip boundary conditions at the shaft and casing:

$$v_\theta(r = R_{rot}) = \Omega R_{rot} \tag{2.60}$$

$$v_\theta(r = R_{st}) = 0 \tag{2.61}$$

where R_{rot} is the rotor radius and R_{st} is the stator radius (i.e. the journal bearing or seal radius):

$$R_{st} = R_{rot} + c \tag{2.62}$$

where c is the centered clearance between the rotor and stator. The tangential velocity, $v_{\theta,}$ reduces to (White, 1995):

$$v_\theta = \Omega R_{rot} \frac{R_{st}/r - r/R_{st}}{R_{st}/R_{rot} - R_{rot}/R_{st}} \tag{2.63}$$

However, for the small clearances involved in the turbine assembly the velocity profile from Eq (2.63) is approximately linear. Applying the no-slip boundary conditions at the walls leads to the linear velocity profile:

$$v_\theta = \Omega R_{rot}\left(1 - \frac{r - R_{rot}}{c}\right) \tag{2.64}$$

For clearances less than 0.002 inch (50.8 micron) the linear approximation in Eq. (2.64) agrees with Eq. (2.63) within 1%; therefore, the linear approximation is used subsequently. Taking the derivative of v_θ with respect to r leads to:

$$\frac{\partial v_\theta}{\partial r} = \frac{\Omega R_{rot}}{c} \tag{2.65}$$

Combining Eqs (2.57) and (2.65) leads to an equation for shear stress at the shaft wall:

$$\tau_w = \frac{\mu \Omega R_{rot}}{c} \tag{2.66}$$

The total friction force, F_f, exerted tangentially at the shaft surface is found by integrating the wall shear stress along the circumference of the rotor:

$$F_f = L \int_0^{2\pi} \tau_w R_{rot}\, d\theta \tag{2.67}$$

Substituting Eq (2.66) into Eq (2.67) and evaluating the integral leads to:

$$F = \frac{2\pi \mu \Omega R_{rot}^2 L}{c} \tag{2.68}$$

which is the well known Petroff equation (Juvinall, 2000). Torque, *T*, and power, $\dot{W}$, are defined according to:

$$T = F_f \, R_{rot} \tag{2.69}$$

$$\dot{W} = \Omega T \tag{2.70}$$

Combining Eqs. (2.68), (2.69), and (2.70) leads to the equation for the friction power ($\dot{W}_f$):

$$\dot{W}_f = \frac{2\pi \mu \Omega^2 R_{rot}^3 L}{c} \tag{2.71}$$

2.3.2 Disk Motion – Thrust Bearing Pad

Estimating the friction produced by the thrust bearing is more complex than that produced by the journal bearing or seal due to the variation of the tangential velocity with radius as well as the possibility of encountering different flow regimes depending on the size (radius) and axial clearance of the thrust bearing. The geometry of an enclosed, rotating disk which represents the thrust bearing is shown schematically in Figure 2-13. The four flow regimes include close clearance laminar which is characterized by merged boundary layers between the stator and rotor (regime I), laminar flow with separate boundary layers (regime II), close clearance turbulent with merged boundary layers (regime III), and finally close clearance turbulent with separate boundary layers (regime IV) according to White (1995).

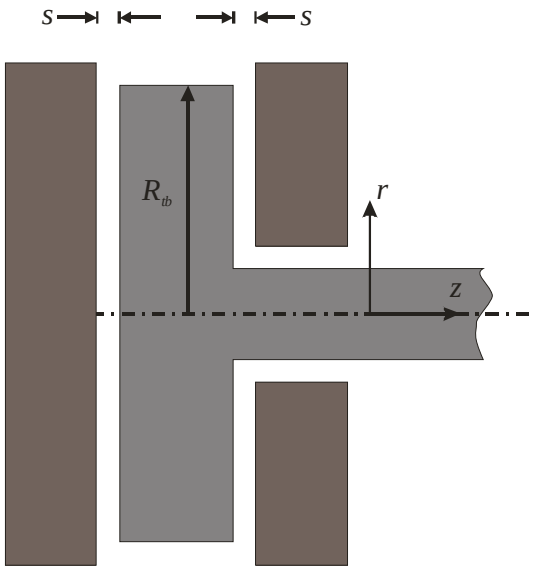

Figure 2-13: Schematic of thrust bearing

Figure 2-14 illustrates the different regimes and their dependence on the ratio of axial clearance, *s*, to bearing radius, R_{tb}, and the disk rotational Reynolds number, Re_{rot}:

$$Re_{rot} = \frac{\Omega R_{tb}^2}{\nu} \tag{2.72}$$

where Ω is the rotational velocity and ν is the kinematic viscosity of helium.

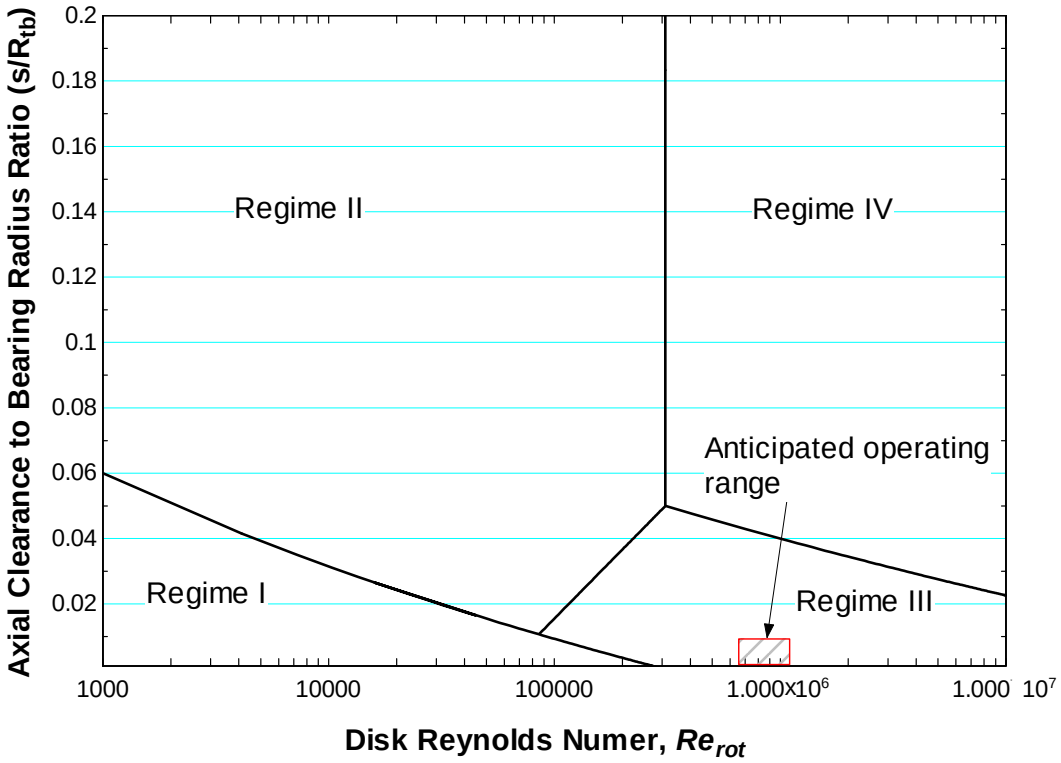

Figure 2-14: Different flow regimes as they relate to the s/R_{tb} ratio and disk Reynolds number

For each regime in Fig. 2-14 there are a different set of empirical correlations used to compute the moment coefficient, C_{mo} as a function of the rotational Reynolds number and clearance ratio s/R_{tb}. The moment coefficients for a smooth, non-ventilated enclosed disk as measured by Daily *et al*. (1960) are:

$$C_{mo,I} = \frac{2\pi}{\left(s/R_{tb}\right) Re_{rot}} \tag{2.73}$$

$$C_{mo,II} = \frac{3.70\left(s/R_{tb}\right)^{0.1}}{Re_{rot}^{0.5}} \tag{2.74}$$

$$C_{mo,III} = \frac{0.08}{\left(s/R_{tb}\right)^{1/6} Re_{rot}^{0.25}} \tag{2.75}$$

$$C_{mo,IV} = \frac{0.102\left(s/R_{tb}\right)^{0.1}}{Re_{rot}^{0.2}} \tag{2.76}$$

In another paper by White (1995) the moment coefficients are given as:

$$C_{mo,I} = \frac{2\pi}{\left(s/R_{tb}\right)Re_{rot}} \tag{2.77}$$

$$C_{mo,II} = \frac{2.66}{Re_{rot}^{0.5}} \tag{2.78}$$

$$C_{mo,III} = \frac{0.0622}{\left(s/R_{tb}\right)^{1/4}\mathrm{Re}_{rot}^{0.25}} \tag{2.79}$$

$$C_{mo,IV} = \frac{0.0836}{Re_{rot}^{0.2}} \tag{2.80}$$

Note that the moment coefficients for regimes I and III reported in the second paper are completely independent of the clearance ratio. The moment coefficient is defined in order to nondimensionalize the torque on the shaft according to:

$$C_{mo} = \frac{T_f}{\frac{\rho}{2}\Omega^2 R_{tb}^{5}} \tag{2.81}$$

where ρ is the helium density and T_f is the total torque resulting from viscous friction on both sides of the thrust disk. The resulting thrust bearing friction power can be calculated using Eq. (2.70). Equations (2.72) through (2.81) were implemented using EES in order to calculate the moment coefficient for a given regime; the average of the results from the two papers was used.

The code for the numerical calculations related to the turboexpander rotor dynamics (natural frequencies, whirl, and friction) can be found in Appendix A.

3. Turboalternator

The turboexpander operates by extracting energy from the incoming helium and converting it into mechanical energy associated with the turbine shaft rotating against a torque. With no additional interference, the turbine shaft would rotate at a speed such that the mechanical power is balanced by the frictional power, discussed in section 2.3. However, the frictional power is low due to the use of gas bearings and is also not adjustable; if the frictional power is too low then the turbine speed will become too high and the critical frequencies discussed in Chapter 2 will be exceeded resulting in damage to the device. Therefore, it is necessary to include a turboalternator that can be used to convert the shaft's mechanical energy into electrical energy; the torque exerted by the turboalternator stator onto the shaft may be controlled by the resistance of the electrical load and therefore the turboalternator provides an effective technique for controlling the turbine speed.

The turboalternator rotor is a permanent, neodymium-iron-boron magnet that is magnetized across its diameter and installed in the shaft bore. The stator consists of six ferrite poles, each with copper wire windings (illustrated in Figure 3-1) that are installed within a ferrite shell. As the magnet rotates past each stator pole, the flux that passes through the stator pole varies which induces an electrical current; the result is the generation of a three-phase sinusoidal electrical signal (one phase for each pair of poles). The windings may be connected via electrical leads to a 3-phase potentiometer located at room temperature and external to the cryocooler in order to dissipate the electrical power

as ohmic heating. By varying the resistance of the potentiometer, the amount of electrical current generated and therefore the magnetic torque exerted on the rotor assembly (i.e. the turbine shaft, thrust bearing, and magnet) can be regulated. This chapter describes an analytical model to predict the turboalternator performance as well as the results of an experimental validation of the model.

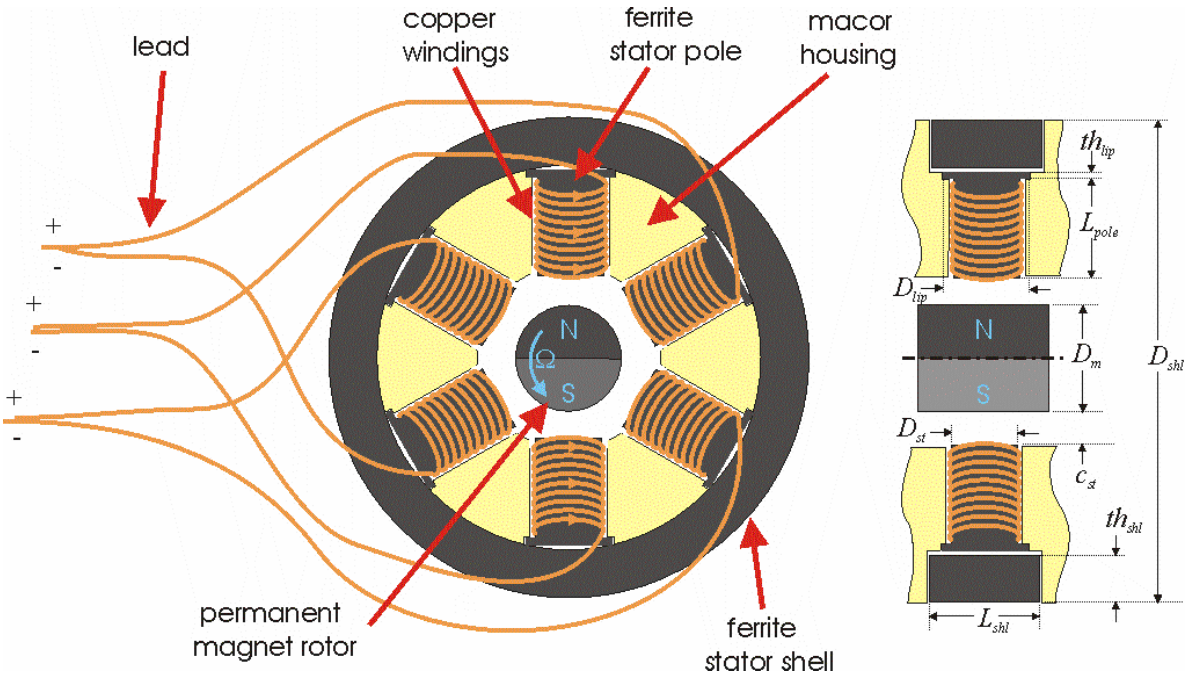

Figure 3-1: Schematic of the turboalternator components

3.1 Model

The model of the turboalternator utilizes a magnetic equivalent circuit in which the reluctance ($\Re$), magnetomotive force (F_m), and magnetic flux (ϕ) of a magnetic circuit are considered to be analogous to the resistance (R), voltage (V), and current (i) in an electrical circuit, as illustrated in Figure 3-2. Additionally, magnetic permeability, μ, is analogous to electrical resistivity which allows the reluctance to be defined as:

$$\Re = \frac{l}{\mu A} \tag{3.1}$$

where l is the flux path length and A is the flux path cross-sectional area.

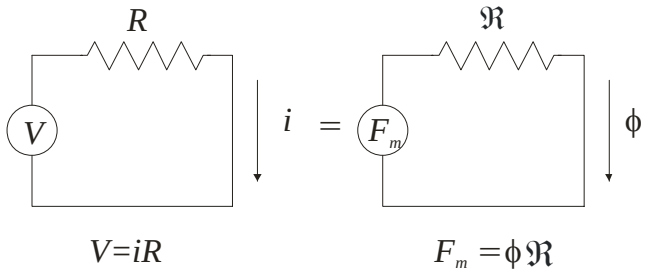

Figure 3-2: Analogous electric (left) and magnetic (right) circuits

Applying the equivalent of Ohm's Law to the turboalternator magnetic circuit provides:

$$F_m = \phi_m \Re_{eq} \tag{3.2}$$

where F_m and ϕ_m are the rotor magnet magnetomotive force and flux density, respectively, and $\Re_{eq}$ is the equivalent reluctance apparent to the magnet.

The magnetomotive force is defined by Lorenz (2000):

$$F_m = \int \vec{H} \cdot d\vec{l} \tag{3.3}$$

where $\vec{H}$ is the magnetic field intensity, and l is the flux path length. The source of the magnetomotive force in the turboalternator is the rotor magnet which is magnetized across its diameter; within the magnet, the magnetic field is parallel to the path length, so that Eq (3.3) can be simplified:

$$F_m = H_m \bar{D} \tag{3.4}$$

where $\bar{D}$ is the mean flux path through the magnet, given by:

$$\bar{D} = \frac{\pi D_m}{4} \tag{3.5}$$

The magnetic flux through a given path is defined by the flux density vector, $\vec{B}$:

$$\phi = \int \vec{B} \cdot \hat{n}\, dA \tag{3.6}$$

where $\hat{n}$ is the unit vector parallel to the flux path and dA is the differential area of the flux path. Within the magnet, the flux density is always normal to the flux path which reduces Eq. (3.6) to:

$$\phi_m = B_m L_m D_m \tag{3.7}$$

where B_m, L_m, and D_m are the flux density, length, and diameter of the magnet, respectively.

The magnetic field strength, H_m, and the flux density, B_m, are material properties related by the demagnetization curve of the permanent magnet in the upper left quadrant of the material's hysteresis plot. Figure 3-3 illustrates the demagnetization curves associated with various grades of neodymium iron boron (ChenYang, 2004). For the operating parameters of the turboalternator, the relation between flux density and magnetic field strength can be approximated as being linear:

$$B_m = B_{max} - H_m \frac{B_{max}}{H_{max}} \tag{3.8}$$

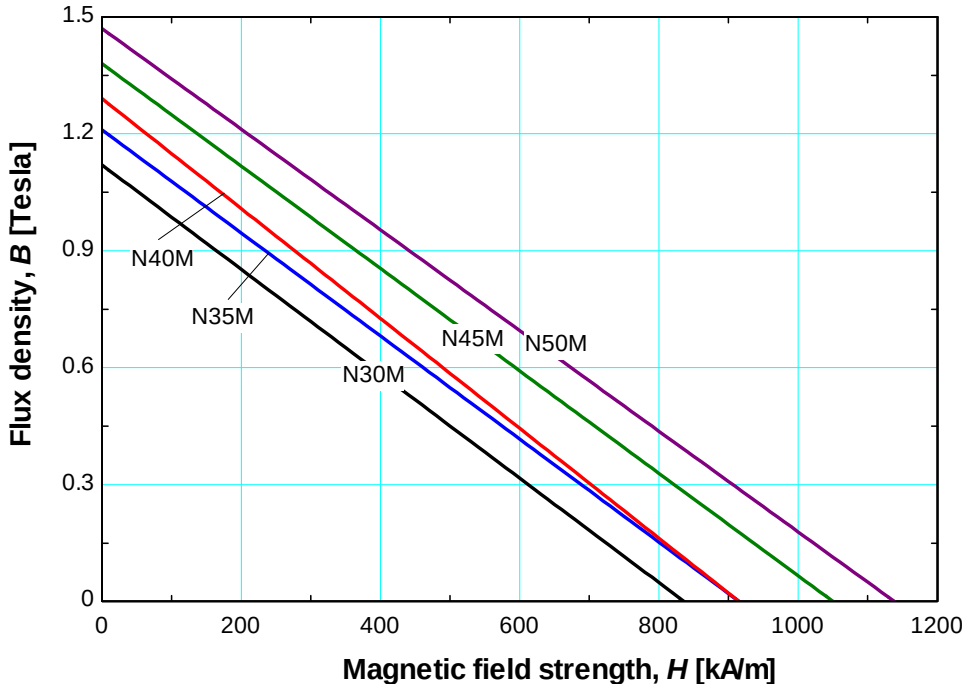

Figure 3-3: Demagnetization curve for various grades of neodymium iron boron (ChenYang, 2004)

Combining Eqs. (3.2), (3.4), and (3.8) leads to an expression for the magnetic field strength of the magnet in terms of the magnet dimensions (L_m and D_m), magnet strength (H_{max} and B_{max}) and the reluctance of the loading circuit ($\Re_{eq}$):

$$H_m = \frac{\Re_{eq} B_{max} L_m D_m}{\bar{D} H_{max} + \Re_{eq} B_{max} L_m D_m} \tag{3.9}$$

Combining Eqs. (3.2), (3.4), and (3.9) yields the flux provided by the magnet:

$$\phi_m = \frac{B_{max} H_{max} L_m D_m}{\bar{D} H_{max} + \Re_{eq} B_{max} L_m D_m} \tag{3.10}$$

Note that if the reluctance of the load is very large then the flux provided by the magnet will go to zero (this is equivalent to open circuiting a power supply). On the other hand, if the reluctance of the load is very small then the flux is related to the maximum flux that

can be pulled from the magnet (this is equivalent to short circuiting a power supply). Traveling between these two extremes is related to moving along one of the demagnetization paths in Fig. 3-3.

The magnetic flux can take one of two paths as it moves from the north to the south pole of the magnet: the flux can either travel through the stator assembly (ϕ_{st}) or through the air gap between the magnet and stator poles (ϕ_{leak}) as illustrated in Figure 3-4 (a). The reluctance of the stator assembly includes the initial air gap from the rotor magnet to the stator pole ($\Re_{g,1}$), the stator pole ($\Re_{pole}$), the air gap from the stator pole to the shell ($\Re_{g,2}$), and the shell ($\Re_{shl}$). Applying Eq. (3.1) to each of these components yields:

$$\Re_{g,1} = \frac{\overline{c}_{st}}{\mu_0 \, \pi \, D_{st}^2} \tag{3.11}$$

$$\Re_{pole} = \frac{2 L_{st}}{\mu_f \, \pi \, D_{st}^2} \tag{3.12}$$

$$\Re_{g,2} = \frac{\overline{c}_{shl}}{\mu_0 \, A_{g,2}} \tag{3.13}$$

$$\Re_{shl} = \frac{\pi \, \left(D_{shl} - 0.5 th_{shl} \right)}{\mu_f \, th_{shl} \, L_{shl}} \tag{3.14}$$

where L_{st} and D_{st} are the radial length and diameter of the stator pole, μ_f and μ_0 are the permeability of ferrite and of free space, and $\overline{c}_{st}$ is the average clearance for between the stator and rotor. $A_{g,2}$ and $\overline{c}_{shl}$ are the average area and average clearance length within the air-gap between the stator. D_{shl}, th_{shl}, and L_{shl} are the outer diameter, thickness, and axial length of the stator shell, respectively. Note that there is also titanium alloy shaft

material between the magnet and stator poles. However, titanium is not magnetic and therefore the magnetic permeability of the titanium alloy is low and assumed to be equal to the magnetic permeability of free space. Also note that the stator poles must include a lip that provides a mechanical stop when it is installed in the Macor housing (see Fig. 3-1); the effect of the presence of the lip on the magnetic circuit was neglected. However, the lip diameter, D_{lip}, was used to determine the stator pole-to-shell air-gap length in Eq. (3.13).

The total reluctance of the stator, $\Re_{st}$, is the equivalent reluctance associated with magnetic circuit illustrated in Figure 3-4 (b):

$$\Re_{st} = 2\left(\Re_{g,1} + \Re_{pole} + \Re_{g,2}\right) + \frac{\Re_{shl}}{2} \tag{3.15}$$

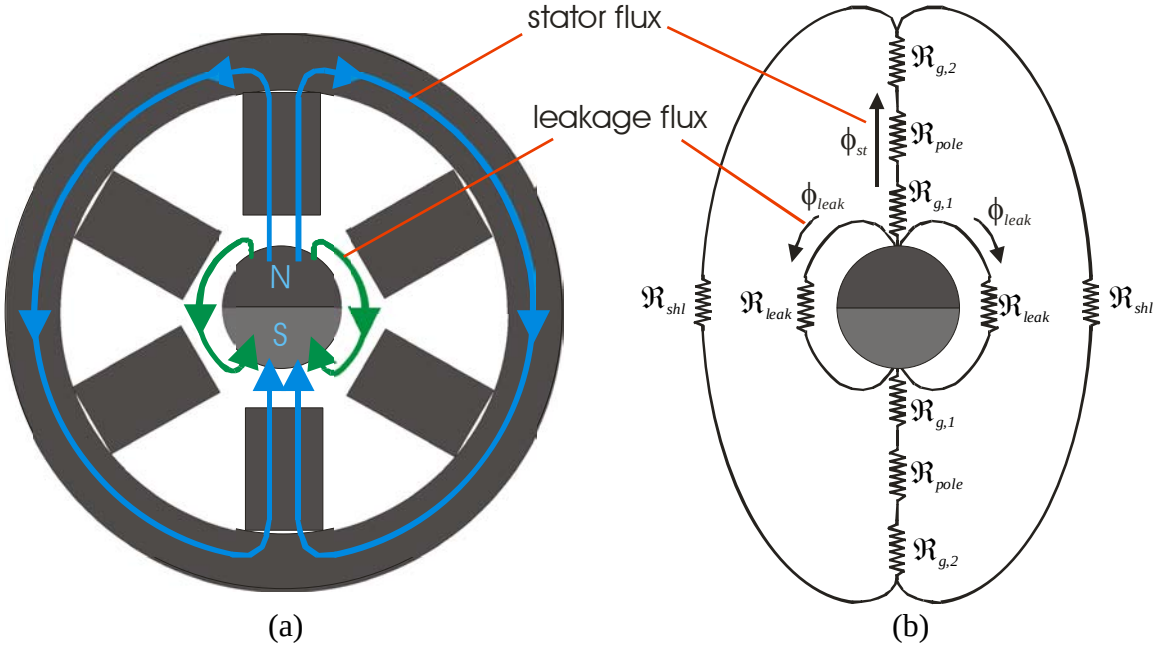

Figure 3-4: Schematic of flux paths (a) and corresponding reluctances (b)

The reluctance associated with the leakage flux ($\Re_{leak}$, the flux that bypasses the stator by going directly from the north to the south pole of the magnet via the clearance between the shaft and stator) is not as well defined by the geometry of the problem. However, the magnet may be analyzed as a number of smaller magnets aligned across the diameter, each with width, *dx*, and varying length, *S*, as illustrated in Figure 3-5. The flux path length, *l*, associated with these differential magnets varies with *x*, as does the magnetomotive force produced by each differential magnet. For example, the flux path length associated with a differential magnet near the edge of the magnet will be very small but it will also have a very small magnetomotive force. The leakage flux reluctance must be computed by averaging the differential flux lengths weighted by the magnetomotive force. From Eq. (3.4), it is evident that this process is equivalent to determining the average with respect to the magnet length which can be defined as a function of the angle β:

$$S = D_m \sin(\beta) \tag{3.16}$$

Therefore the leakage reluctance for either side of the magnet is estimated by:

$$\Re_{leak} = \frac{\int_0^{\pi/2} S\,\Re\, d\beta}{\int_0^{\pi/2} S\, d\beta} \tag{3.17}$$

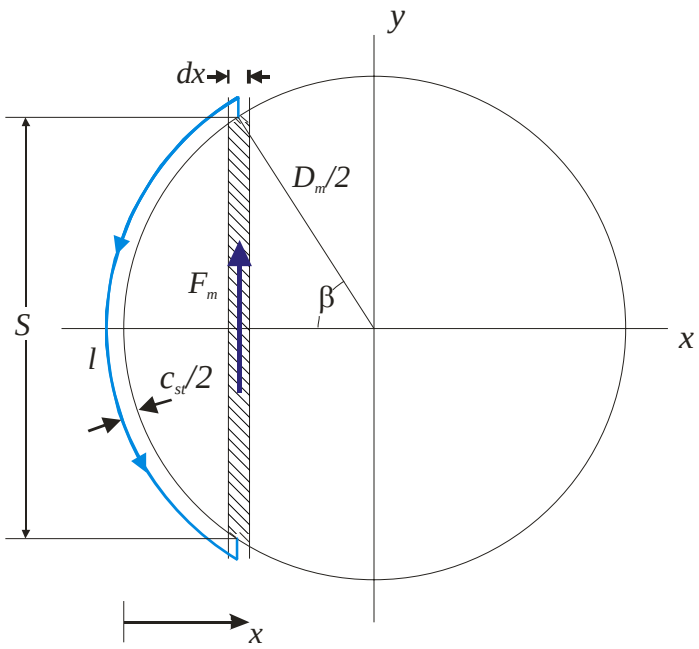

Figure 3-5: Schematic of discretized magnet

The flux path length of each section, *l*, is estimated as the arc length evaluated at a radius that includes one half the clearance between the magnet and stator pole, c_{st}:

$$l = \beta\left(D_m + c_{st}/2\right) \tag{3.18}$$

Combining Eqs. (3.1) and (3.16) through (3.18) gives:

$$\Re_{leak} = \frac{\left(D_m + c_{st}/2\right)}{\mu_0 A_{leak}} \frac{\int_0^{\pi/2} \beta \sin(\beta)\, d\beta}{\int_0^{\pi/2} \sin(\beta) d\beta} \tag{3.19}$$

where A_{leak} is the cross-sectional area of the leakage flux path, approximated by:

$$A_{leak} = c_{st}\, L_m \tag{3.20}$$

Evaluating Eq. (3.19) yields the expression for the leakage flux reluctance:

$$\Re_{leak} = \frac{\left(D_m + c_{st}/2\right)}{\mu_0\, c_{st}\, L_m} \tag{3.21}$$

The reluctances associated with the stator assembly and the leakage flux represent two paths in parallel. The equivalent reluctance seen by the magnet is given by:

$$\Re_{eq} = \left[\frac{1}{\Re_{st}} + \frac{1}{\Re_{leak}} \right]^{-1} \tag{3.22}$$

The amount of the total flux that passes through the stator rather than the leakage path is determined by applying a relation analogous to the current divider in an electric circuit. Combined with Eq. (3.6) this leads to the expression for the stator flux:

$$\phi_{st} = \frac{\Re_{eq}}{\Re_{st}} \phi_m \sin(\theta) \tag{3.23}$$

where θ is the angle between the rotor and stator pole. The voltage produced by the turboalternator is a result of a time-varying magnetic field captured by the windings, as stated in Faraday's Law:

$$V = -\frac{d\lambda}{dt} \tag{3.24}$$

where V is the voltage produced and λ is the flux linkage as defined by:

$$\lambda = N\phi \tag{3.25}$$

where N is the total number of turns of wire around a pair of stator poles.

Combining Eqs. (3.23) and (3.25) leads to the flux linkage through the stator:

$$\lambda = N\phi_m \frac{\Re_{eq}}{\Re_{st}} \sin(\theta) \tag{3.26}$$

The sine of the angle of the rotor, θ, can also be written as the sine of the product of rotor angular velocity, Ω, and time, t:

$$\sin(\theta) = \sin(\Omega t) \tag{3.27}$$

Substituting Eq. (3.27) into Eq. (3.26) and taking the derivative with respect to time yields the voltage produced by one pair of stator poles:

$$V = \Omega N \phi_m \frac{\Re_{eq}}{\Re_{st}} \cos(\Omega t) \tag{3.28}$$

The root mean square voltage produced (V_{rms}) is:

$$V_{rms} = \frac{\Omega N \phi_m \Re_{eq}}{\Re_{st}\sqrt{2}} \tag{3.29}$$

The current provided to the load potentiometer can be determined by examining the electrical circuit associated with the windings, leads, and the potentiometer. The impedance, Z, for a circuit composed only of resistors and inductors (i.e. neglecting any capacitance) is given by:

$$Z = \sqrt{Z_R^2 + Z_L^2} \tag{3.30}$$

where Z_R is the resistive impedance:

$$Z_R = R_{eq} \tag{3.31}$$

and Z_L is the inductive impedance:

$$Z_L = \Omega L \tag{3.32}$$

R_{eq} and L are the equivalent resistance and inductance of the circuit, respectively. The equivalent resistance for one stator pole pair is the total resistance of the windings ($R_{winding}$), the potentiometer (R_{load}), and two leads (R_{lead}), all in series:

$$R_{eq} = R_{winding} + R_{load} + 2\,R_{lead} \tag{3.33}$$

The resistance of one lead is:

$$R_{lead} = \frac{4\,\bar{\rho}_e\,l_{lead}}{\pi\,D_{wire}^2} \tag{3.34}$$

where D_{wire} is the diameter of the wire, l_{lead} lead is the length the lead, and $\bar{\rho}_e$ is the integrated average electrical resistivity of the wire (assumed to be copper) between the temperature of the turboalternator (assumed to be equal to the temperature of the bearings), $T_{bearing}$, and room temperature, T_0:

$$\bar{\rho}_e = \frac{\int_{T_{bearing}}^{T_0} \rho_e(T)\,dT}{T_0 - T_{bearing}} \tag{3.35}$$

The resistance of one set of windings is given by:

$$R_{winding} = \frac{4\,N\,D_{st}\,\rho_{e,T=T_{bearing}}}{D_{wire}^2} \tag{3.36}$$

where $\rho_{e,T=T_{bearing}}$ is the resistivity of the wire at the bearing temperature determined according to Giancoli (1995).

The inductance of the magnetic circuit is given by Lorenz (2000):

$$L = \frac{N^2}{\Re_{eq}} \tag{3.37}$$

Combining Eqs. (3.30)-(3.33) and Eq. (3.37) provides the *rms* current, I_{rms}:

$$I_{rms} = \frac{V_{rms}}{\sqrt{\left(\Omega \frac{N^2}{\Re_{eq}}\right)^2 + \left(R_{winding} + R_{load} + 2R_{lead}\right)^2}} \tag{3.38}$$

The total power dissipated at the potentiometer outside of the cryocooler ($\dot{W}_{load}$) is the sum of the electrical power dissipated by the three phases of the circuit:

$$\dot{W}_{load} = 3 I_{rms}^2 R_{load} \tag{3.39}$$

The power delivered to the load is the difference between the power generated at the turbine and the losses which include the frictional losses and ohmic losses within the stator and leads. The power delivered to the potentiometer and the voltage can be used to estimate the required load resistance. The potentiometer used in the turboexpander must be controllable near this estimated required resistance in order provide adequate control over the turboexpander speed. This will be discussed further in Chapter 6.

The turboalternator model is implemented in Engineering Equation Solver, EES (Klein, 2004). The code is included in Appendix B.

3.2 Experimental Validation

3.2.1 Materials and Equipment

A room temperature test apparatus was constructed with the dimensions summarized in Table 3-1. The magnet, shown in Figure 3-6, is made of cryogenic grade Neodymium

Iron Boron and the stator components, shown in Figures 3-7 and 3-8, are sintered ferrite. The shaft, shown in Figure 3-9, was machined from titanium alloy. The turbine consists of a rudimentary system of 8 straight notches; any complex, optimized design for the room temperature test using compressed air would be ineffective for helium at cryogenic temperatures. The journal bearing cartridge in which the turboalternator components are installed, shown in Figure 3-10, is Macor machineable ceramic. The turbine nozzles are 8 tangential inlet slots machined into a brass end-piece. The nozzle piece mounts against a spacer forming closed nozzle cavities; the spacer would be replaced by the seal for the fully functional turboexpander.

All of the components were installed within a brass facility, shown in Figure 3-11 with stainless steel tubing bringing compressed air to the turbine and journal bearings. The cross-sectional view of the solid model assembly is shown in Figure 3-12. Note that turbine inlet passages, which direct the inlet air to the turbine nozzles, are not visible in the drawing. Exhaust was to ambient conditions; pathways were machined into the journal bearing cartridge such that the bearing exhaust air was allowed to exit past the thrust bearing. Voltage and speed measurements were taken with a Tektronix TDS2014 oscilloscope, which has a vertical (voltage) accuracy of ± 2% and a speed accuracy of ± 0.002%.

Table 3-1: Parameters used for experimental validation of turboalternator model

Parameter	**Symbol**	**Dimension**
Rotor magnet diameter	D_m	0.12 in (3.05 mm)
Rotor magnet length	L_m	0.30 in (7.62 mm)
Ferrite shell thickness	th_{shl}	0.125 in (3.18 mm)
Ferrite shell outer diameter	D_{shl}	1.25 in (3.18 cm)
Stator pole lip thickness	th_{lip}	0.03 in (0.762 mm)
Stator pole lip diameter	D_{lip}	0.26 in (6.5 mm)
Stator pole diameter	D_{pole}	0.125 in (3.18 mm)
Stator pole length	L_{pole}	0.24 in (6.09 mm)
Clearance between rotor and stator	c_{st}	0.114 in (2.89 mm)
Diameter of winding and lead wires	D_{wire}	0.005 in (127 μm)
Number of winds per stator pole pair	N	240
Magnet maximum flux density	B_{max}	1.35 Tesla
Magnet maximum magnetic field strength	H_{max}	1.12 E6 A/m
Ferrite magnetic permeability	μ_f	400 μ_0

Figure 3-6: Neodymium iron boron magnets used inside turbine shaft

Figure 3-7: Stator poles with and without windings

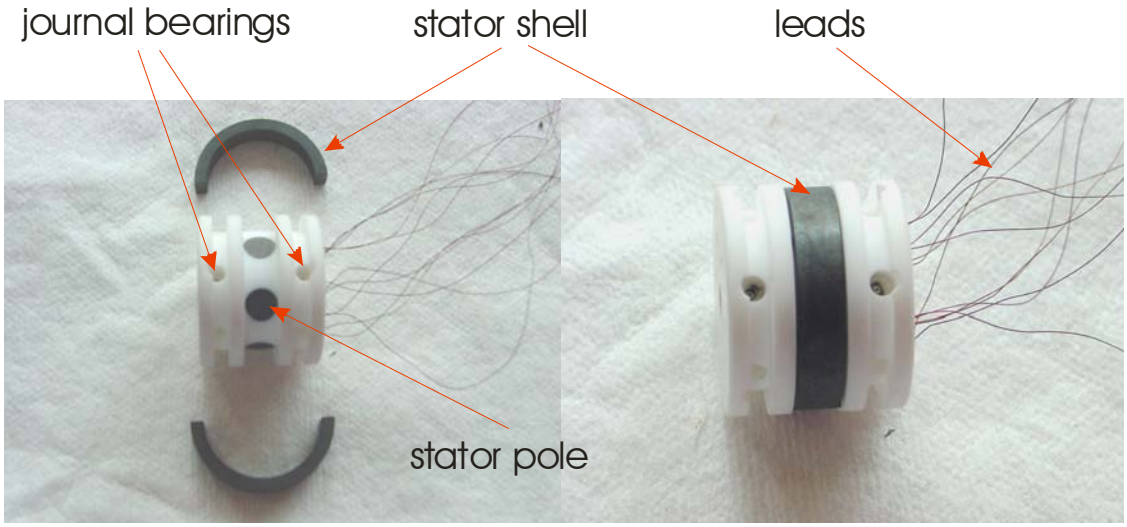

Figure 3-8: The journal bearing cartridge with installed turboalternator components

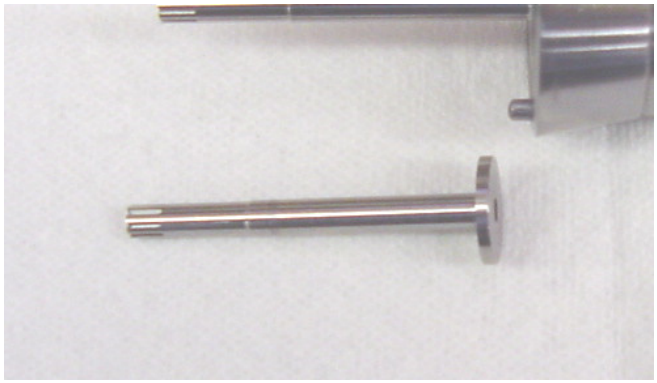

Figure 3-9: Titanium alloy shaft and thrust bearing with straight turbine blades

Figure 3-10: Turbine nozzle plate

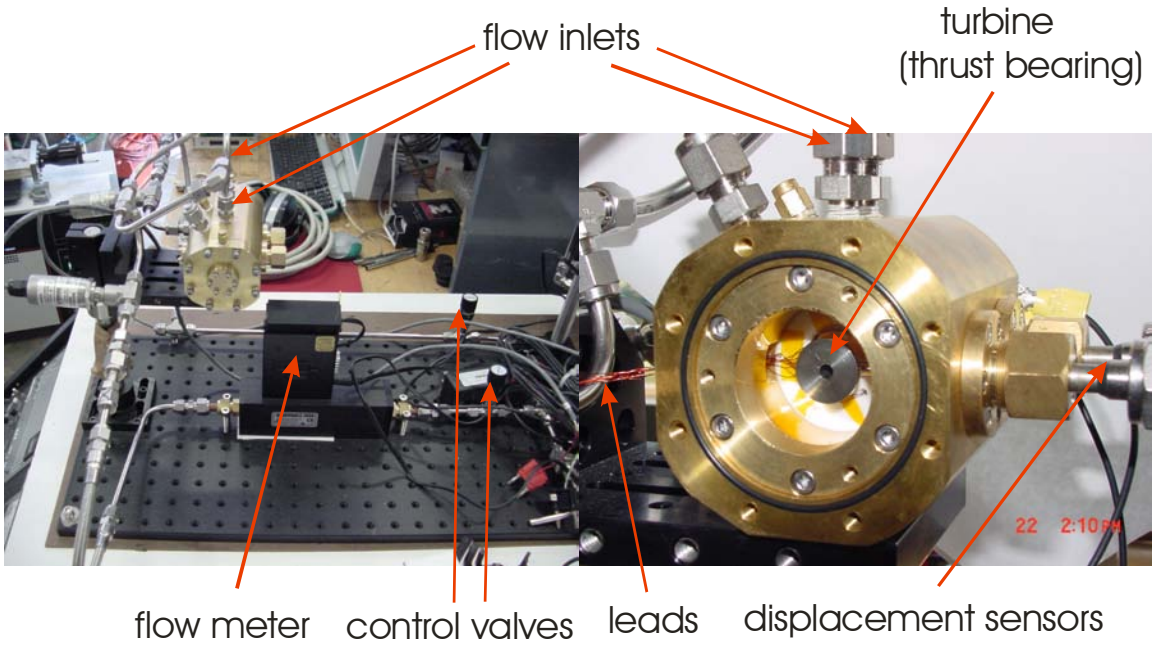

Figure 3-11: Turboalternator and journal bearing test facility

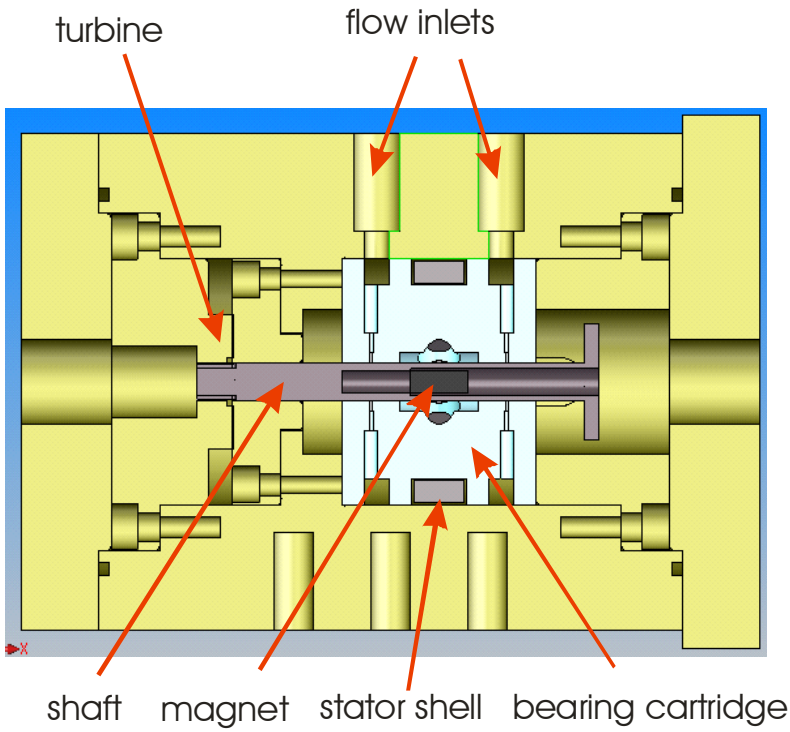

Figure 3-12: Solid model assembly

3.2.2 Procedure

A torque was placed on the shaft by providing compressed air to the nozzles. The open-circuit voltage (i.e., the voltage with no external resistive load) was measured as a function of speed up to 320 Hz. The voltage and speed data were captured by the oscilloscope by observing the sinusoidal voltage signal and period for each of the stator poles pairs (each pole was connected to a separate channel of the oscilloscope). The data were exported to a computer were the rms voltage was calculated from the voltage signal for each speed. Figure 3-13 illustrates the voltage signal measured by the oscilloscope as well as the rms voltage calculated for each pair of stator poles for a shaft speed of 321 Hz.

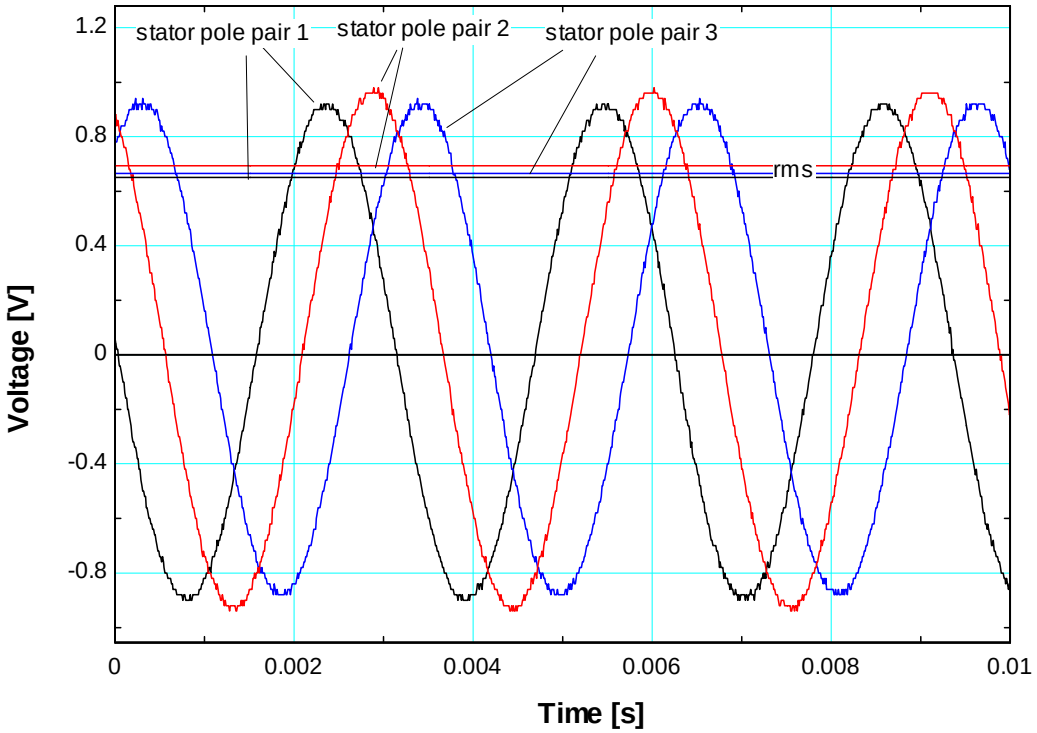

Figure 3-13: Three phase voltage signal measured by oscilloscope and respective calculated rms voltages for a speed of 321 Hz

Figure 3-14 illustrates the voltage obtained by the experimental setup for stator pole 1 (i.e. channel 1 of the oscilloscope) as well as the voltage predicted by the model. The maximum error between the voltage predicted by the model and data is 15%, with the model under-predicting the voltage at all speeds. The error bars for the experimental data illustrate that only a small amount of error is associated with the voltage measurement; the speed error is negligible. The number of winds around the stator poles was estimated by counting the number of windings of the outer (fourth) layer of windings and assuming all layers have an equal number of turns. The model is very sensitive to this number, and this is likely a large source of the disagreement between the model and experimental data. Figure 3-14 also displays the model prediction for ± 3 windings (corresponding to the dotted lines in the modeled result). If the number of turns were 33 instead of the 30 that was initially estimated then the data would agree within 3 % of the values predicted by the model.

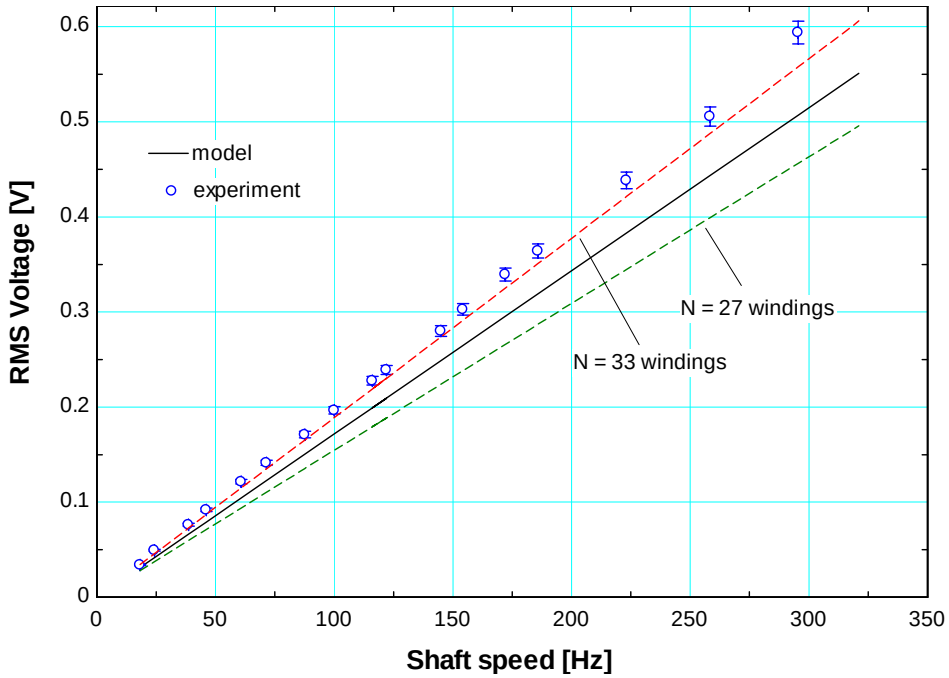

Figure 3-14: The rms voltage as a function of shaft speed produced by the experimental setup and as predicted by the model

4 Seal

The gas leaving the turbine nozzle will be at a different pressure than the gas in the exhaust passages of the bearing cartridge even if some effort is taken to balance these pressures; any pressure difference that exists between these locations will drive a leakage flow through the seal. Because the turbine and bearings are at substantially different temperatures, even a relatively small leakage rate can have a large impact on the turbine performance. This chapter discusses a model of the seal that can evaluate its effect on the cycle thermal performance (i.e., the effect that the seal has on the refrigeration capacity) as well as its effect on the hydrodynamic characteristics (i.e., its ability to restrict the flow rate and therefore the feasibility of controlling the seal leakage).

A well-designed seal will minimize the leakage flow rate from the turbine to the bearings ($\dot{m}_{leak}$) as well as the conductive heat leak into the turbine ($\dot{q}_{cond,turb}$). The seal will consist of a cylinder of length L_{seal} and thickness th_{seal} that encases the shaft; the presence of the seal results in a small annulus through which helium may flow, as shown in Figure 4-1. A number of grooves may be added on the internal surface of the seal in order to introduce inertial pressure losses as well as to reduce the rotordynamic impact of the seal (as was discussed in section 2.2).

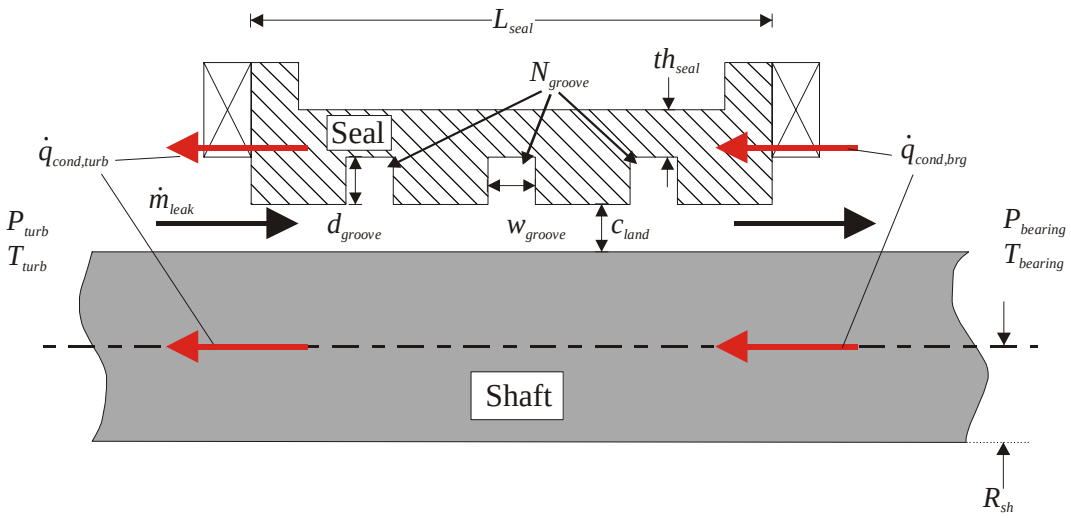

Figure 4-1: Schematic of the seal illustrating heat and mass flows

4.1 Thermal Model

To estimate the overall heat transfer rate that reaches the turbine side of the seal ($\dot{q}_{cond,turb}$ in Fig. 4-1), a one-dimensional numerical model was developed that includes conduction through the shaft and seal, the advective energy related to the leakage mass flow rate, and the heat generated by friction in the seal. The pressure difference across the seal must be balanced manually in any practical design; this is accomplished by throttling the bearing exhaust so that it closely matches the nozzle exit pressure. The sign of the pressure difference across the seal can range from slightly negative (i.e., the nozzle pressure is higher than the bearing cartridge pressure) if the throttle valve is wide open to very positive (i.e., the bearing cartridge pressure is substantially higher than the nozzle pressure) if the throttle valve is closed. It is clear that flow from the bearings to the turbine has a large and very negative effect on cycle performance as it represents a large flow of energy directly to the cold end of the cycle. However, a very small flow from the

turbine to the bearings intercepts some of the conductive heat leak that flows down the shaft and therefore there is a small range of leakage flow that results in a very small impact on the cycle performance. A desirable operating point will therefore provide a very small pressure difference driving a flow from the nozzle to the bearings and the leakage mass flow rate for this analysis is assumed to be in this direction.

4.1.1 Model

The governing equation balances conductive heat flow and frictional heat addition with the enthalpy change of the flow in the seal. Figure 4-2 illustrates the discretization that was used to develop the numerical model; note that each control volume encompasses the entire cross-section of the seal and therefore includes the stationary seal, the annular gap for helium, and the rotating shaft. The fluid-to-solid temperature difference at any axial location (x) is assumed to be negligibly small throughout the seal and therefore the metal and fluid are assumed to have the same temperature (T); this implies a high heat transfer coefficient in the annular gap which is supported by the small seal clearance. The temperature at each node (T_i) refers to both the solid material and helium gas at that node.

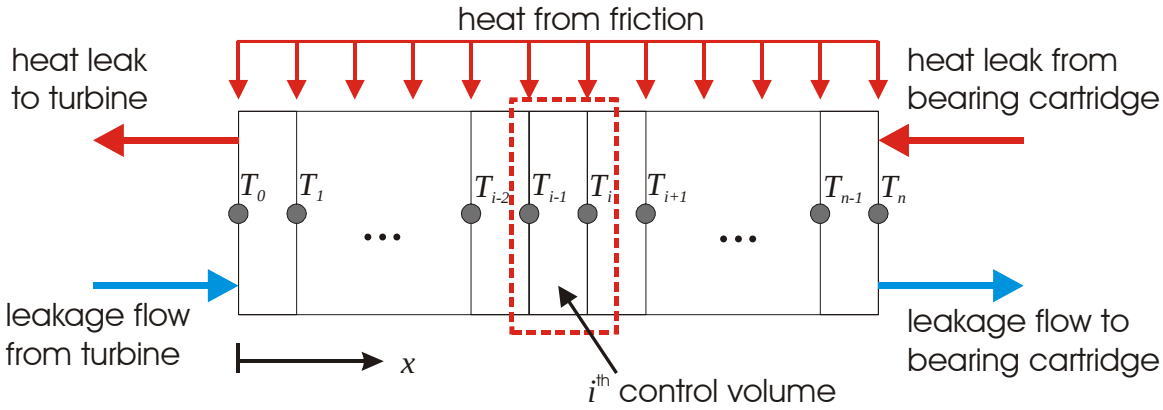

Figure 4-2: Discretization and energy flows of the seal

The energy flows that are incident on the i^{th} control volume, illustrated in Fig. 4-3, include conduction from each of the adjacent control volumes ($\dot{q}_{RHS,i}$ and $\dot{q}_{LHS,i}$), enthalpy flows associated with the leakage entering ($hf_{LHS,i}$) and leaving ($hf_{RHS,i}$) the control volume, and the heat generation due to fluid friction ($\dot{g}$).

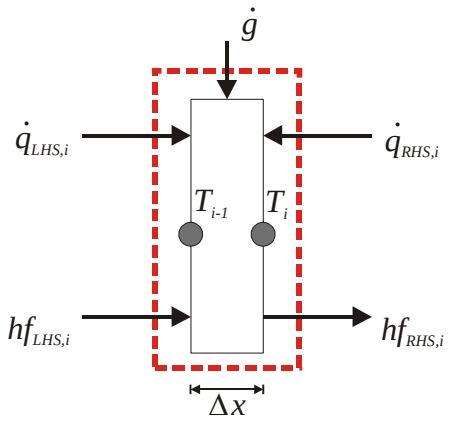

Figure 4-3: Energy flows for i^{th} control volume of the seal

The conductive heat transfer from the adjacent volumes, $\dot{q}_{RHS,i}$ and $\dot{q}_{LHS,i}$, can be written as:

$$\dot{q}_{RHS,i} = \left(k_{sh,i}\, A_{sh} + k_{seal,i}\, A_{seal}\right)\left[\frac{\frac{T_i + T_{i+1}}{2} - \frac{T_i + T_{i-1}}{2}}{\Delta x}\right] \tag{4.1}$$

$$\dot{q}_{LHS,i} = \left(k_{sh,i-1}\, A_{sh} + k_{seal,i-1}\, A_{seal}\right)\left[\frac{\frac{T_{i-2} + T_{i-1}}{2} - \frac{T_i + T_{i-1}}{2}}{\Delta x}\right] \tag{4.2}$$

where A_{sh} and A_{seal} are the effective cross sectional areas for conduction through the shaft and the seal, respectively, $k_{sh,i}$ and $k_{seal,i}$ are the thermal conductivity of the shaft and the seal material, respectively. The thermal conductivities are temperature dependent and are

evaluated at the nodal temperature T_i. The axial length of the control volume (Δx) is defined as:

$$\Delta x = \frac{L_{seal}}{n} \tag{4.3}$$

where L_{seal} is the axial length of the seal and n is the number of control volumes used in the discretization. The effective shaft cross sectional area is the actual cross sectional area of the shaft, as the shaft geometry does not vary axially within the seal. However, the stationary seal may contain grooves. To account for this, the effective seal cross sectional area is estimated according to the length-averaged cross sectional area:

$$\begin{aligned} A_{seal} = {} & \frac{N_{groove}\, w_{groove}}{L_{seal}} \left[\frac{\pi\left(\left(R_{sh} + c_{land} + d_{groove}\right)^2 - \left(R_{sh} + c_{land}\right)^2\right)}{2} \right] \\ & + \left(1 - \frac{N_{groove}\, w_{groove}}{L_{seal}}\right) \left[\frac{\pi\left(\left(R_{sh} + c_{land} + th_{seal}\right)^2 - \left(R_{sh} + c_{land}\right)^2\right)}{2} \right] \end{aligned} \tag{4.4}$$

where R_{sh} is the shaft radius, w_{groove} is the width of the labyrinth grooves, c_{land} is the seal clearance, N_{groove} is the number of labyrinth grooves, and th_{seal} is the thickness of the grooved area of the seal. The enthalpy flows on either side of the control volume can be written as:

$$hf_{LHS,i} = \dot{m}_{leak}\, h_{i-1} \tag{4.5}$$

$$hf_{RHS,i} = \dot{m}_{leak}\, h_i \tag{4.6}$$

where $\dot{m}_{leak}$ is the leakage mass flow rate, determined using a fluid-dynamic model in section 4-2, and h_i is the enthalpy of the helium working fluid evaluated at T_i and P_{turb}. Note that the pressure P_{turb} at which the enthalpies are evaluated is arbitrary as the difference between the turbine and bearing pressures will produce a negligible enthalpy change; the real gas effect associated with helium is not large enough to matter at the operating conditions within the seal.

The generation term, $\dot{g}$, is the friction power that was calculated previously in section 2.3. However, the thermal model temperature distribution allows the generation to vary in the axial direction due to the strongly temperature dependent viscosity of helium. For a plain seal, the generation at each node, $\dot{g}_i$, can be determined by using Eq (2.71) for the length of the seal while evaluating the viscosity μ at the local temperature at T_i.

$$\dot{W}_f = \frac{2\pi\mu\Omega^2 R_{rot}^3 L}{c} \tag{2.71}$$

For a seal that includes labyrinth grooves, $\dot{g}_i$ is estimated by determining the friction power within each land based on an average temperature and distributing that power evenly over the nodes within that land and the adjacent grooves:

$$g_i = \begin{cases} \Delta x \dfrac{\dot{W}_{f,land,j}}{w_{land} + w_{groove}} & \text{for } j = 2..N_{land-1} \\ \Delta x \dfrac{\dot{W}_{f,land,j}}{w_{land}} & \text{for } j = 1,\ j = N_{land} \end{cases} \tag{4.7}$$

where $\dot{W}_{f,land,j}$ is the frictional power generated in land j (for 1..j lands) as determined by evaluating Eq (2.71) for a length of w_{land} and the viscosity at the temperature at the center of the land, $T_{land,j}$. For the lands at either end of the seal (j=0 and j=N_{land}) the power is only distributed within the length of the land.

At steady state, the five energy flows illustrated in Figure 4-3 must balance leading to the governing equation:

$$\dot{q}_{LHS,i} + \dot{q}_{RHS,i} + hf_{LHS,i} + \dot{g}_i = hf_{RHS,i} \quad i = 1..(n-1) \tag{4.8}$$

Substituting equations (4.1), (4.2), (4.5), and (4.6) into (4.8) and simplifying leads to:

$$\left(k_{sh,i-1} A_{sh} + k_{seal,i-1} A_{seal}\right)\left[\frac{T_{i-2} - T_i}{2\Delta x}\right] + \left(k_{sh,i} A_{sh} + k_{seal,i} A_{seal}\right)\left[\frac{T_{i+1} - T_{i-1}}{2\Delta x}\right] + \dot{g}_i = \dot{m}_{leak}\left(h_i - h_{i-1}\right) \quad i = 1..(n-1) \tag{4.9}$$

Using the definition of specific heat capacity allows Eq. (4.9) to be rewritten as:

$$\left(k_{sh,i-1} A_{sh} + k_{seal,i-1} A_{seal}\right)\left[\frac{T_{i-2} - T_i}{2\Delta x}\right] + \left(k_{sh,i} A_{sh} + k_{seal,i} A_{seal}\right)\left[\frac{T_{i+1} - T_{i-1}}{2\Delta x}\right] + \dot{g}_i = \dot{m}_{leak} c_{p,i}\left(T_i - T_{i-1}\right) \quad i = 1..(n-1) \tag{4.10}$$

where $c_{p,i}$ is the specific heat capacity of helium evaluated at T_i. Equation (4.10) can be written for each of the n-1 internal control volumes (i.e., i=1..(n-1)). The hot and cold ends of the seal are assumed to be at fixed temperatures, providing the necessary boundary conditions:

$$T_0 = T_{cold} \tag{4.11}$$

$$T_n = T_{hot} \tag{4.12}$$

where T_{cold} and T_{hot} are the operating temperature of the turbine and the bearing cartridge (taken to be the 1st and 2nd stage load temperatures), respectively. Equations (4.10), (4.11), and (4.12) represent n+1 equations for the unknown n+1 unknown temperatures. The temperature dependent properties make this equation set nonlinear and therefore the problem is implemented using the Engineering Equation Solver software, EES (Klein, 2005).

The key results of the model are the conductive heat transfer rates from the bearing cartridge ($\dot{q}_{cond,brg}$) and to the turbine ($\dot{q}_{cond,turb}$). These quantities are calculated based on:

$$\dot{q}_{cond,turb} = \frac{2\left(k_{seal,0}\, A_{seal} + k_{sh,0}\, A_{sh}\right)}{\Delta x}\left[\frac{T_0 + T_1}{2} - T_0\right] \tag{4.13}$$

$$\dot{q}_{cond,brg} = \frac{2\left(k_{seal,n}\, A_{seal} + k_{sh,n}\, A_{sh}\right)}{\Delta x}\left[T_n - \frac{T_n + T_{n-1}}{2}\right] \tag{4.14}$$

The numerical thermal model is included in Appendix C.

4.1.2 Analytical Verification

An analytical model was developed in order to verify the numerical thermal model described in Section 4.1.1 in the limit of constant helium and material properties and no generation due to friction. Figure 4-4 illustrates the energy flows that are incident on a control volume of differential length (dx) of the shaft, seal, and helium.

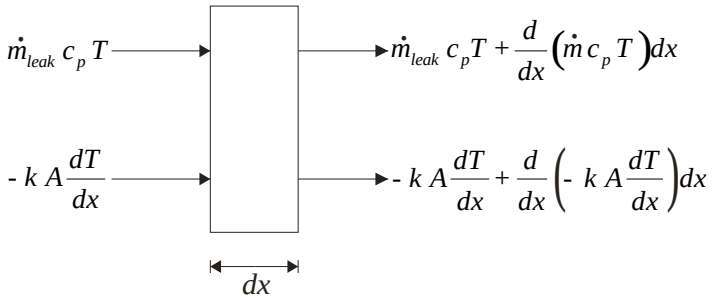

Figure 4-4: Energy flows for differential volume of the seal

The energy balance on the differential volume yields:

$$\dot{m}_{leak}\, c_p\, T - k\, A\frac{dT}{dx} = \dot{m}_{leak}\, c_p\, T + \frac{d}{dx}\left(\dot{m}\, c_p\, T\right)dx - k\, A\frac{dT}{dx} + \frac{d}{dx}\left(-k\, A\frac{dT}{dx}\right)dx \quad (4.15)$$

where k is the conductivity of the shaft and seal (which are assumed to be made of the same material) and A is the total cross-sectional area of the shaft and seal. Eq. (4.15) reduces to:

$$\frac{d}{dx}\left(\dot{m}\, c_p\, T\right)dx = \frac{d}{dx}\left(-k\, A\frac{dT}{dx}\right)dx \quad (4.16)$$

For a constant mass flow rate, specific heat capacity, thermal conductivity, and cross-sectional area, Eq. (4.16) becomes:

$$\dot{m}\, c_p\, \frac{dT}{dx} = -k\, A\frac{d^2T}{dx^2} \quad (4.17)$$

Rearranging leads to:

$$\frac{d^2T}{dx^2} + \frac{\dot{m}\, c_p}{k\, A}\frac{dT}{dx} = 0 \quad (4.18)$$

which can be put in the form:

$$\frac{d^2T}{dx^2} + \lambda \frac{dT}{dx} = 0 \tag{4.19}$$

where

$$\lambda = \frac{\dot{m} c_p}{k A} \tag{4.20}$$

Eq. (4.19) is a second order linear homogeneous equation with the general solution:

$$T = C \exp(a x) \tag{4.21}$$

where:

$$a^2 - \lambda a = 0 \tag{4.22}$$

and C is a constant. The parameter a has two solutions related to the two roots of Eq. (4.22):

$$a_1 = 0 \quad a_2 = \lambda \tag{4.23}$$

which can be used to find the general temperature distribution:

$$T = C_1 + C_2 \exp(\lambda x) \tag{4.24}$$

where C_1 and C_2 are constants. Applying the boundary condition at the cold end leads to:

$$T_{cold} = C_1 + C_2 \exp(0) \tag{4.25}$$

$$C_2 = T_{cold} - C_1 \tag{4.26}$$

Applying the boundary condition at the warm end leads to:

$$T_{hot} = C_1 + C_2 \exp(\lambda L_{seal}) \tag{4.27}$$

Substituting Eq. (4.26) into (4.27) yields:

$$T_{hot} = C_1 + (T_{cold} - C_1)\exp(\lambda L_{seal}) \tag{4.28}$$

$$C_1 = \frac{T_{hot} - T_{cold}}{1 - \exp(\lambda L)} \tag{4.29}$$

Substituting Eqs. (4.26) and (4.29) into equation (4.24) leads to the temperature distribution:

$$T = \frac{T_{hot} - T_{cold}}{1 - \exp(\lambda L)} + \left(T_{cold} - \frac{T_{hot} - T_{cold}}{1 - \exp(\lambda L)} \right) \exp(\lambda L) \tag{4.30}$$

Finally, substituting Eq. (4.20) and simplifying yields:

$$T = T_{cold} + \frac{T_{hot} - T_{cold}}{\exp\left(\frac{\dot{m} c_p}{k A} L \right) - 1} \left[\exp\left(\frac{\dot{m} c_p}{k A} x \right) - 1 \right] \tag{4.31}$$

Eq (4.31) can be rewritten in terms of dimensionless temperature, θ, axial position, $\bar{x}$, and Graetz number (i.e. the capacitance rate divided by the conductive heat transfer), γ:

$$\theta = \frac{T - T_{cold}}{T_{hot} - T_{cold}} \tag{4.32}$$

$$\bar{x} = \frac{x}{L_{seal}} \tag{4.33}$$

$$\gamma = \frac{\dot{m} c_p L}{k A} \tag{4.34}$$

$$\theta = \frac{1 - \exp(\gamma \bar{x})}{1 - \exp(\gamma)} \tag{4.35}$$

The heat transfer to the turbine is defined as:

$$\dot{q}_{turb} = \left.\frac{dT}{dx}\right|_{x=0} \tag{4.36}$$

The dimensionless heat transfer to the turbine, α, can be written as:

$$\alpha = \left.\frac{d\theta}{d\bar{x}}\right|_{\bar{x}=0} \tag{4.37}$$

which simplifies to:

$$\alpha = \frac{\gamma}{\exp(\gamma)-1} \tag{4.38}$$

The most important result (i.e. the result that will be used in the system-level model) is the heat transfer to the turbine and therefore this aspect of the solution will be evaluated for verification purposes. The percent difference between the dimensionless heat transfer predicted by the analytical and numerical model (with constant properties and no generation) is shown as a function of the number of control volumes, *n*, in Figure 4-5. A value of *n* greater than 100 will result in an error of less than 0.5%; therefore subsequent calculations of axial conduction will use 100 control volumes.

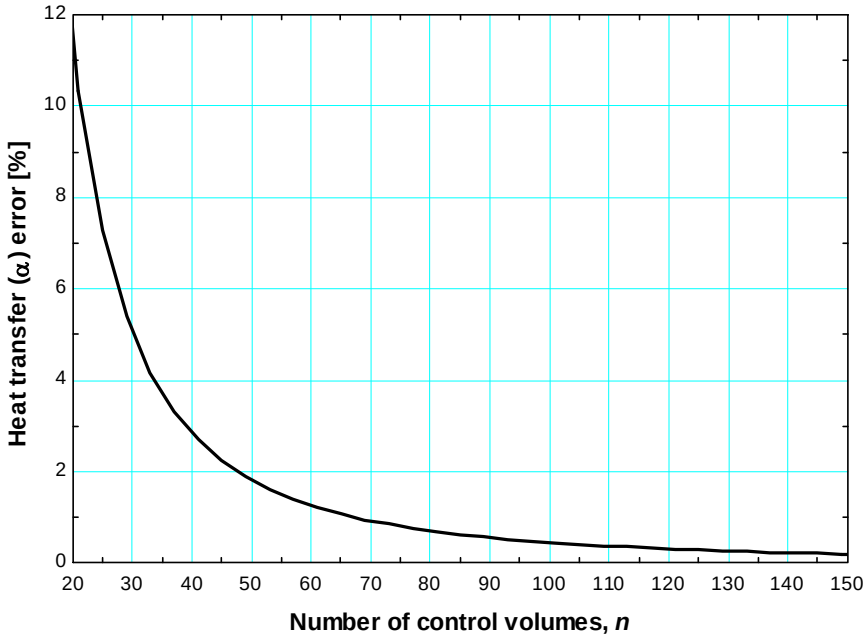

Figure 4-5: The error in dimensionless heat transfer (α) for the numerical model compared to the analytical model as a function of the number of control volumes (n)

Figure 4-6 illustrates the dimensionless temperature distribution predicted by the analytical and numerical models. Figure 4-7 illustrates the dimensionless heat transfer to the turbine side of the seal, α, as a function of the dimensionless mass flow, γ, predicted by both models. Notice in Fig. 4-6 that at $\gamma = 0$ (i.e., with no leakage flow) there is a linear temperature distribution which is consistent with conductive heat transfer. The heat transfer to the turbine is also the maximum at this point, as seen in Fig. 4-7. As γ increases, the conductive heat leak decreases but there is diminishing return. A high mass leakage rate will intercept the entire heat leak; however, it will pose a severe penalty on the load capability of the turbine due to the resulting unbalance in the recuperative heat exchanger. The relationship between the leakage mass flow rate and

the cycle performance will be discussed in section 6.2. The EES code for the thermal verification model is included in Appendix C.

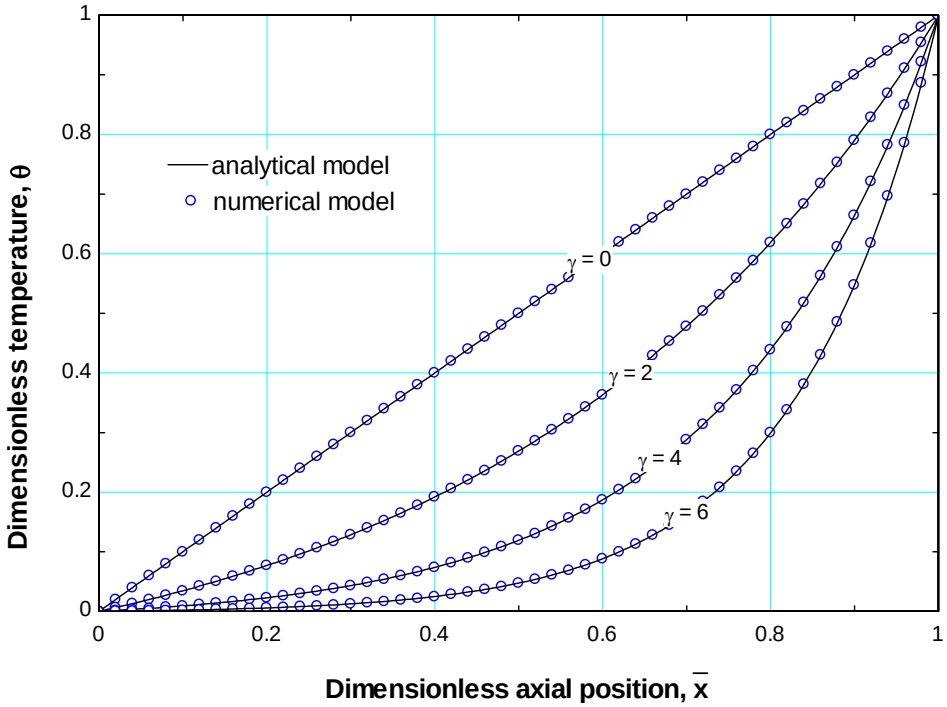

Figure 4-6: Dimensionless temperature distribution (θ) determined by analytical and numerical methods at values of the Graetz number

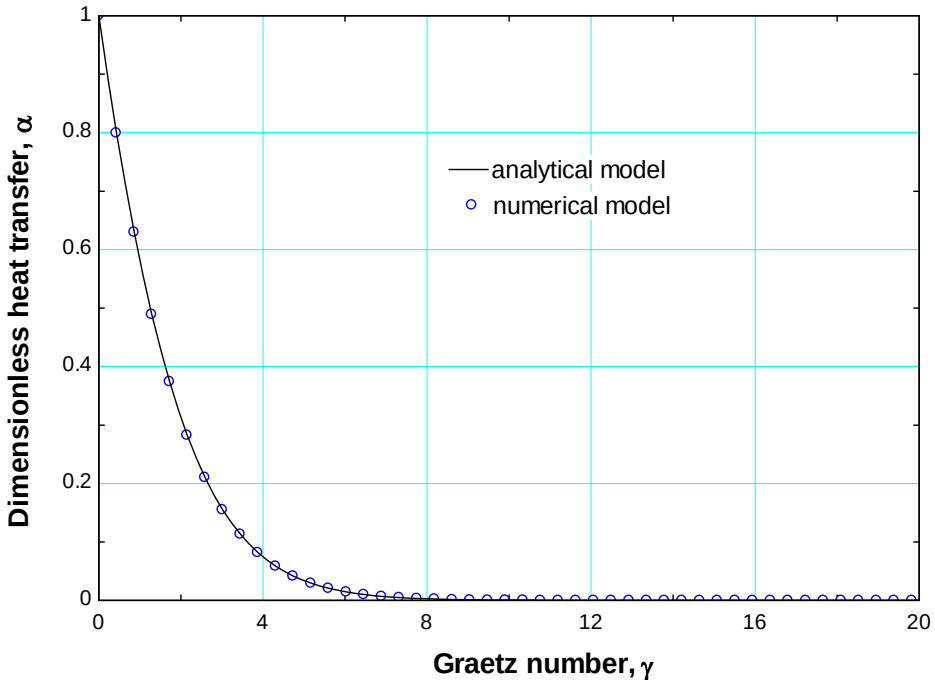

Figure 4-7: Dimensionless heat transfer (α) as it varies with the Graetz number (γ)

4.2 Leakage Flow Model

Section 4.1 discussed the thermal model of the seal; given a leakage mass flow rate through the seal, the thermal model predicted the temperature distribution through the seal. This section discusses a hydrodynamic model of the seal that predicts the leakage flow given the pressure difference and temperature distribution. Clearly then the two models are coupled (the leakage flow affects the temperature distribution and vice versa) and therefore the seal model is iterative.

It is likely that the seal will consist of a series of close clearance lands that are separated by grooves, as shown in Fig. 4-1. The grooves serve several purposes: they provide an inertial pressure drop due to expansion and contraction of the fluid, they serve to limit the

hydrodynamic forces that are generated by the close clearance lands, and they result in a developing region of flow at the inlet to each land that causes an increase in the viscous shear and therefore flow resistance associated with that land. Of these, the reduction of the rotordynamic forces is the most important.

The seal consists of N_{groove} grooves that are installed in the seal which has a total length of L_{seal} (see Fig. 4-1). The width of each groove is w_{groove} and the depth is d_{groove}. The radial clearance between the shaft and the lands is c_{land}. The radius of the shaft is R_{sh}. Assuming that the grooves are equally spaced through the seal, the width of each close-clearance land (w_{land}) is:

$$w_{land} = \frac{L_{seal} - N_{groove}\, w_{groove}}{N_{groove} + 1} \tag{4.39}$$

The axial location of the center of each groove ($x_{groove,i}$) is given by:

$$x_{groove,i} = \frac{i}{N_{groove} + 1} L_{seal} \quad \text{for } i = 1...N_{groove} \tag{4.40}$$

where the position is measured from the cold (turbine) end of the seal. The axial location of the center of the 1st land ($x_{land,1}$, the one closest to the cold end) is:

$$x_{land,1} = \frac{w_{land}}{2} \tag{4.41}$$

The axial locations of the center of the remaining lands ($x_{land,i}$) are given by:

$$x_{land,i} = x_{land,i-1} + w_{land} + w_{groove} \quad \text{for } i = 2...\left(N_{groove} + 1\right) \tag{4.42}$$

The average temperature within each of the grooves ($T_{groove,i}$) is given by:

$$T_{groove,i} = T\left(\frac{x_{groove,i}}{L_{seal}}\right) \quad \text{for } i = 1...N_{groove} \tag{4.43}$$

where T is the temperature as a function of axial position as calculated by the thermal model. Similarly, the average temperature within each land ($T_{land,i}$) is the temperature at the axial position as given by the thermal model:

$$T_{land,i} = T\left(\frac{x_{land,i}}{L_{seal}}\right) \quad \text{for } i = 1...\left(N_{groove}+1\right) \tag{4.44}$$

The cross-sectional area for flow in the lands ($A_{c,land}$) is given by:

$$A_{c,land} = 2\pi R_{sh} c_{land} \tag{4.45}$$

The hydraulic diameter of the flow passage ($D_{h,land}$) is given by:

$$D_{h,land} = 2c_{land} \tag{4.46}$$

The average viscosity and density within each land and groove ($\mu_{land,i}$, $\rho_{land,i}$, $\mu_{groove,i}$, and $\rho_{groove,i}$) are computed according to the turbine pressure (P_{turb}) and the respective groove and land average temperatures. The property correlations for helium are included internally in the Engineering Equation Solver (EES) software. The average velocity within each land ($v_{land,i}$) is given by:

$$v_{land,i} = \frac{\dot{m}_{leak}}{\rho_{land,i} A_{c,land}} \quad \text{for } i = 1...\left(N_{groove}+1\right) \tag{4.47}$$

where $\dot{m}_{leak}$ is the leakage mass flow rate through the seal. The Reynolds number characterizing the flow within the lands ($Re_{land,i}$) is given by:

$$Re_{land,i} = \frac{v_{land,i}\, D_{h,land}\, \rho_{land,i}}{\mu_{land,i}} \quad \text{for } i = 1...\left(N_{groove}+1\right) \tag{4.48}$$

The dimensionless length of each land with respect to hydrodynamic flow development ($w^{+}_{land,i}$) is given by:

$$w^{+}_{land,i} = \frac{w_{land}}{D_{h,land}\, Re_{land,i}} \quad \text{for } i = 1...\left(N_{groove}+1\right) \tag{4.49}$$

The apparent friction factor for a hydrodynamically developing, laminar flow in a slot ($f_{land,i}$) is given by Guyer and Brownell (1989):

$$f_{land,i} = \frac{3.44}{Re_{land,i}\sqrt{w^{+}_{land,i}}} + \frac{24 + \dfrac{0.674}{4\, w^{+}_{land,i}} - \dfrac{3.44}{\sqrt{w^{+}_{land,i}}}}{Re_{land,i}\left(1 + \dfrac{0.00029}{\left(w^{+}_{land,i}\right)^{2}}\right)} \quad \text{for } i = 1...\left(N_{groove}+1\right) \tag{4.50}$$

The pressure drop across each land ($\Delta P_{land,i}$) is therefore:

$$\Delta P_{land,i} = \frac{\rho_{land,i}\, v^{2}_{land,i}}{2}\, f_{land,i}\, \frac{w_{land,i}}{D_{h,land}} \quad \text{for } i = 1...\left(N_{groove}+1\right) \tag{4.51}$$

There is an inertial pressure drop associated with the fluid entering the seal at the cold end (ΔP_{inlet}) that can be written as:

$$\Delta P_{inlet} = K_{c,inlet}\, \frac{\rho_{inlet}\, v^{2}_{inlet}}{2} \tag{4.52}$$

where ρ_{inlet} is the density of the gas entering the seal at the turbine temperature and nominal pressure, v_{inlet} is the velocity of the gas in the initial close clearance region, and

$K_{c,inlet}$ is the contraction coefficient for the inlet. The velocity of the gas entering the seal is:

$$v_{inlet} = \frac{\dot{m}_{leak}}{A_{c,land}\,\rho_{inlet}} \tag{4.53}$$

The contraction coefficient for the inlet will be approximated assuming that the gas is entering from a very large plenum so that $K_{c,inlet} = 0.42$ (White, 1999).

Within each groove there is an expansion and contraction pressure loss, the sum of which ($\Delta P_{groove,i}$) can be written as:

$$\Delta P_{groove,i} = \left(K_{c,groove} + K_{e,groove}\right)\frac{\rho_{groove,i}\,v_{groove,i}^2}{2} \quad \text{for } i = 1...N_{groove} \tag{4.54}$$

where $v_{groove,i}$ is the velocity of the fluid in the close clearance regions immediately adjacent to the groove and $K_{c,groove}$ and $K_{e,groove}$ are the contraction and expansion coefficients, respectively, for the groove. The velocity is estimated according to:

$$v_{groove,i} = \frac{\dot{m}_{leak}}{A_{c,land}\,\rho_{groove,i}} \quad \text{for } i = 1...N_{groove} \tag{4.55}$$

The contraction and expansion coefficients are assumed to depend only on geometry and therefore are the same for all of the grooves in the seal. The contraction coefficient is estimated according to White (1999):

$$K_{c,groove} = \begin{cases} 0.42\left(1-\dfrac{D_{h,land}^2}{D_{h,groove}^2}\right) & \text{for } \dfrac{D_{h,land}}{D_{h,groove}} \le 0.76 \\ \left(1-\dfrac{D_{h,land}^2}{D_{h,groove}^2}\right)^2 & \text{for } \dfrac{D_{h,land}}{D_{h,groove}} > 0.76 \end{cases} \tag{4.56}$$

where $D_{h,groove}$ is the hydraulic diameter associated with the flow of gas in the groove:

$$D_{h,groove} = \frac{2\left(\left(R_{sh}+c_{land}+d_{groove}\right)^2-\left(R_{sh}\right)^2\right)}{\left(R_{sh}+c_{land}+d_{groove}\right)+\left(R_{sh}\right)} \tag{4.57}$$

The expansion coefficient is estimated according to White (1999):

$$K_{e,groove} = \left(1-\frac{D_{h,land}^2}{D_{h,groove}^2}\right)^2 \tag{4.58}$$

The pressure drop associated with the expansion of the fluid into the bearing cartridge (ΔP_{exit}) is given by:

$$\Delta P_{exit} = K_{e,exit}\,\frac{\rho_{exit}\,v_{exit}^2}{2} \tag{4.59}$$

where ρ_{exit} is the density of the gas exiting the seal at the bearing temperature and pressure, v_{exit} is the velocity of the gas in the initial close clearance region, and $K_{e,exit}$ is the expansion coefficient for the exit. The velocity of the gas exiting the seal is:

$$v_{exit} = \frac{\dot{m}_{leak}}{A_{c,land}\,\rho_{exit}} \tag{4.60}$$

The expansion coefficient for the exit will be approximated assuming that the gas is exiting into a very large plenum so that $K_{e,exit}$ = 1.0 (White, 1999).

The total pressure drop through the seal (ΔP_{seal}) is the sum of the pressure drops calculated above:

$$\Delta P_{seal} = \Delta P_{inlet} + \sum_{i=1}^{N_{groove}+1} \Delta P_{land,i} + \sum_{i=1}^{N_{groove}} \Delta P_{groove,i} + \Delta P_{exit} \tag{4.61}$$

The leakage flow model is implemented in EES, the code is included in Appendix D. The number of grooves chosen for the seal depends on both adequate suppression of the leakage flow rate as well as the additional destabilizing stiffness that a seal with fewer grooves will provide (discussed in section 2.2). This trade-off is discussed further in Chapter 6.

4.3 Seal Thickness

Section 4.1 describes how the heat leak is highly dependent on the shaft and seal cross sectional area. Therefore, minimizing the seal thickness will minimize the conductive cross sectional area for a given shaft radius. Clearly the optimal design that minimizes the heat leak will be the thinnest possible seal. However, the high absolute pressure within the seal can cause a large tensile stress which may yield the seal. Even if the seal material remains in the elastic region, the effect of the pressure might be a substantial increase in the seal clearance which will lead to an increased leakage mass flow rate and possibly a higher performance penalty on the turboexpander. The practical lower limit of the seal thickness is governed by the ability to machine the titanium alloy; the nominal minimum machinable thickness is 0.025 inch (0.635 mm).

The pressure within a cylinder will impose a tangential tensile stress, known as the hoop stress (σ_{hoop}), as illustrated in Figure 4-8. The magnitude of the stress can be estimated based on the force produced by the seal absolute pressure, P_{seal}, acting on the area A_2 in Figure 4-8:

$$\sigma_{hoop} = \frac{P_{seal}\, A_2}{A_1} \tag{4.62}$$

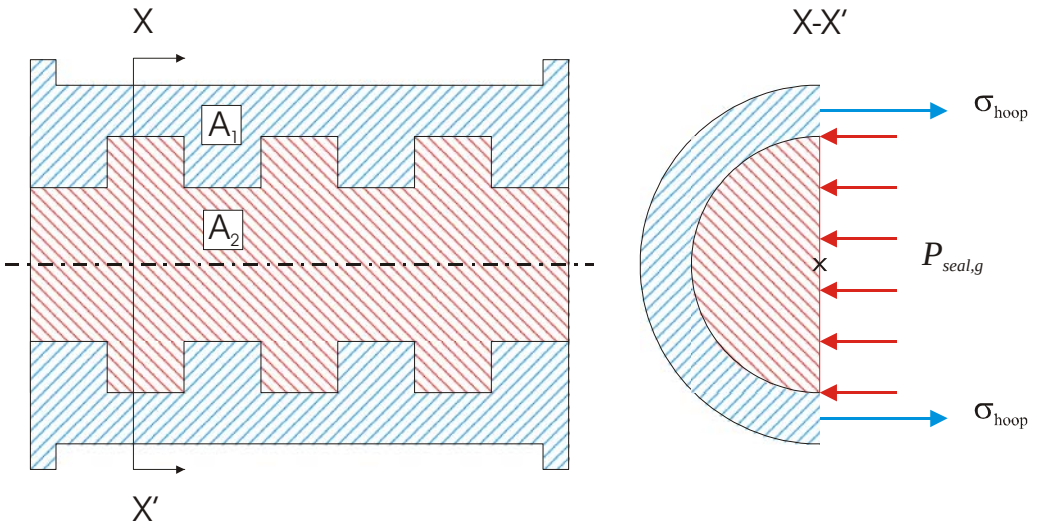

Figure 4-8: Schematic of seal cross sections and internal forces

The areas A_1 and A_2 are given by:

$$A_1 = L_{seal}\, th_{seal} + N_{land}\, w_{land}\, d_{groove} \tag{4.63}$$

$$A_2 = L_{seal}\left(R_{sh} + c_{land}\right) + N_{groove}\, w_{groove}\, d_{groove} \tag{4.64}$$

The strain (ε) within the elastic region of a material is defined by Hooke's Law:

$$\varepsilon = \frac{\sigma_{hoop}}{E} \tag{4.65}$$

where E is the modulus of elasticity of the seal material. Due to the isotropic material properties the strain in the tangential direction will be equal to the strain in the radial direction. Therefore, the change in the seal clearance, Δc_{land}, is given by:

$$\Delta c_{land} = \varepsilon \, c_{land} \tag{4.66}$$

Combining Eqs (4.62) through (4.66) yields:

$$\Delta c_{land} = \frac{P_{seal,g} \, R \left[L_{seal} \left(R_{sh} + c_{land} \right) + N_{groove} \, w_{groove} \, d_{groove} \right]}{E \left[L_{seal} \, th_{seal} + N_{land} \, w_{land} \, d_{groove} \right]} \tag{4.67}$$

The increase in seal clearance, and thus the heat transfer due to helium leakage, is inversely proportional to the seal thickness. The conductive heat transfer to the turbine, however, is linearly proportional to the seal thickness. These competing effects are examined in section 6-2 in order to determine the seal thickness for optimal cycle efficiency.

5 Integrated Model

The preceding chapters have described several independent component models that make up the turboexpander. To determine the cycle performance of the turboexpander these models must interact dynamically. Additionally, several supplementary models are required in order to obtain a complete model of the recuperative stage. This chapter describes these supplementary models as well as the process of integrating the sub-models to form the complete turboexpander model.

5.1 Supplementary Models

Several models are necessary to arrive at a complete model of the recuperative stage; these include the turbine aerodynamic performance, the recuperative heat exchanger, and the journal bearings.

5.1.1 Turbine Aerodynamic Performance

The turbine operates by extracting energy from the entering, high pressure helium stream as its pressure is reduced. In an ideal cycle, the mechanical power imparted to the turbine would be equal to the reduction in the enthalpy of the gas consistent with an isentropic expansion. However, the actual turbine will not perform optimally and its performance is indicated by the aerodynamic efficiency.

The aerodynamic efficiency of a well-designed turbine will be a strong function of the ratio of the isentropic nozzle velocity, v_{isen}, and the blade tip velocity, v_{tip}, shown in Figure 5-1:

$$v_{isen} = \sqrt{2\,\Delta h_s} \tag{5.1}$$

$$v_{tip} = \Omega\, R_{sh} \tag{5.2}$$

$$\lambda = \frac{v_{tip}}{v_{isen}} \tag{5.3}$$

where Δh_s is the isentropic enthalpy drop through the turbine, Ω is the shaft rotational velocity, and R_{sh} is the shaft radius. The maximum efficiency typically occurs when the velocity ratio, λ, is approximately 0.7.

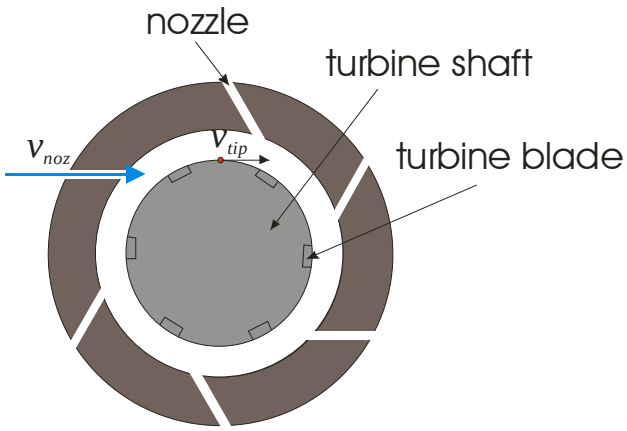

Figure 5-1: Schematic of turbine velocities

The aerodynamic efficiency, η_s, is used to calculate the exit enthalpy of the turbine:

$$\eta_s = \frac{h_{turb,in} - h_{turb,out}}{h_{turb,in} - h_{turb,out,s}} \tag{5.4}$$

where $h_{turb,in}$, $h_{turb,out}$, and $h_{turb,out,s}$ are the inlet, actual exit, and isentropic exit enthalpies, respectively. The turbine power is subsequently calculated from the actual enthalpy drop and the turbine mass flow rate, $\dot{m}_{turb,in}$:

$$\dot{W}_{turb} = \dot{m}_{turb,in}\left(h_{turb,in} - h_{turb,out}\right) \tag{5.5}$$

Figure 5-2 illustrates the relation between the aerodynamic efficiency and the velocity ratio as presented by Baines (2005). The computer model implements the variation shown in Figure 5-2 using a lookup table and interpolation. Note that the actual efficiency of the turbine will depend on achieving the correct turbine blade design, and therefore the final design may not achieve the same maximum efficiency; however, the shape of the curve will be similar.

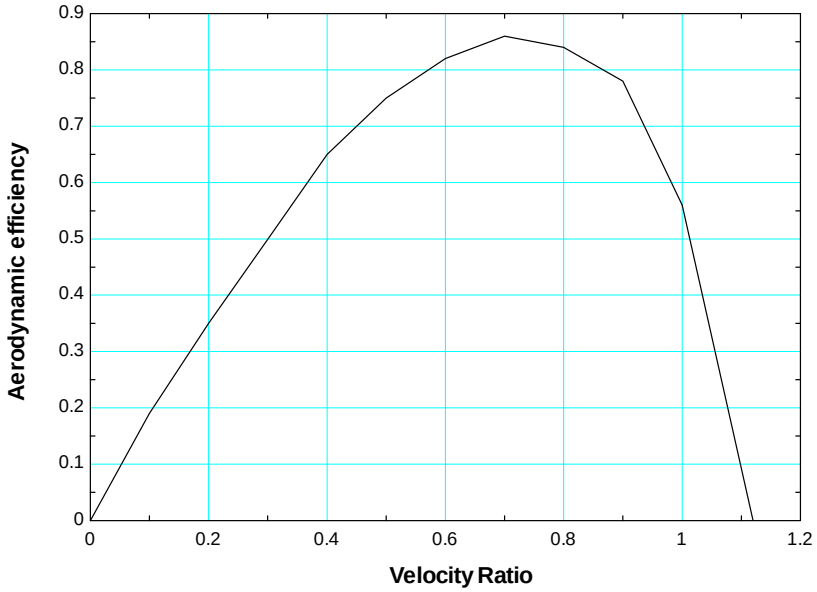

Figure 5-2: Aerodynamic efficiency as a function of the velocity ratio, λ

5.1.2 Recuperative Heat Exchanger

The performance of the lower stage of the hybrid cryocooler depends on the recuperator exit temperature (state 2 in Figure 5-3) while the recuperator performance depends simultaneously on the turbine exit temperature and refrigeration load (if any); therefore, the recuperator performance depends on the predicted performance of the turboexpander performance through state 3. In order to accurately determine the turboexpander performance, a recuperator model with the ability to iterate must be used.

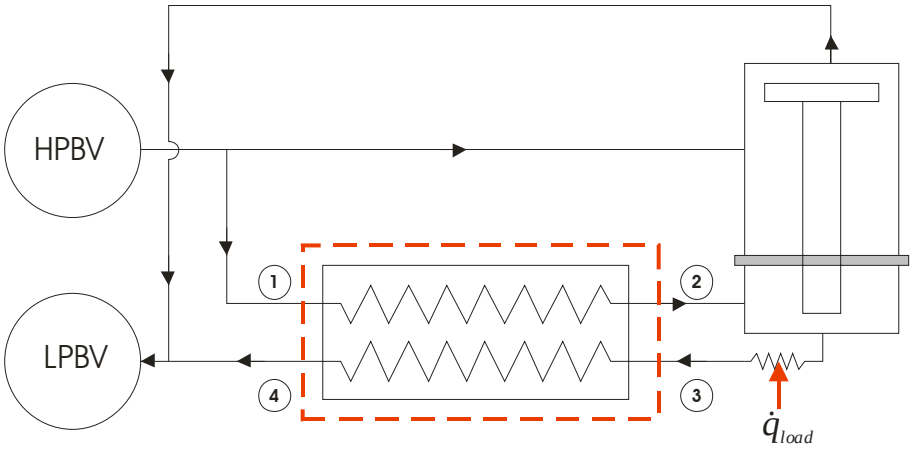

Figure 5-3: Schematic of reverse Brayton cycle emphasizing the recuperator conditions

Heat exchanger performance is commonly modeled using the effectiveness-NTU method which assumes constant fluid properties throughout the heat exchanger, in particular the specific heat capacity and its variation has a strong effect on performance. However, near the target turbine operating temperature of 10 K, the specific heat of helium depends strongly on temperature and pressure, as illustrated in Figure 5-4. To account for this change, the heat exchanger must be considered more carefully.

The heat exchanger is discretized by dividing it into several (N) parts, each of which can be assumed to have a constant fluid heat capacity as illustrated in Figure 5-5.

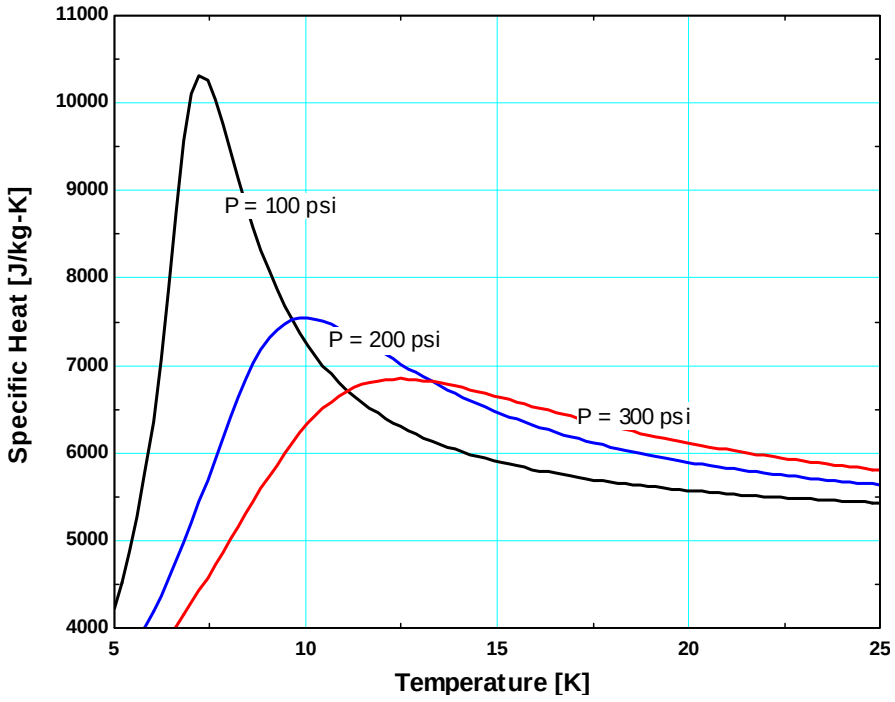

Figure 5-4: The specific heat of helium as it varies with temperature for various pressures

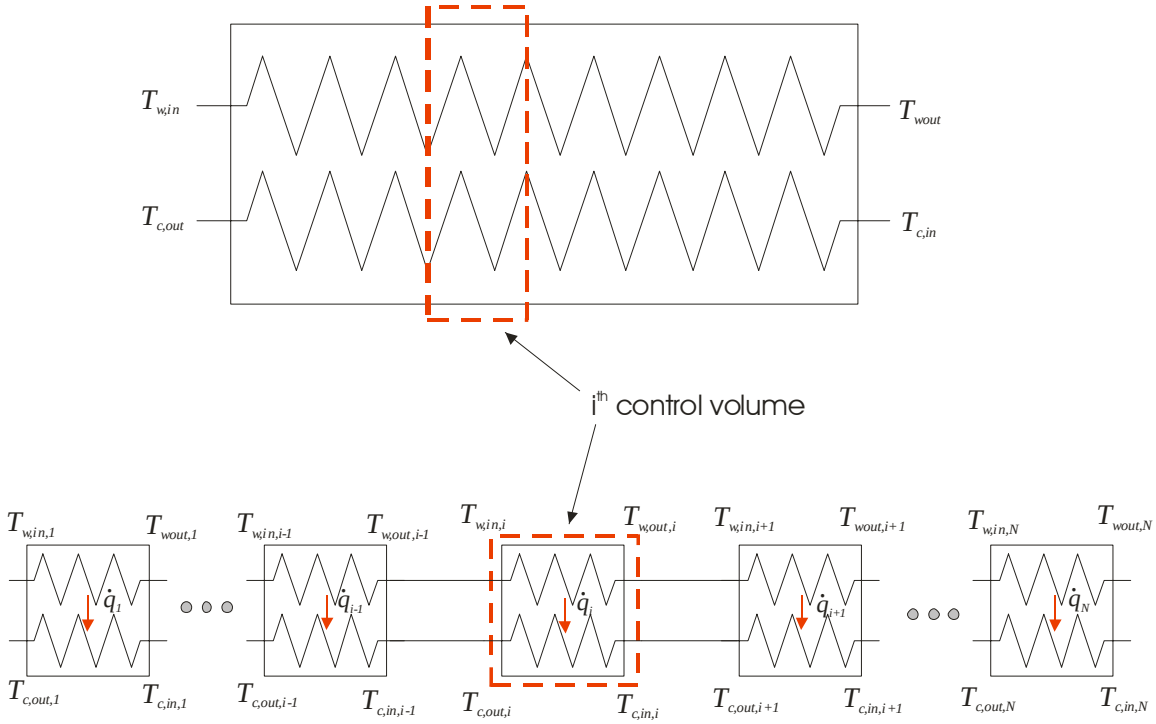

Figure 5-5: Complete and discretized heat exchanger

The overall recuperator area-heat transfer product (UA_{total}) has been calculated using a more detailed, geometry-specific model (which is not part of this work but has been developed as part of a companion project); the detailed model does not consider the variation in the fluid properties within the recuperator. The total conductance (UA_{total}) is a function of the cold and warm stream inlet temperatures, $T_{c,in}$ and $T_{w,in}$, respectively; and the cold and warm stream pressures, P_c and P_w, respectively:

$$UA_{total} = f\left(T_{c,in}, T_{w,in}, P_{c,in}, P_{w,in}\right) \tag{5.6}$$

The conductance of each control volume (UA_i) for the recuperator is therefore constrained so that:

$$UA_{total} = \sum_{1}^{N} UA_i \tag{5.7}$$

The heat transfer within each control volume ($\dot{q}_i$) is the same and defined as:

$$\dot{q}_i = \frac{\dot{q}_{total}}{N} \tag{5.8}$$

where $\dot{q}_{total}$ is the total stream-to-stream heat transfer in the recuperator. Note that the control volumes are not equal size but rather represent an equal amount of heat transfer; progressing through the control volumes represents a steady increase in the total heat transferred between the streams. If the specific heat capacity within each control volume can be considered constant then the effectiveness-NTU relations can be applied. The effectiveness (ε_i) and number of transfer units (NTU_i) of each control volume are:

$$\varepsilon_i = \frac{\dot{q}_i}{\dot{q}_{\max,i}} \tag{5.9}$$

$$NTU_i = \frac{UA_i}{C_{min,i}} \tag{5.10}$$

where $\dot{C}_{min,i}$ is:

$$\dot{C}_{min,i} = \begin{cases} \dot{C}_{w,i} & \text{for } \left(\dot{C}_{w,i} < \dot{C}_{c,i}\right) \\ \dot{C}_{c,i} & \text{for } \left(\dot{C}_{c,i} < \dot{C}_{w,i}\right) \end{cases} \tag{5.11}$$

and $\dot{C}$ is the capacitance rate defined by:

$$\dot{C} = \dot{m}\, c_p \tag{5.12}$$

evaluated at either the cold stream, $\dot{C}_c$, or warm stream, $\dot{C}_w$. The maximum heat transfer within each control volume, $\dot{q}_{\max,i}$, is given by:

$$\dot{q}_{\max,i} = \dot{C}_{\min,i}\left(T_{w,in,i} - T_{c,in,i}\right) \tag{5.13}$$

For a counterflow heat exchanger, the effectiveness and NTU are related by Incropera Dewitt (2002):

$$NTU_i = \begin{cases} \dfrac{1}{C_{r,i}-1}\ln\left(\dfrac{\varepsilon_i - 1}{\varepsilon_i C_{r,i} - 1}\right) & \text{for}\,(C_{r,i} < 1) \\ \dfrac{\varepsilon_i}{1-\varepsilon_i} & \text{for}(C_{r,i} = 1) \end{cases} \tag{5.14}$$

Equations (5.6) through (5.14) allow for the calculation of the exit cold stream temperature given the inlet stream temperatures and pressures.

Due to the large peak in specific heat shown in Figure 5-4 and the strong dependence of the recuperator performance on the specific heat, it is important to choose an adequate number of control volumes. Figure 5-6 illustrates the recuperator effectiveness as a

function of the number of control volumes. Note that for a low number of control volumes the effectiveness is above 1, a non-physical value. The effectiveness does asymptote eventually to its physical solution. A value of 250 control volumes is used in subsequent calculations involving the recuperator due to the relatively low variation in the effectiveness as well as the large calculation time associated with larger values.

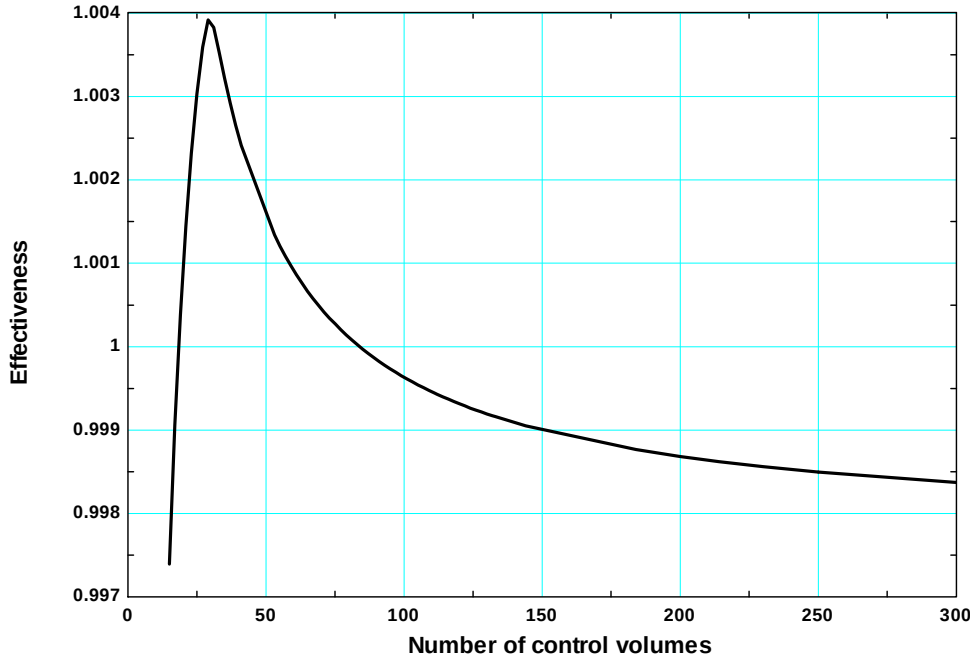

Figure 5-6: The recuperator effectiveness as a function of the number of control volumes used in the model

The axial conduction within the recuperator is determined using a conductive resistance that is determined by the previously mentioned, detailed geometry-based model. The conduction penalty, $\dot{q}_{ac}$, is added to the enthalpy flows of the exit streams:

$$h_{w,out,ac} = h_{w,out} + \frac{\dot{q}_{ac}}{\dot{m}_{turb,in}} \tag{5.15}$$

$$h_{c,out,ac} = h_{c,out} - \frac{\dot{q}_{ac}}{\dot{m}_{turb,out}} \tag{5.16}$$

where $h_{w,out,ac}$ and $h_{c,out,ac}$ are the exit enthalpies of the warm and cold stream, respectively, including axial conduction. The corresponding temperatures are calculated using these enthalpies and the associated pressures. The pressure loss within the recuperative heat exchanger is predicted to be negligibly small and is therefore neglected in this model.

5.1.3 Journal Bearings

The hydrostatic journal bearings operate by passing a high pressure gas through several pockets located radially around the shaft housing, as shown in Figure 5-7. A centered shaft will result in zero net force acting upon the shaft. If the shaft is offset a distance, *e*, there will be a resultant force, *F*, in the opposite direction of the perturbation; the stiffness (k_{jb}) is defined from this offset and resultant force:

$$k_{jb} = \frac{dF}{de} \tag{5.17}$$

The bearing stiffness and mass flow consumption are calculated using an existing model (Evans, 2003) which determines the stiffness and mass flow ($\dot{m}_{jb}$) from the pressure drop ($\Delta P_{bearing}$), inlet temperature ($T_{bearing}$), and shaft radius. The geometry of the bearings themselves was not modified from the initial model. Note that the values are representative of each bearing rather than the combination of the two journal bearings.

$$k_{jb} = f\left(T_{bearing}, \Delta P_{bearing}, R_{sh}\right) \tag{5.18}$$

$$\dot{m}_{jb} = f\left(T_{bearing}, \Delta P_{bearing}, R_{sh}\right) \tag{5.19}$$

The pressure drop through the bearings is defined as the difference between the inlet pressure, $P_{bearing,in}$, and the exit pressure, $P_{bearing,out}$. The exit pressure will be approximately the pressure of the low pressure buffer volume; however, the inlet pressure may be throttled in order to adjust the mass flow consumption and stiffness of the journal bearings. The inlet pressure is given in terms of a throttle constant, x_{jb}:

$$P_{bearing,in} = P_H - x_{jb}\left(P_H - P_L\right) \tag{5.20}$$

For a throttle constant of 1 (i.e. fully restricted) there is no pressure drop and therefore no mass flow; for a throttle constant of 0 (i.e. unthrottled) the full pressure drop is realized.

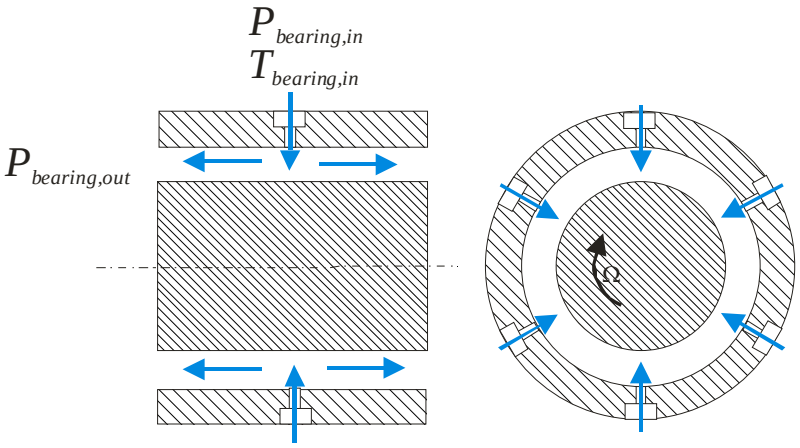

Figure 5-7: Schematic of hydrostatic journal bearings with incident helium flow

5.2 Model Integration

The models have been developed and discussed independently. However, in order to determine the performance of the recuperative stage, the models must be integrated; that is, the input to each model represents either a design input or a predicted output from another model. Figure 5-8 illustrates the high extent of interdependency between the models. The complete cycle model is able solve automatically given only the component

geometries and the pulse tube stage performance. Additionally, any model may be turned off allowing for the direct input of the data. For example, the seal leakage model may be turned off and the leakage flow input directly.

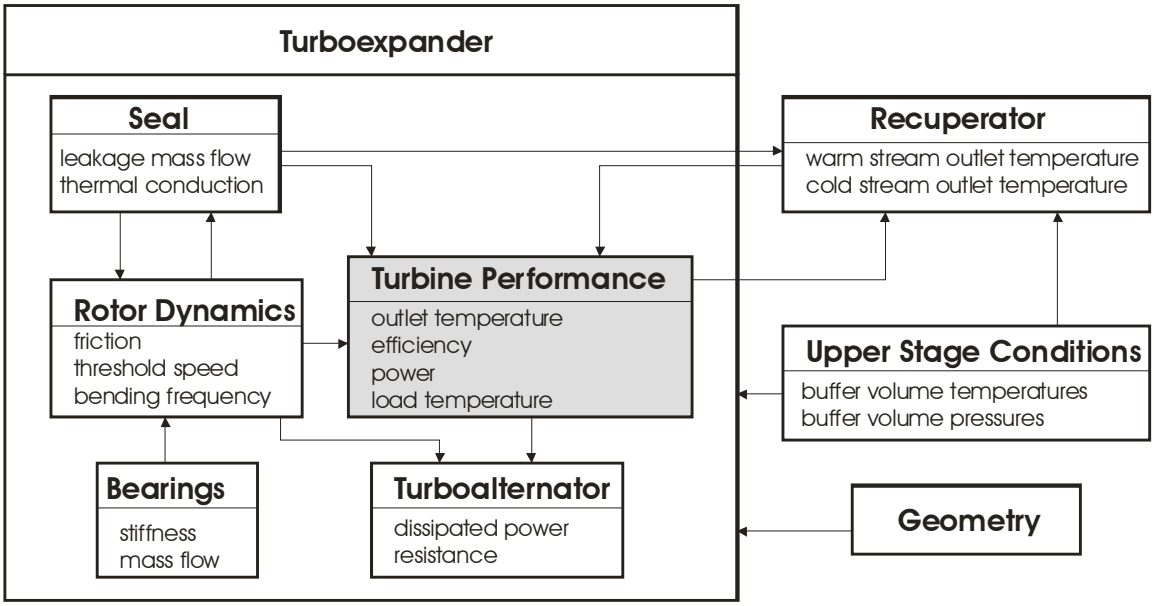

Figure 5-8: Flow diagram of the cycle model interdependencies with important output variables for each sub-model listed

5.2.1 Turbine Mass and Heat Leak

The conductive heat leak that is not intercepted by the seal leakage flow must be added to the turbine mass flow, as illustrated in Figure 5-9. It is assumed that the full heat leak is absorbed by the incoming turbine mass flow, $\dot{m}_{turb,in}$, before it splits into the exit mass flow stream, $\dot{m}_{turb,out}$, and the leakage mass flow stream, $\dot{m}_{leak}$:

$$\dot{m}_{turb,in}\, h_{turb,in} + \dot{q}_{cond} = \dot{m}_{turb,out}\, h_{turb,out} + \dot{m}_{leak}\, h_{turb,out} \tag{5.21}$$

where $h_{turb,in}$ and $h_{turb,out}$ are the turbine inlet and exit enthalpies and are a function of the respective temperatures and pressures.

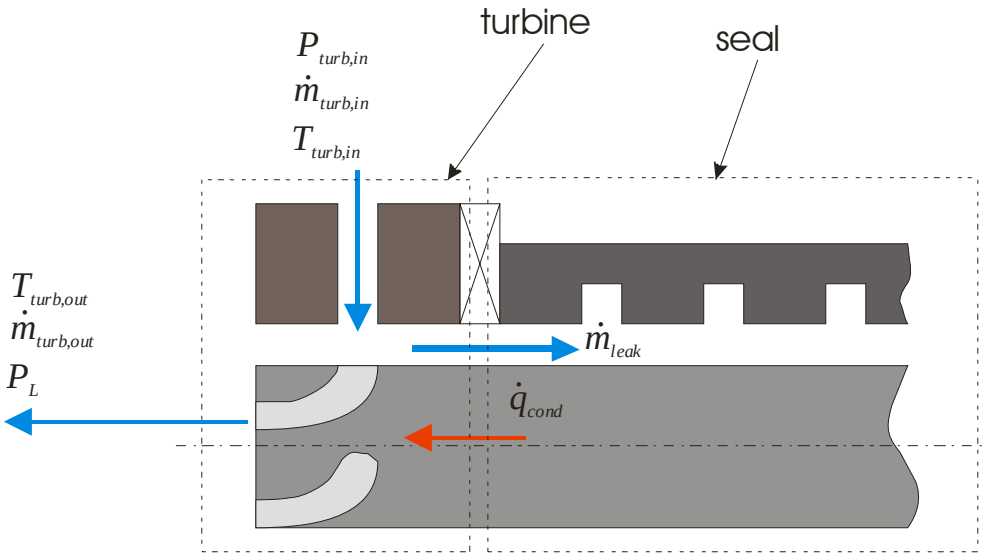

Figure 5-9: The heat and mass flows between the turbine and seal

5.2.2 Load

The heat load is added to the turbine exit stream by a simple energy balance:

$$\dot{m}_{turb,out}\, h_{turb,out} + \dot{q}_{load} = \dot{m}_{turb,out} h_{load} \tag{5.22}$$

where h_{load} is the helium enthalpy after the heat load is added. The load temperature can be determined from the load enthalpy and turbine exit pressure of the helium:

$$T_{load} = T\left(h_{load}, P_L\right) \tag{5.23}$$

5.2.3 Recuperator

The recuperator inputs consist of the inlet temperatures and pressure of each the cold and warm stream. The pressure drop across the recuperator is assumed to be negligible in which case the pressure at both the inlet and exit of each stream are equal. The inlet temperature and pressure of the warm stream is a model input given as the high pressure buffer volume properties which are functions of the upper stage performance. The inlet

and exit pressure of the cold stream are given by the low pressure buffer volume which is again an input to the process related to the upper stage performance. The cold stream temperature, however, is the temperature of the helium after the load, T_{load}. The mass flow through the warm stream is a given value while the mass flow through the cold stream is the warm steam mass flow less the seal leakage mass flow.

5.2.4 Rotordynamics

To account for the limiting speeds, the model has the ability to operate at a fraction of the threshold speed, which is considered to be the lowest absolute limiting speed. Operation at or even near the threshold speed will result in destructive instabilities; therefore, a realistic value that is less than the threshold speed must be used. The model also accounts for a variable threshold speed because several of the variables upon which the threshold speed depends may be varied parametrically. The value chosen for most cases is an operating speed that is 80% of the threshold speed.

6 Results

The turbine performance depends on a multitude of parameters, many of which are interrelated by the several sub-models of the turboexpander which are not completely integrated and there are a number of constraints on the design, some of which are related to manufacturability. Therefore, the turbine model does not lend itself to a straightforward optimization of the overall design. This chapter describes the method used to determine the dimensions and operating conditions necessary for optimum performance. Table 6-1 lists the nominal turboexpander parameter values; unless otherwise noted, all calculations and plots presented subsequently in this chapter use the values presented in Table 6-1.

This chapter describes the perturbation analyses used to estimate the optimal cycle parameters. The effects of varying the shaft geometry, seal parameters, refrigeration load, and 1st stage performance parameters are analyzed. The resulting turboalternator performance is also examined.

Table 6-1: Nominal values for the turboexpander parameters

	Variable description	Symbol	Nominal Value	
			English	Metric
Shaft	Shaft radius	R_{sh}	0.10 in	2.54 mm
	Thrust bearing radius	R_{tb}	0.30 in	7.62 mm
	Thrust bearing thickness	th_{tb}	0.1 in	2.54 mm
	Thrust bearing axial clearance	$c_{tb,a}$	0.001 in	25.4 μm
	Thrust bearing radial clearance	$c_{tb,r}$	0.001 in	25.4 μm
	Magnet bore length	$L_{bore,1}$	1.0 in	2.54 cm
	Length of extended bore	$L_{bore,2}$	0.5 in	1.27 cm
	Diameter of extended bore	$\phi_{bore,2}$	0.1 in	2.54 mm
	Length of turbine (past seal)	$Lturb$	0.25 in	6.35 mm
	Space between journal bearing cartridge and seal	L_{sp1}	0.16 in	4.06 mm
Seal	Seal length	L_{seal}	0.50 in	1.27 cm
	Number of grooves in seal	N_{groove}	10	
	Width of each seal groove	w_{groove}	0.05 in	1.27 mm
	Depth of each seal groove	d_{groove}	0.05 in	1.27 mm
	Seal land clearance	c_{seal}	0.0005 in	12.7 μm
	Pressure drop across seal	ΔP_{seal}	3 inH_2O	747 Pa
Upper stage	High pressure buffer volume pressure	P_H	250 psi	1.72 MPa
	Pressure ratio	P_R	1.2	
	Mass flow to turbine	$\dot{m}_{turb}$		1 g/s
	Upper stage temperature	T_w	60 K	
Operating conditions	Shaft rotational velocity	N_{Hz}	0.80*Ω_{th}	
	Load	$\dot{q}_{load}$	0 W	
	Percent throttle of turbine inlet pressure	x_{turb}	0	
journal bearings	Journal bearing cartridge length	L_{cart}	1.00 in	2.54 cm
	Journal bearing clearance	c_{jb}	0.0005 in	12.7 μm
	Percent throttle of bearing exit pressure	$x_{bearing}$	0	
	Journal bearing pad length	$L_{bearing}$	0.3 in	7.62 mm
Turboalternator	Magnet length	L_m	0.3 in	7.62 mm
	Magnet diameter	D_m	0.12 in	3.05 mm
	Stator pole diameter	D_{st}	0.125 in	3.18 mm
	Stator pole length	L_{st}	0.240 in	6.10 mm
	Stator pole lip diameter	D_{lip}	0.260 in	6.60 mm
	Stator pole lip thickness	th_{lip}	0.030 in	762 μm
	Wire diameter	d_{wire}	0.0050 in	127 μm
	Stator shell outer diameter	D_{shl}	1.25 in	3.18 cm
	Stator shell thickness	th_{shl}	0.125 in	3.18 mm

6.1 Shaft Geometry

Altering the shaft radius will have multiple effects on the turboexpander. An increase in the shaft radius will increase the total mass of the shaft and therefore the mass supported by each bearing. This will reduce the rigid body natural frequency and therefore the threshold speed (see Figure 6-1, which shows the threshold speed as a function of the shaft radius). The increase in radius will also increase the bending frequency of the shaft (i.e., the threshold speed related to the flexing of the shaft); however, the threshold speed for the nominal design is on the order of half the bending frequency and therefore the bending frequency can be neglected as a design constraint under most conditions; this is true provided that the threshold speed is not drastically increased or the shaft geometry substantially modified. For example, the bending frequency for a radius of 0.07 inch (1.78 mm) and length of 2 inches (5.08 cm) is over 3500 Hz, which is well above the threshold speed for whirl instability for the nominal design.

Although increasing the radius causes the rotational speed to decrease, the linear velocity of the turbine tip actually increases and therefore the aerodynamic efficiency initially increases with shaft radius. Figure 6-2 illustrates the aerodynamic efficiency as a function of shaft radius; the shape of this curve is related to the variation of aerodynamic efficiency with the ratio of isentropic nozzle velocity to tip velocity (see section 5.2).

Figure 6-2 suggests that an increase in the shaft radius from 0.07 inch to 0.10 inch would improve the system performance; however, increasing the shaft radius also leads to an increase in the cross-sectional area available for both the heat transfer and helium leakage

through the seal, as shown in Figure 6-3. The result of these conflicting effects is evident in Figure 6-4, which illustrates the turbine no-load temperature as a function of the shaft radius. The lowest temperature achievable through varying the shaft radius is approximately 10.1 K at a radius of about 0.082 in (2.08 mm). Note that the nominal shaft radius is very near to the optimal value.

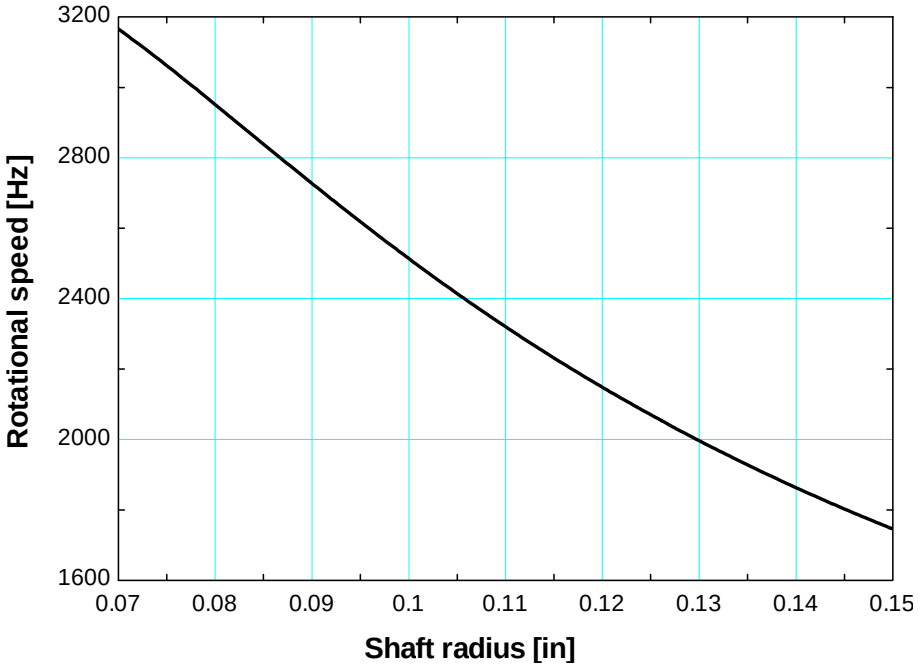

Figure 6-1: Threshold speed as a function of shaft radius (note that the threshold speed is related to the rigid body natural frequency).

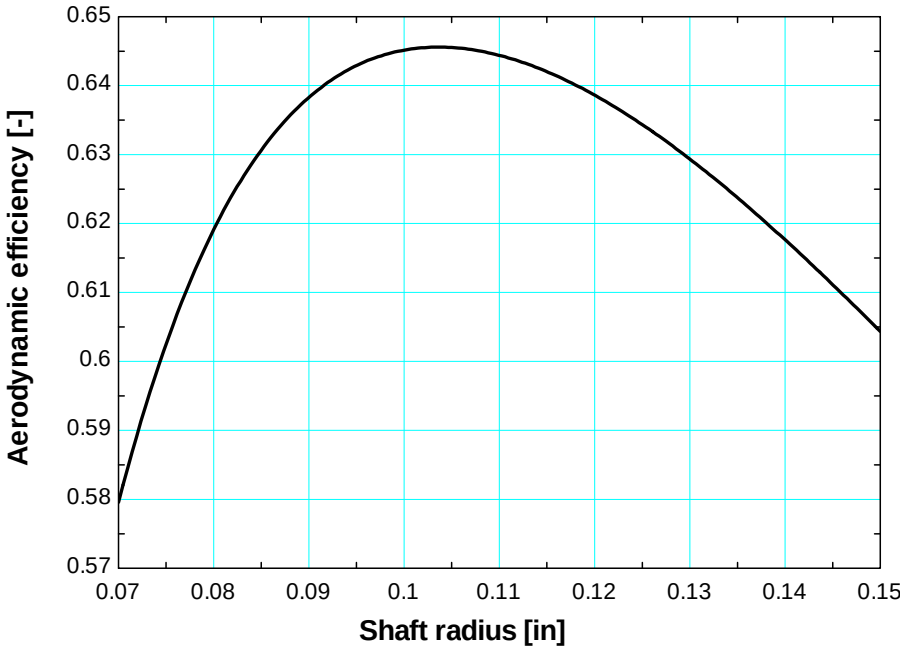

Figure 6-2: Aerodynamic efficiency as a function of shaft radius (for values listed in Table 6-1); note that the shaft speed is always constrained to be 80% of the threshold speed.

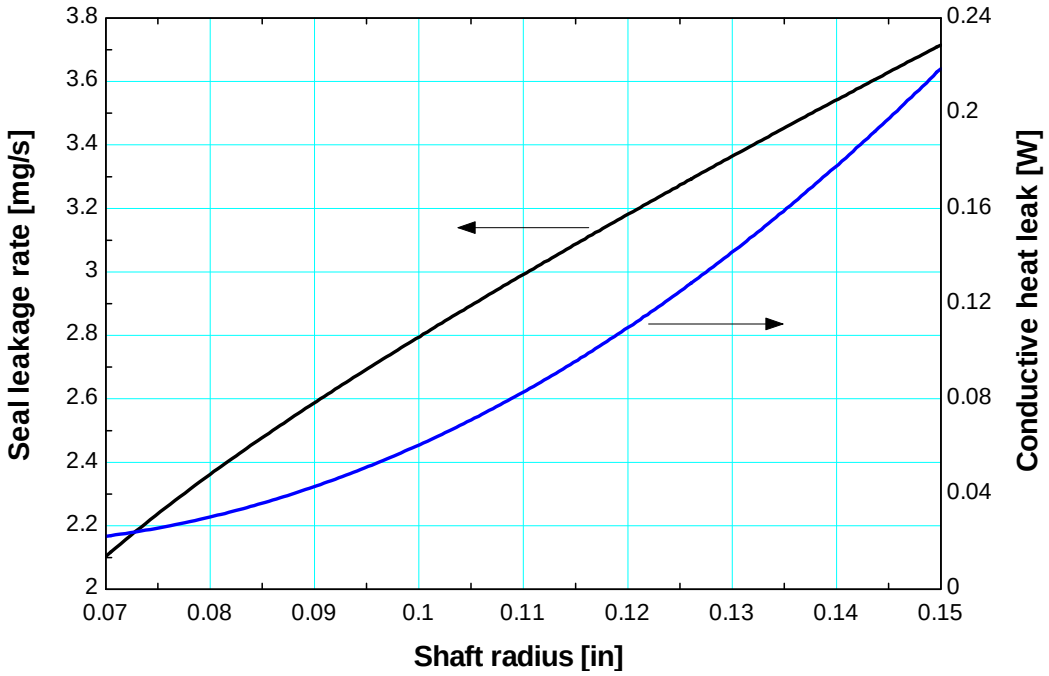

Figure 6-3: Seal leakage rate and conductive heat leak to turbine as a function of shaft radius

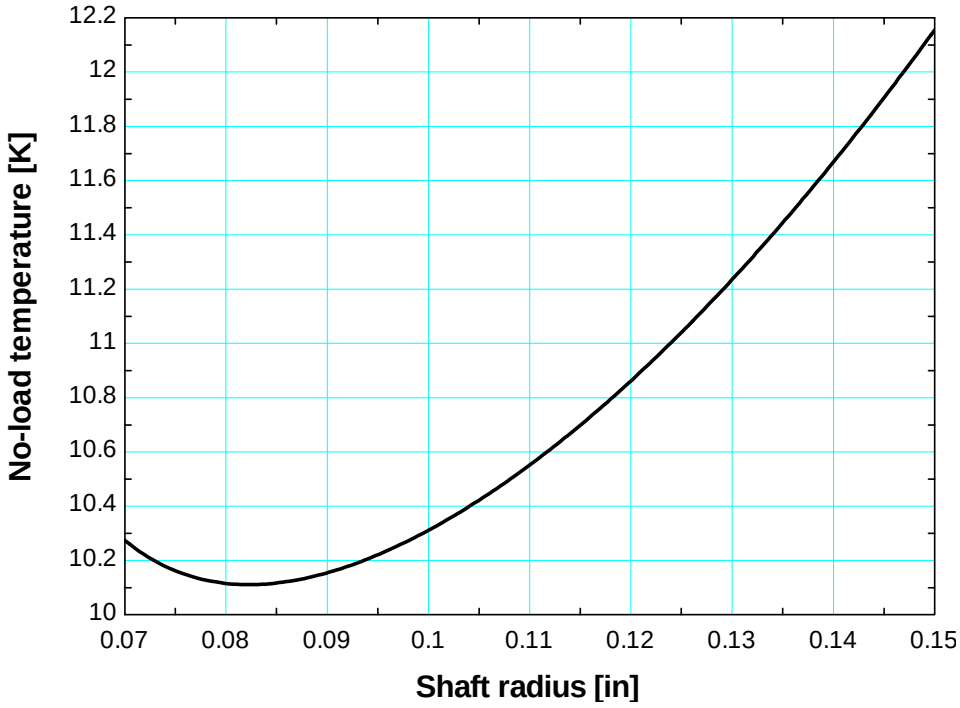

Figure 6-4: No-load temperature as a function of shaft radius

Changing the shaft radius will also change the axial position of the center of mass of the shaft. Figures 6-1 through 6-4 assume the space between the journal bearing and thrust bearing and magnet position are always adjusted so that the center of mass remains centered on the journal bearings, thereby maximizing the rigid body natural frequency associated with each of the journal bearings by correctly distributing the mass of the rotating assembly.

The length of the shaft is also adjusted during the parametric study so that the spaces and lengths presented in Table 6-1 remain valid. The variation of the shaft length and the space between the thrust bearing and journal bearing cartridge are presented in Figure 6-5 as a function of the shaft radius. Note that below a shaft radius of approximately 0.075 in (1.9 mm) the thrust bearing to journal bearing space becomes negative; clearly this is not

possible and therefore, by extension, it is not possible to distribute the mass equally for small shaft radii. A more correct parametric study would account for this effect and the result would be seen in Figure 6-4 as the no-load temperature below a radius of 0.075 in (1.9 mm) would increase more rapidly. However, because the optimal value of the radius is above 0.075 inch the parametric study was not adjusted.

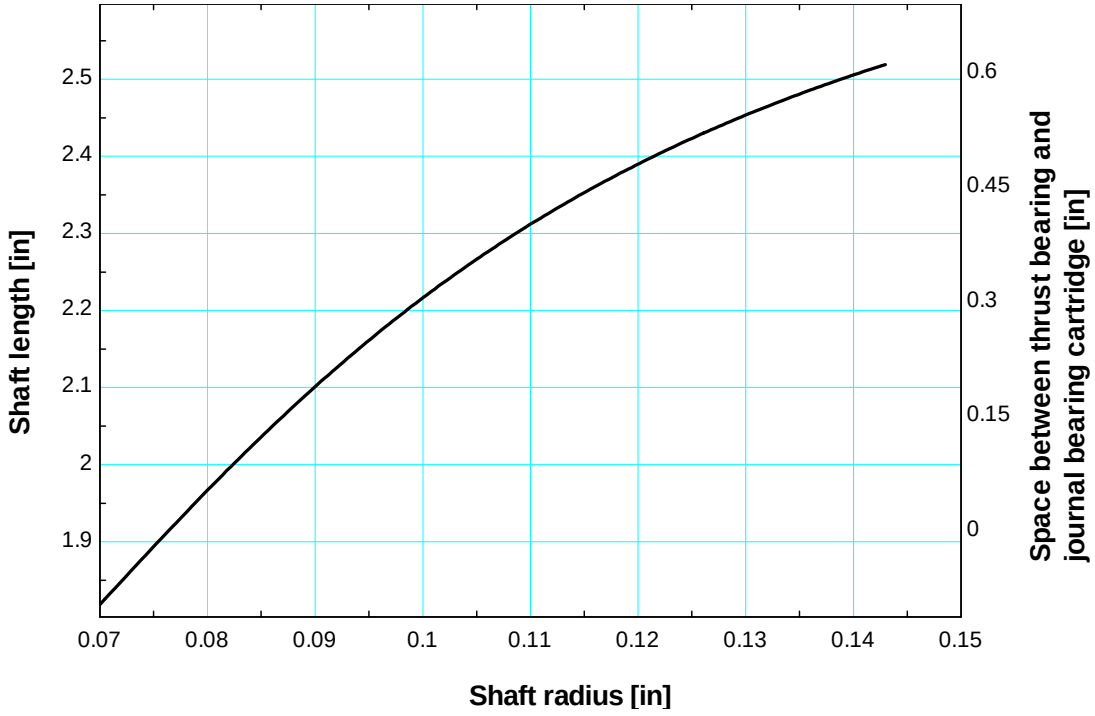

Figure 6-5: Shaft length and journal bearing cartridge to thrust bearing length as they vary with shaft radius for an axially balanced shaft on the journal bearings

6.2 Seal

The characteristics of the seal affect almost every aspect of the cycle performance. The helium leakage through the seal will unbalance the recuperator (more mass flow will be present on the low pressure side than the high pressure side) and therefore impose a direct penalty on its performance. Figure 6-6 illustrates the cold side temperature difference for

a constant cold stream inlet temperature of 10 K. Figure 6-7 illustrates the ideal, isentropic temperature drop the turbine will produce as a function of inlet temperature. At an inlet temperature of 10 K, the ideal temperature drop is about 0.7 K. Therefore, the maximum mass flow penalty from Figure 6-6 is about 7 mg/s. However, when accounting for other penalties and efficiency, the leakage must be kept below approximately 5 mg/s.

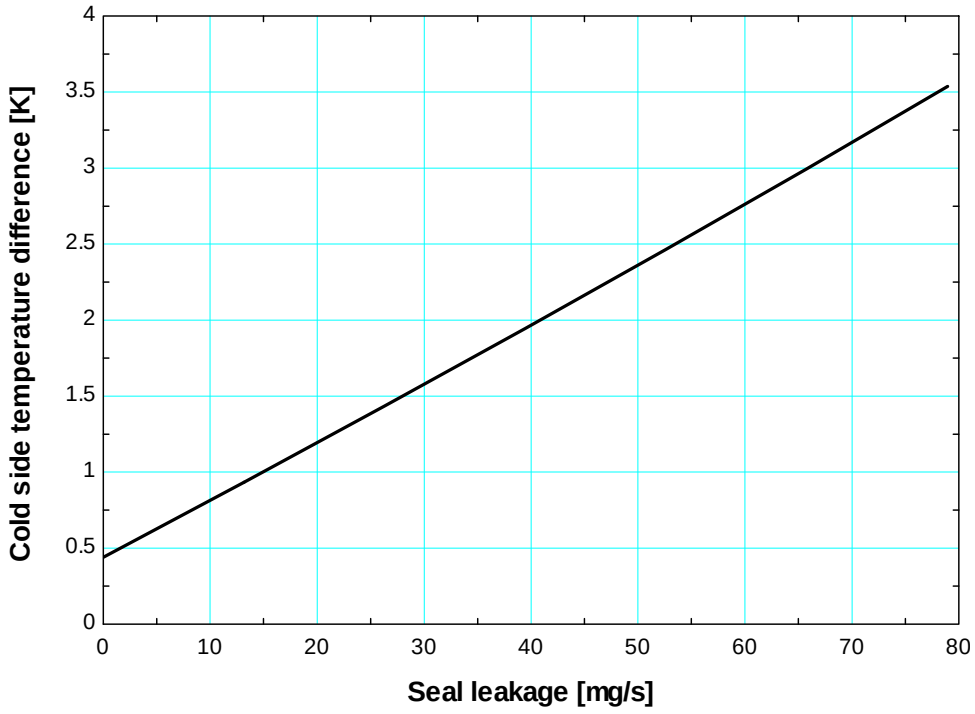

Figure 6-6: The recuperator cold side temperature difference as a function of seal mass flow leakage

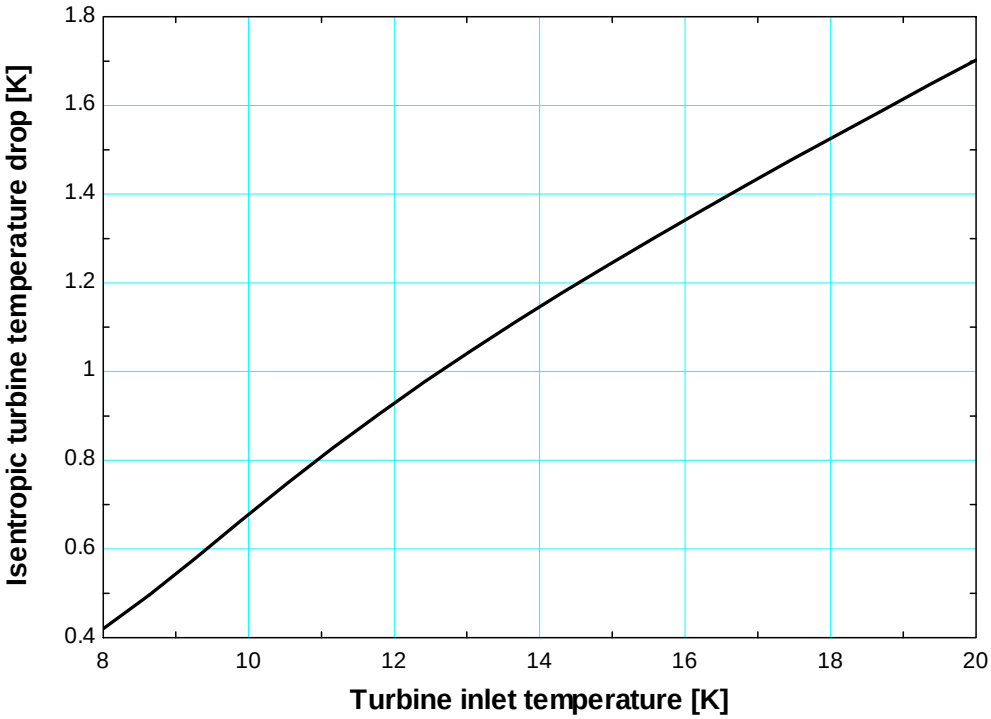

Figure 6-7: The isentropic turbine temperature drop as a function of the turbine inlet temperature

For the turboexpander to perform well, it is imperative that the seal leakage flow rate be minimized. Figure 6-8 shows contours of constant turbine no-load temperature in the parameter space of seal leakage and operating speed. Notice that in order to reach a no-load temperature of 10 K while operating at 2000 Hz, the leakage must be kept to approximately 2 mg/s, or 0.2% of the flow to the turbine. Also note that the no-flow condition represents the minimum temperature that is attainable for a given geometry. Although a temperature of 9 K can be attained with a speed of 1800 Hz, to achieve 8 K would require a speed of approximately 3000 Hz which is a speed that is not likely to be achieved using conventional hydrostatic bearings due to whirl instability. To change these no-flow temperatures would require that the cross-sectional area for conduction be modified or that the recuperator must be redesigned to increase its performance.

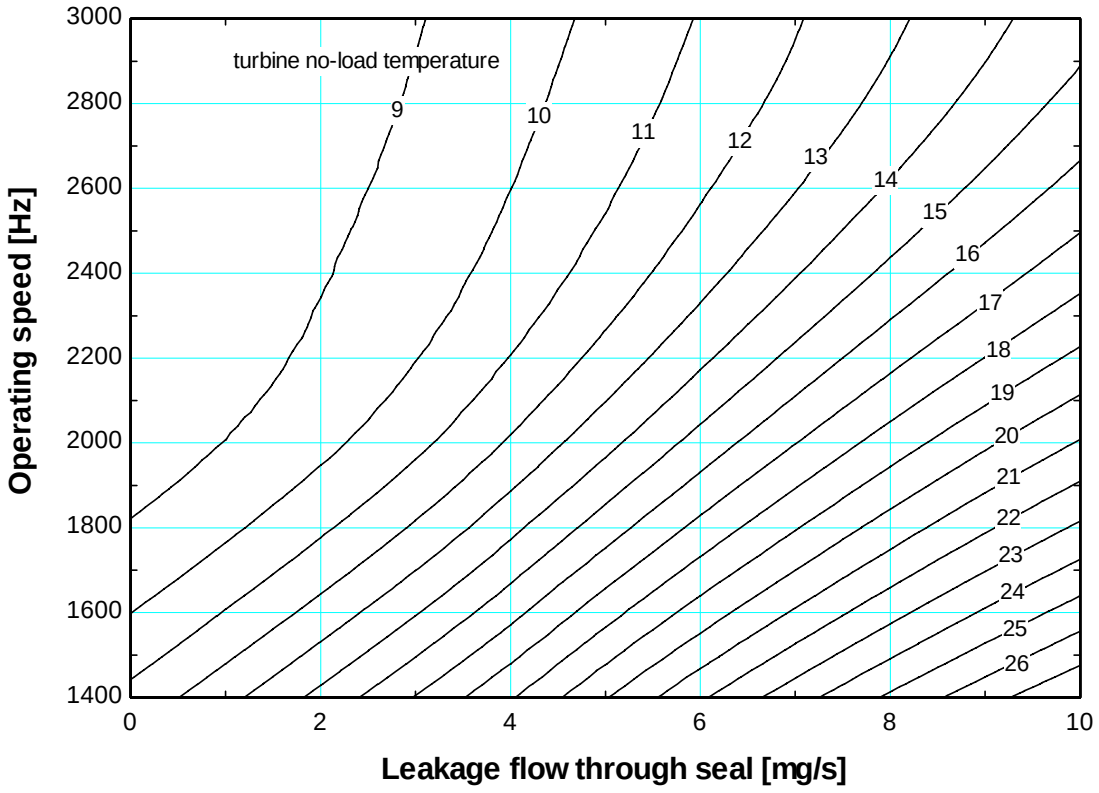

Figure 6-8: Contours of no-load temperature in the parameter space of turbine operating speed and seal leakage rate.

The leakage flow through the seal can be controlled by either changing the pressure difference (i.e. the driving potential for leakage) or the seal geometry and clearance (i.e. the flow resistance to leakage). Though controlling the pressure difference will change the flow rate, the exit temperature of the turbine will also play a role. Lower temperatures will result in a decreased helium viscosity causing a higher leakage rate. This increases the difficulty associated with achieving low temperatures and emphasizes the need for a well designed seal. Figure 6-9 illustrates contours of constant seal leakage rate in the parameter space of seal pressure drop and turbine exit temperature. In order to achieve a temperature of 10 K at a speed of 2000 Hz and a leakage rate of 2 mg/s, the pressure drop must be maintained at approximately 2.6 inH_2O (645 Pa). Note, however,

that this conclusion apply for a labyrinth seal geometry with 10 grooves and a clearance of 0.0005 in.

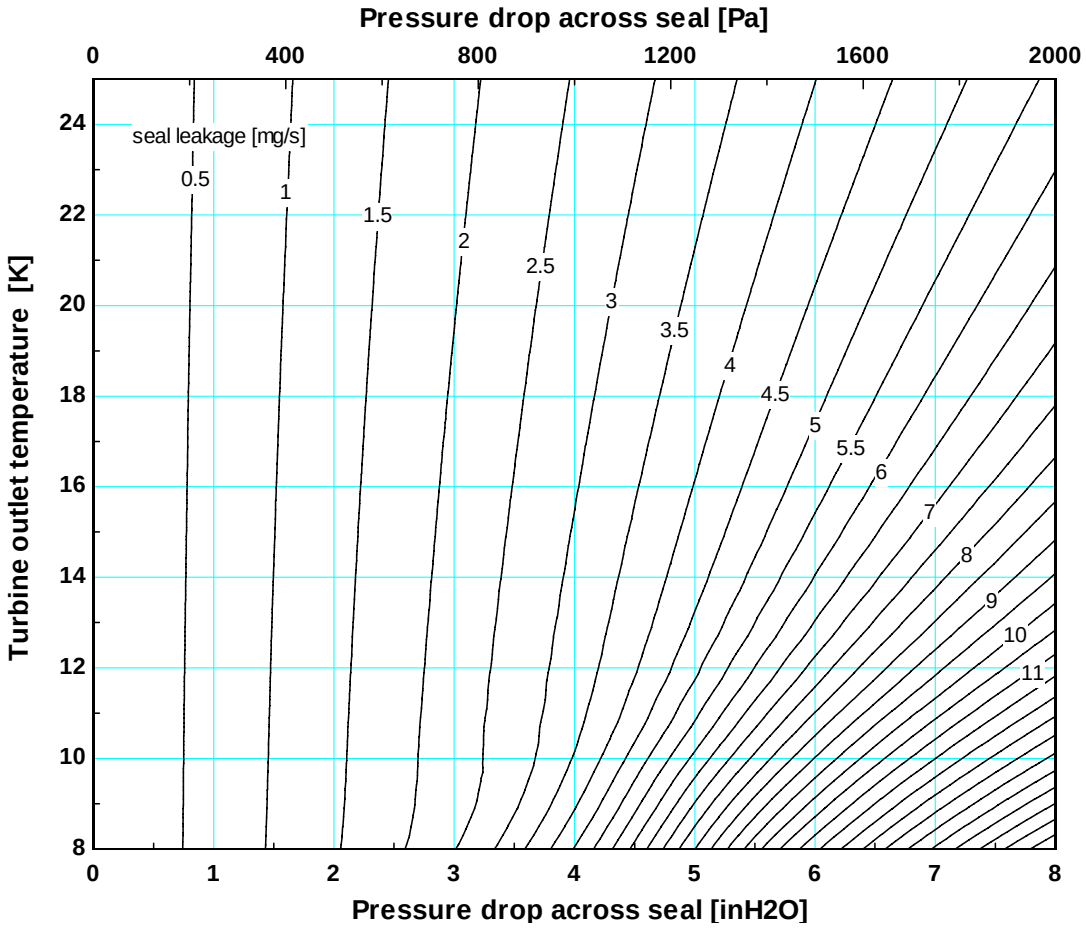

Figure 6-9: Contours of constant seal leakage flow in the parameter space of seal pressure drop and turbine exit temperature.

An interesting result of increasing the pressure drop at low temperatures is the presence of two distinct regimes. This is shown more clearly in Figure 6-10 which shows the seal leakage flow rate and conductive heat leak as a function of the pressure drop and can also be seen in Figure 6-9 as a decrease in contour spacing at a constant, low temperature as the pressure difference rises. The regime change occurs at the relatively sharp discontinuity in the slope of seal leakage with pressure drop (in Figure 6-10) and

corresponds to the point where conductive heat leak down the shaft approaches zero (i.e. the heat leak is fully intercepted by the leakage flow). The explanation for this phenomenon is related to the impact of the leakage on the temperature profile. At low values of leakage, the temperature profile through the seal will be nearly linear (note that the heat leak is proportional to the slope of the temperature profile at the turbine side of the seal). However, as the leakage increases the temperature profile begins to flatten out at the cold end and the average temperature within the seal becomes lower. As a result, the average viscosity within the seal decreases and thus the resistance to flow decreases as well; this manifests itself as a dramatic rise in the slope of mass flow rate with pressure drop. Figure 6-11 illustrates the temperature profile in the seal for various pressure drops. Between a pressure drop of 4 and 5 inH_2O, the heat leak approaches zero (as shown in Figure 6-10) and the temperature distribution within the seal changes dramatically, as shown in Figure 6-11

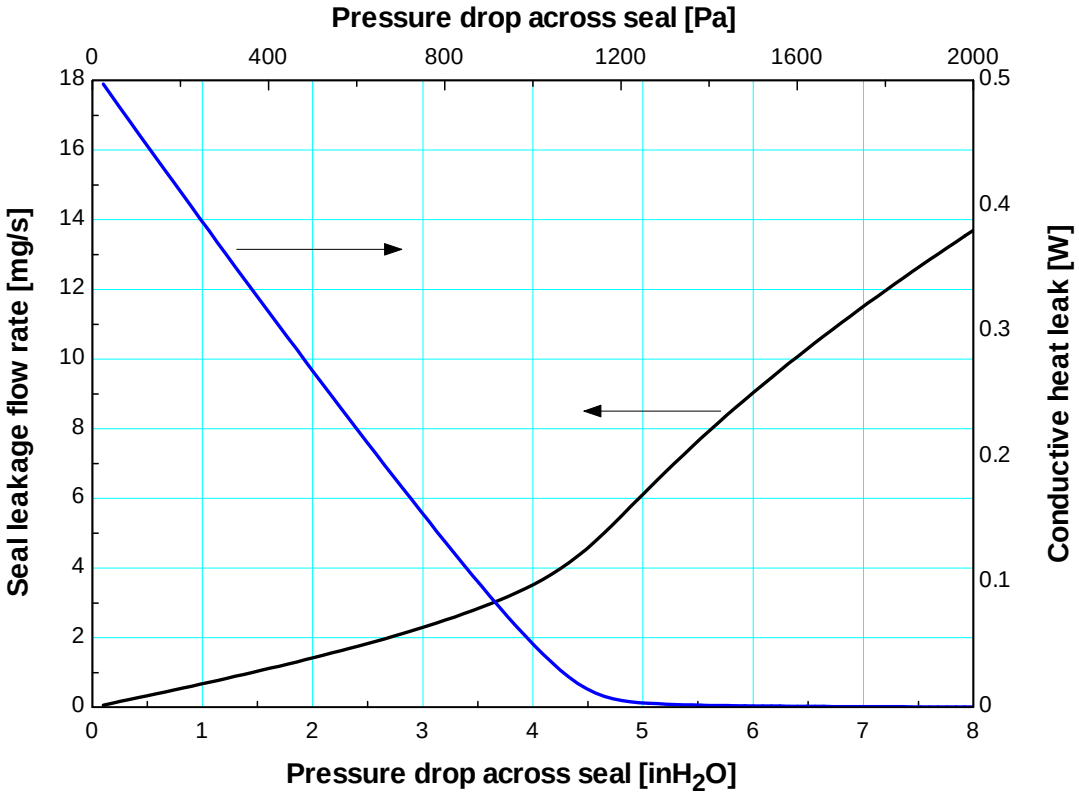

Figure 6-10: Seal leakage flow rate and conductive heat leak as they vary with the seal pressure drop for a turbine exit temperature of 10 K

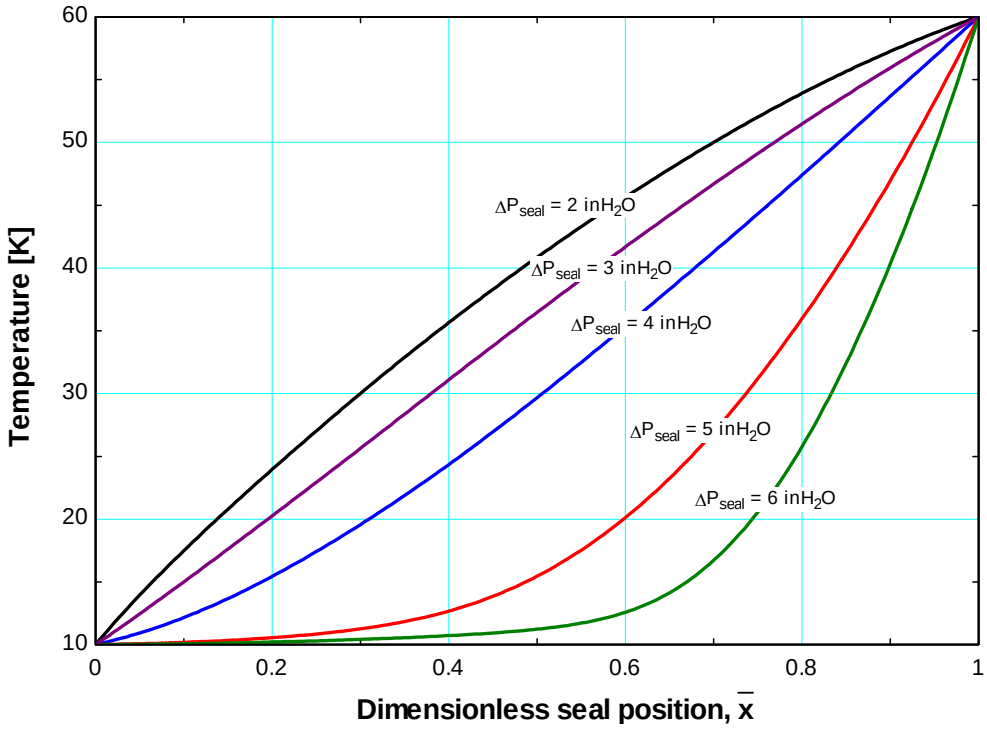

Figure 6-11: Temperature within seal as a function of dimensionless seal position for a turbine exit temperature of 10 K at various seal pressure drops

Though a perfect balance between the turbine and bearing pressures would be ideal, a value of 3 inH2O (750 Pa) was assumed to be an attainable and necessary value; for subsequent calculations this value is assumed. It should be noted, however, that a failure to balance the turbine and bearing pressures to within this value in practice will result in a large penalty; conversely balancing to a lower value can substantially improve the performance.

Figures 6-9 through 6-11 are only valid for a single seal geometry and clearance; however, proper control of the geometry and clearance of the seal is critical to control the leakage rate as well as the conductive heat leak. Figures 6-12 and 6-13 illustrate the turbine no-load temperature as a function of turbine speed for a plain and labyrinth seal,

respectively, and include the threshold speed, friction limit speed (i.e. the speed at which the friction power is equal to the turbine power), and bending frequency. It is immediately obvious from Figures 6-12 and 6-13 that the labyrinth seal will perform better than the plain seal for several reasons. First, the minimum attainable speed for the labyrinth seal will be less than if the plain seal were used with the same clearance, regardless of limitations on the operating speed. Second, the threshold speed, which will be the ultimate speed limit (except for clearances lower than 0.0005 in which case the friction limit may occur at a lower speed than the threshold speed), will be substantially higher in the case of the labyrinth seal.

An interesting feature of Figures 6-12 and 6-13 is the similarity of the friction limit. The plain seal would intuitively provide more friction due to the larger close-clearance length. However, as the plain seal is operating at higher no-load temperatures, the turbine power increases due to the larger isentropic enthalpy drop. The larger turbine power can overcome larger frictional power dissipation and the similarity between the values is a coincidence.

An important note about the plain seal is that it uses a length-averaged viscosity to calculate the leakage flow friction, whereas the labyrinth seal uses the local average viscosity of each land. This assumption may distort the overall performance of the turbine using a plain seal by altering the leakage flow rate because it does not account for a varying friction factor. However, the threshold speed of the plain seal is accurate, and this effect alone is sufficient to suggest that a labyrinth seal must be used. At the low

clearances that are required for a low leakage rate regardless of seal type, the threshold speed must be as high as possible. This can only be done through the use of a labyrinth seal due to it's the low amount of destabilizing forces produced.

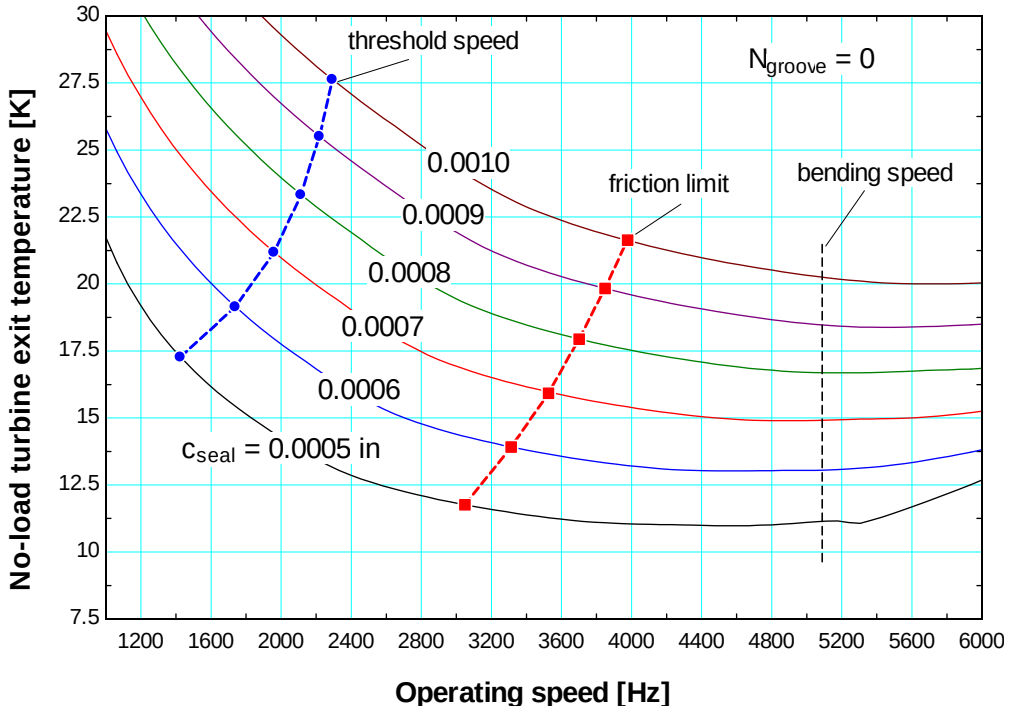

Figure 6-12: No-load turbine exit temperature as a function of operating speed for various clearances using a plain seal

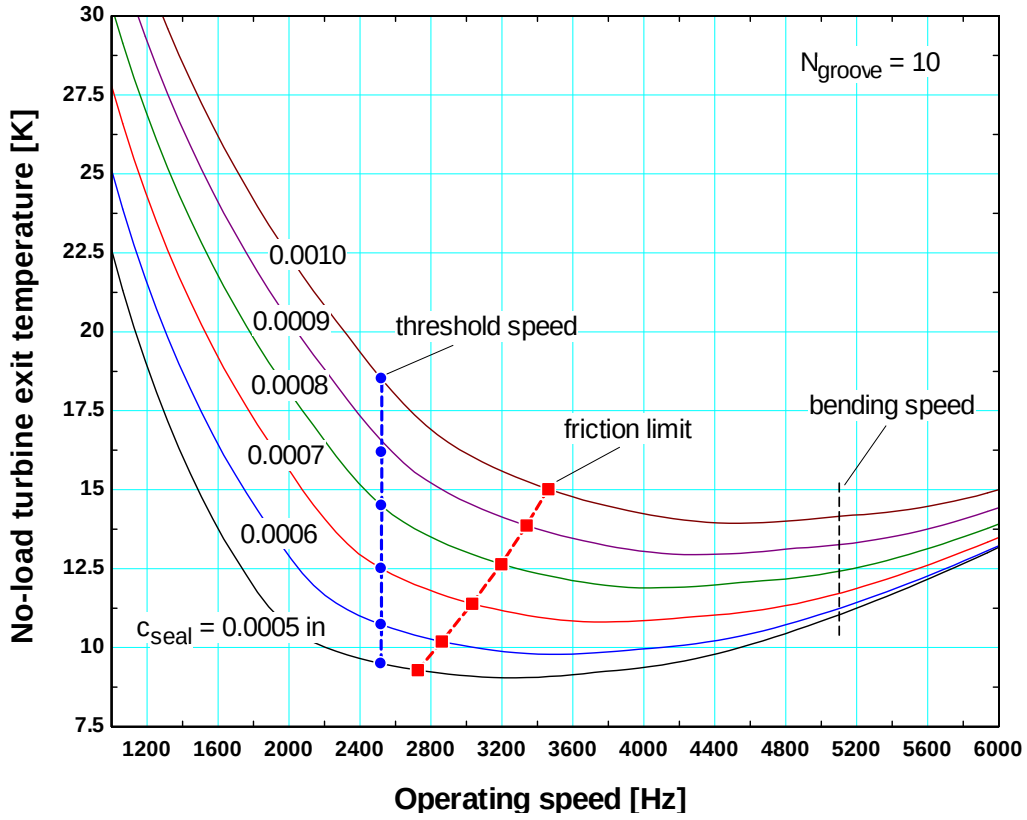

Figure 6-13: No-load turbine exit temperature as a function of operating speed or various clearances using a labyrinth seal with 10 grooves

The number of grooves for the labyrinth seal was chosen to be 10. However, a reduction in the number of grooves may reduce the temperature slightly as illustrated in Figure 6-14. Decreasing the number of grooves will also increase the length-to-diameter ratio for each of the seal lands, which is an important parameter affecting the bearing tangential stiffness. When the number of grooves is reduced below 5, the short bearing approximation becomes invalid. Therefore to verify that the lands can be approximated as short bearings and also due to the relatively low improvement of performance associated with decreasing the number of grooves (i.e. the maximum decrease in

temperature is approximately 0.15 K), the number of grooves was maintained at 10 for the design.

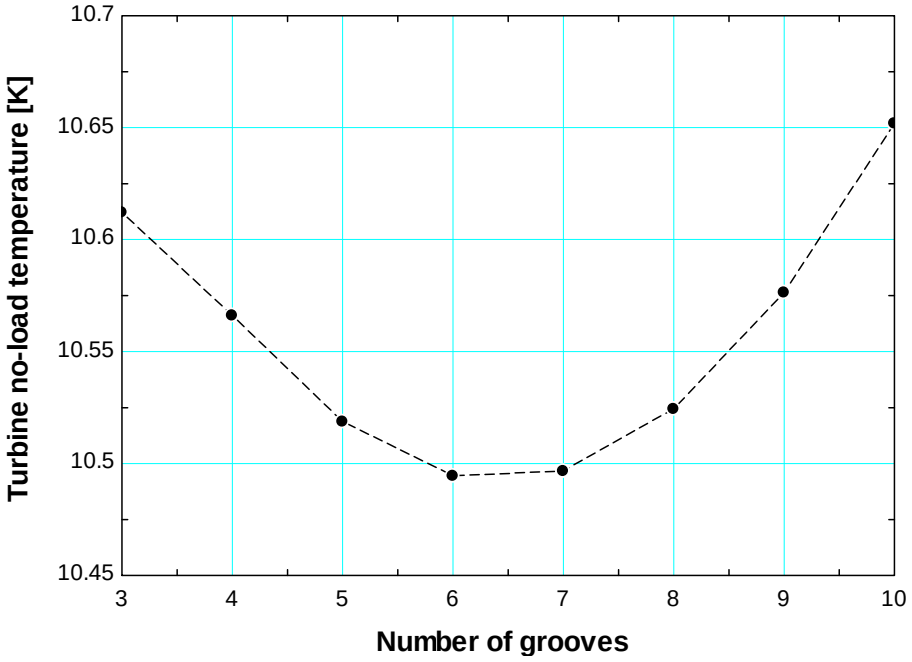

Figure 6-14: Turbine no-load temperature as a function of the number of grooves in a labyrinth seal

Though the seal will have a large impact on the threshold speed, the journal bearing normal stiffness is the most important parameter and a sufficient increase in the journal bearing stiffness could increase the threshold speed beyond the bending critical speed. This situation, however, would require an excessive amount of mass flow and most likely a larger pressure ratio than the upper stage can realistically provide. However, by reducing the journal bearing clearance, the normal stiffness can also be increased. Figure 6-15 illustrates contours of constant no-load temperature in the parameter space of seal and journal bearing clearance. A clearance of 0.0005 inch (13 μm) for both the seal and journal bearings, which is estimated to be the limit of available machining processes, is

necessary to achieve temperatures near 10 K. An increase in either clearance will drastically increase the no-load temperature; in either case (journal bearing or seal clearance), the impact is approximately 4 K per 0.0001 inch of clearance increase.

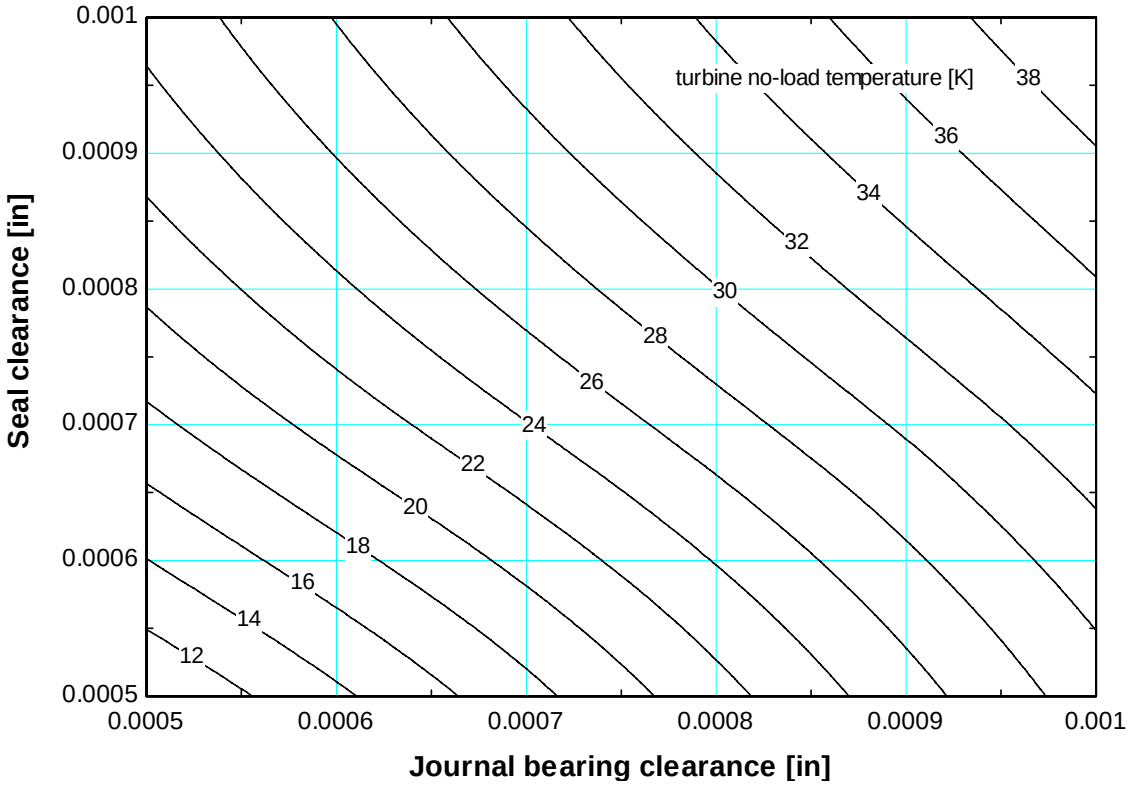

Figure 6-15: No-load temperature contours for varying journal bearing and seal clearance

The ideal seal clearance for all cases was below the assumed minimal machinable thickness of 0.025 inch (0.635 mm). This is due to the mass flow penalty due to seal distortion from pressure being lower than the benefit from the lower cross-sectional area for conduction. The seal thickness must therefore be 0.025 inch (0.635 mm) or the lowest allowable through available machining methods.

6.3 Load Performance

All calculations up to this point have presented the turbine exit temperature for no cooling load; the temperature exiting the turbine under no load is equal to the cold stream temperature entering the recuperator. In practice, the helium leaving the turbine must receive a cooling load prior to returning to the recuperator. Figure 6-16 illustrates the load temperature as a function of the cooling load. At the nominal design load of 1 W, the load temperature is approximately 17 K.

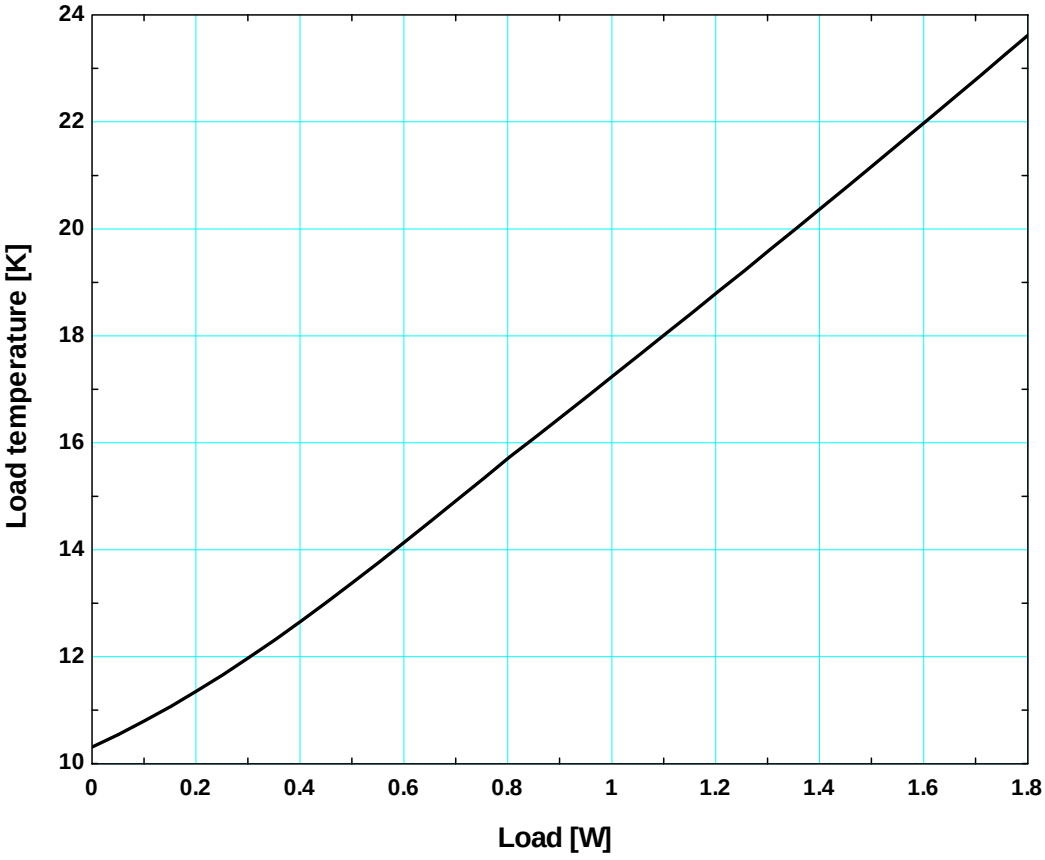

Figure 6-16: Turboexpander load performance

6.4 Turboalternator

The primary requirement of the turboalternator is that it must dissipate the turbine power that is not consumed by fluid friction at the design temperature, which is approximately 1 to 2 watts. The turboalternator design is not dependent on other sub-models; only space requirements are important. Figure 6-17 illustrates the operating speed contours for varying load resistance and power dissipated. Each speed has a corresponding maximum power the turboalternator is able to dissipate.

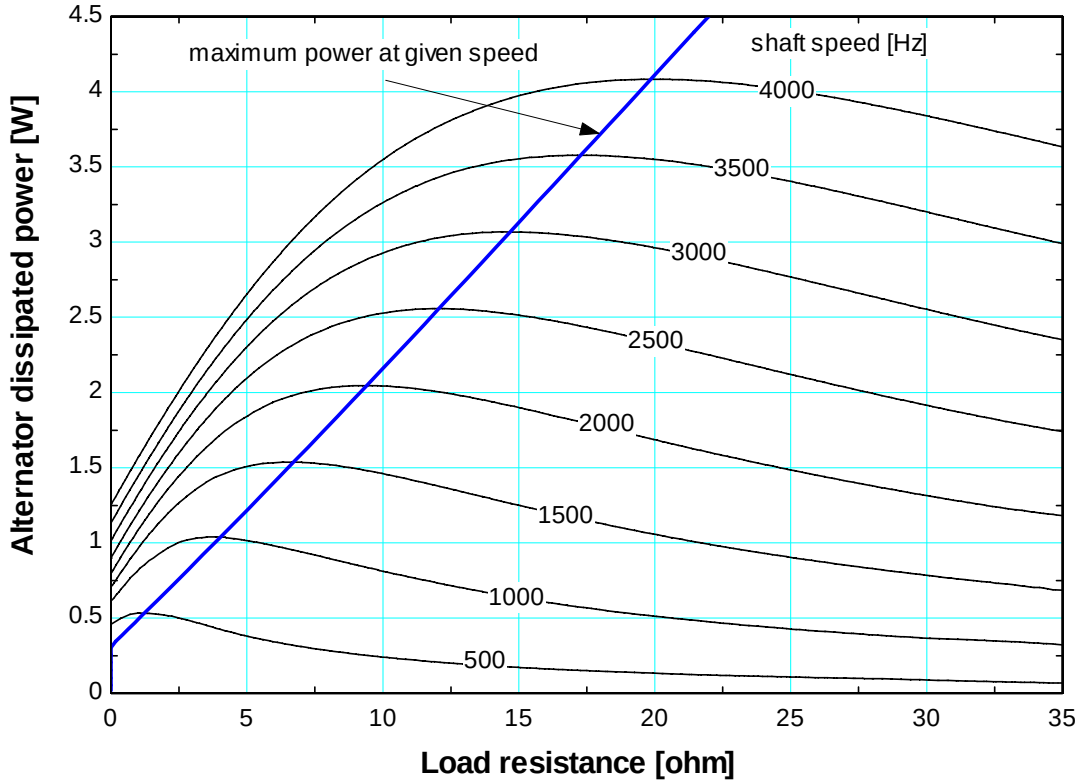

Figure 6-17: Shaft speed contours for varying turboalternator dissipated power and load resistance

Figure 6-18 illustrates the total turbine power, excess turbine power (i.e. the power not consumed by friction), the maximum turboalternator power, and the friction power as

they vary with the operating speed. The turbine power will exceed the maximum turboalternator power for speeds less than approximately 2300 Hz. This is due primarily to the high temperatures associated with the low operating speeds. Therefore, below a speed of 2100 the turboalternator must be modified or the mass flow and pressure difference, and thus the turbine power, must be reduced through the use of a throttle.

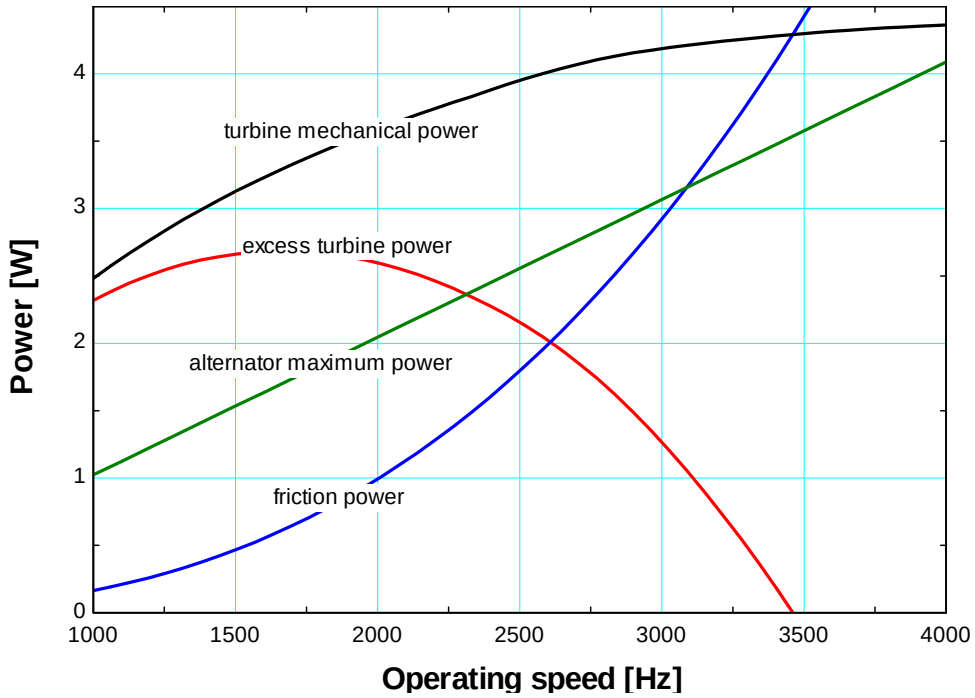

Figure 6-18: Turbine power, excess turbine power, maximum turboalternator power, and friction power as they vary with turbine operating speed

6.5 Upper Stage Performance

The upper stage performance of the pulse tube must be considered when determining the optimal hybrid operating conditions. The performance of the turboexpander will strongly depend on the pressures and temperature produced by the upper pulse tube stage. Figure 6-19 shows contours of no-load temperature as a function of the high pressure buffer

volume pressure and the pressure ratio and shows that the turboexpander will operate at lower temperatures given a high pressure ratio and low high pressure buffer volume (HPBV) pressure. However, the pulse tube will perform better at higher charge pressures providing a higher HPBV pressure. This is the fundamental mismatch between the cycles and one of the reasons that the hybrid concept is not as favorable as initially anticipated. The nominal design is a HPBV pressure of 250 psi (1.72 MPa) and a pressure ratio of 1.2 which will result in a turbine temperature of approximately 10.2 K for the parameters listed in Table 6-1.

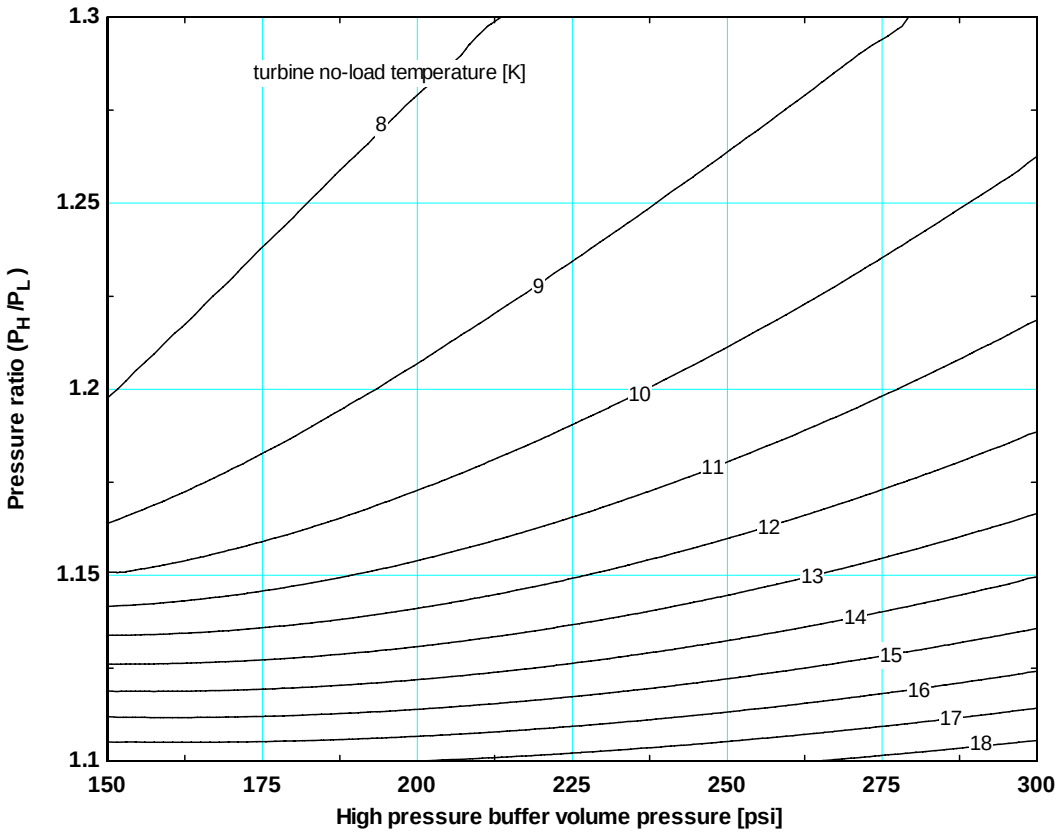

Figure 6-19: Turbine no-load temperature contours for varying pressure ratio and high pressure buffer volume pressure

The HPBV temperature (i.e., the temperature at the cold end of the upper stage) will also affect the turboexpander performance. Decreasing in HPBV temperature will decrease

the helium viscosity and reduce the fluid friction within the journal and thrust bearings. The performance of the recuperative heat exchanger will improve as it has to span a smaller temperature difference. The lower temperature difference between the turbine and bearings will also reduce the conductive heat leak. However, the decrease in viscosity within the seal will result in a higher leakage flow rate. These competing effects result in a minimum turboexpander temperature at a HPBV temperature of approximately 56 K, as shown in Figure 6-20 (note that the turboexpander operating speed is set to be 80% of the threshold speed). However, the decrease in temperature (i.e. increase in performance) from the nominal pulse tube temperature of 60 K is negligible. The additional electrical power required and possibly many hours spent adjusting the pulse tube in order to operate at 56 K to reach the minimum turbine temperature will likely not be worthwhile; there are several other components, such as the journal bearings, which have the ability to yield a higher turbine performance increase with less effort input.

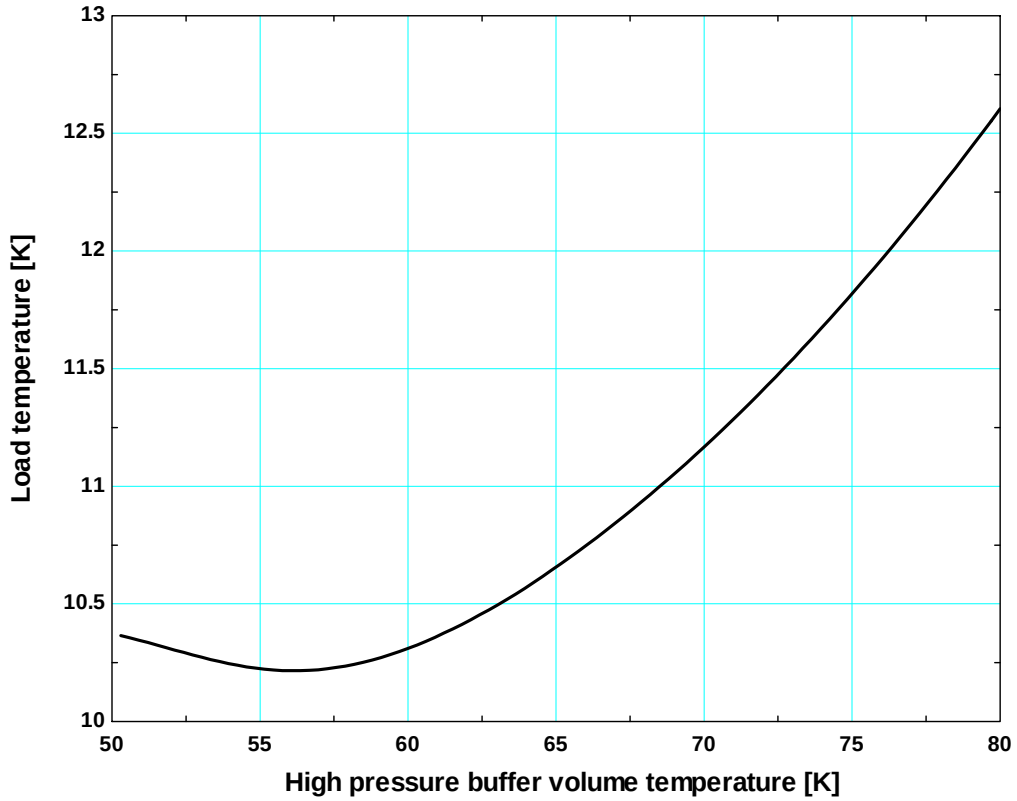

Figure 6-20: Turbine no-load temperature as a function of pulse tube temperature

7 Conclusions

The hybrid pulse tube-reverse Brayton cycle cryocooler has the potential for cooling to temperatures on the order of 10 K. By using the rectifying interface which converts the oscillating pulse tube flow to a continuous flow, both vibrations and low temperature regenerator losses are overcome, making the hybrid an ideal candidate for cooling infrared focal plane arrays which demand low temperature and low vibration. A model was developed to predict the performance of the reverse Brayton cycle stage; the model focused on the turboexpander and its sub-components but also considers the recuperative heat exchanger. The turboexpander was modeled in some detail and sub-models considering the rotordynamics, seal, and turboalternator were developed. Finally, a parametric analysis was carried out in order to determine the optimal design and operating conditions for the turboexpander.

In order to achieve temperatures near 10 K, the turboexpander components must be carefully designed and machined to very close tolerances. The clearances in both the seal and journal bearings must be as small as can realistically be achieved using conventional machining processes. Every increase of 0.0001 inch (2.5 μm) of either the seal or journal bearing clearance will result in a penalty of approximately 4 K on the no-load temperature that can be reached. Additionally, the turbine must be run at the highest possible speed within the limits of the critical speeds. The current design will allow the turbine to run up to approximately 2000 Hz before the onset of whirl instability. A labyrinth seal must be utilized in order to produce the minimal tangential stiffness while

maintaining a low leakage rate. The pressure drop across the seal will need to be closely monitored and minimized through active control.

An option that would provide improved performance is the use of more advanced journal bearing designs that would provide an increased threshold speed; these designs may either increase the tangential damping coefficient or normal stiffness. Some advanced bearing concepts might use tangentially directed gas supply holes, pneumatic phase shifting cavities, or lead pad activation. The use of advanced bearing designs may be the only practical alternative to make the hybrid cryocooler cycle competitive with pulse tube technology if the low clearances and well-balanced seal pressure drop cannot be achieved.

Although the seal is a critical component with regards to preventing both heat and mass flow, the redesign of the seal produces a limited increase in cycle performance. As Figure 6-8 illustrates, the performance with no leakage rate (i.e. a perfectly designed and pressure-balanced seal) will only perform well if the turbine speed is sufficiently high or if the seal and shaft cross sectional area are decreased. As section 6.1 demonstrated, a shaft radius of 0.082 inch (2.08 mm) will perform marginally better than the nominal value of 0.10 inch (2.54 mm) due to the decrease in cross sectional area.

The upper stage performance must also be adequate for the turboexpander to perform at the expected temperature range. The pulse tube cold temperature must be on the order of 60 K. The pressure ratio must be as high as possible, and the high pressure buffer

volume pressure must be kept as low as possible while maintaining acceptable pulse tube temperatures.

References

Baines R, “Radial Turbines: An Integrated Design Approach,” Concepts ETI, Inc, 2005

ChenYang Engineering ISM, “Neodymium Iron Boron Magnets”, 2004

“COSMOSWorks”, Structural Research & Analysis Corporation, 2005

Daily J W, Nece R E, “Chamber Dimensional Effects on Induced Flow and Frictional Resistance of Enclosed Rotating Disks”, *Journal of Basic Engineering*, March 1960

Dubois G B., Ocvirk F W, “Analytical derivation and experimental evaluation of short-bearing approximation for full journal bearing”, National Advisory Committee for Astronautics (NACA) Report 1157, 1953

Fay J A, *Introduction to Fluid Mechanics*, MIT Press, Cambridge, MA, 1994.

Giancoli D C, Physics, 4th Ed, Prentice Hall, (1995)

Guyer E C, and Brownell D L, Eds., *Handbook of Applied Thermal Design*, McGraw-Hill, New York, (1989).

Hitachi Metals America, Ltd., “Neodymium,” http://www.hitachimetals.com/product/permanentmagnets/neodymium/, 2006

Incropera F P, DeWitt D P , *Introduction to Heat Transfer*, John Wiley & Sons, New York (2002)

Juvinall R C, Marshek K M, *Fundamentals of Machine Component Design*, 3rd Edition, John Wiley and Sons, 2000

Klein S A, "EES – Engineering Equation Solver, version 7.571", F-Chart Software, www.fchart.com, 2006

Lorenz R D, Haines L P, *Understanding Modern Power Conversion*, 3rd Edition, RDL/LPH(2000)

Qui L M, He Y L, Gan Z H, Chen G B, "A single-stage pulse tube cooler reached 12.6 K," *Cryogenics*, Volume 45, 641-643, 2005

San Andres L, "Dynamics of a Rigid Rotor-Fluid Film Bearing System", MEEN 626 Fluid Bearings, Lecture 5, 2000

Sandor B I; Roloff R, Birn S M; Jawad M H, Brown M L; "Mechanics of Solids," *Mechanical Engineering Handbook*, Boca Raton: CRC Press LLC, 1999

"SolidWorks 2005 SP3.1," SolidWorks Corporation, 2006

White F M, Fluid Mechanics, 4th Edition, McGraw Hill, 1999

White F M, Ed, "Drag-Rotating Nonventilated Enclosed Rotating Disks," *Heat Transfer and Fluid Flow*, Section 408.4. Genium Publishing, August 1995

Appendix A: Rotordynamics Model EES Code

```
"!*****************************************************************************************************************"
"-----------------------------------------------------------------------------------------------------------------"
"!<<<<<<<<<<<<<<<<<<<<<<<<<<<ROTOR DYNAMICS>>>>>>>>>>>>>>>>>>>>>>>>>>>"
"-----------------------------------------------------------------------------------------------------------------"
"!*****************************************************************************************************************"

$IF RotorDynamics$ = 'on'
"-----------------------------------------------------------------------------------------------------------------"
"================Rigid Body Natural Frequency of Shaft on Bearings================"
$IF thresholdspeed$='on'

L_jbcart_e = L_jb1_e + L_jb2_e + L_stsp_e;    L_jbcart = L_jbcart_e*convert(in,m)        "total length of journal bearing cartridge"
L_bore1 = L_sp2 + L_jb2 + L_stsp/2 + L_rot/2; L_bore1 = L_bore_1_e*convert(in,m)       "length of bore 1"

x_F_jb1 = L_sp2 + L_jb2 + L_stsp + L_jb1/2          "position of journal bearing force 1"
x_F_jb2 = L_sp2 + L_jb2/2                           "position of journal bearing force 2"

"shaft broken into 7 sections to perform moment balance"

"length of each section"
L[1] = L_sh - (L_bore2 + L_bore1+ L_sp1/2)
L[2] = L_sh - (L_bore2 + L_bore1 + L[1])
L[3] = L_bore1 + L_bore2 - x_F_jb1
L[4] = L_bore2 - L[2]
L[5] = L_rot
L[6] = L_bore1 - L_rot - th_tb
L[7] = th_tb

"axial position of center of mass for each section"
cm[1] = L[3] + L[2] + L[1]/2
cm[2] = L[3] + L[2]/2
cm[3] = L[3]/2
cm[4] = L[4]/2
cm[5] = L[4] + L[5]/2
cm[6] = L[4] + L[5] + L[6]/2
cm[7] = L[4] + L[5] + L[6] + L[7]/2
cm_jb2 = L_jb1/2 + L_stsp + L_jb2

"cross sectional area of each section"
Ac[1] = pi*D_sh_2^2/4
Ac[2] = pi*D_sh^2/4
Ac[3] = pi*(D_sh^2 - phi_bore2^2)/4
Ac[4] = Ac[3]
Ac[5] = pi*(D_sh^2 - D_rot^2)/4
Ac_m[5] = pi*D_rot^2/4              "magnet"
Ac[6] = Ac[5]
Ac[7] = pi*(D_tb^2 - D_rot^2)/4
```

```
"mass of each section"
m[1] = rho_Ti*Ac[1]*L[1]
m[2] = rho_Ti*Ac[2]*L[2]
m[3] = rho_Ti*Ac[3]*L[3]
m[4] = rho_Ti*Ac[4]*L[4]
m[5] = rho_Ti*Ac[5]*L[5] + rho_m*Ac_m[5]*L[5]
m[6] =  rho_Ti*Ac[6]*L[6]
m[7] =  rho_Ti*Ac[7]*L[7]

duplicate i = 1,7
F[i] = g#*m[i]        "total force = weight"
Mo[i] = F[i]*cm[i]
end

Mo_ccw = Mo[1] + Mo[2] + Mo[3] + F_jb_2*cm_jb2  "counterclockwise moment about front
journal bearing"
Mo_cw = sum(Mo[i],i=4,7)                        "clockwise moment about front journal
bearing"
Mo_ccw = Mo_cw                                  "moment balance"

m_tot = sum(m[i],i=1,7)
F_jb_1 + F_jb_2 = Weight_tot
Weight_tot = m_tot*g#

DELTAP_bearings = P_bearing_in - P_bearing_out                  "pressure drop across
journal bearings"
DELTAP_bearings = DELTAP_bearings_e*convert(psi,Pa)

"Input inlet temperature (T_gas [K]) and pressure (Pse_gage [psi]), pressure drop through
bearings (DELTAP [psi]), and bearing clearance (c_e [in])"
CALL jbconst(T_bearing,DELTAP_bearings_e,P_H_e,c_jb_e,R_sh_e:C_k_jb,C_m_jb)

k_jb= C_k_jb*(DELTAP_bearings)*(2*R_sh)^2/c_jb          "stiffness of journal bearings
(each)"
m_dot_jb = C_m_jb*P_H*c_jb^3*(DELTAP_bearings)/(R_He*T_bearing*mu_bearing)    "helium
mass flow through journal bearings"

$IF FrictionModel$ = 'off'
R_He = R/M_He                       "helium gas constant"
M_He = molarmass(Helium)
R = R#
$ENDIF
                                    "journal bearing stiffness constant"
masscheck = F_jb_1/g# + F_jb_2/g#       "should equal m_tot"
omega_n1 = sqrt(k_jb/(F_jb_1/g#))       "rigid body nat freq on journal bearing 1 (for)"
omega_n2 = sqrt(k_jb/(F_jb_2/g#))       "rigid body nat freq on journal bearing 2 (aft)"

N_f_jb1 = 2*omega_n1*convert(rad/s,Hz)      "threshold speed for jb 1"
N_f_jb2 = 2*omega_n2*convert(rad/s,Hz)      "threshold speed for jb 2"
N_f_min = 2*sqrt(k_jb/m_tot)*convert(rad/s,Hz)    "minimum possible threshold speed - when
centered axially"

omega_n = MIN(omega_n1,omega_n2)        "the rigid body natural frequency is lesser of the
two - when system becomes unstable"
```

```
"=========================================================================="
"Threshold Speed including the additional seal and thrust bearing tangential stiffenesses"

"Centered"

"Thrust Bearing"
e_0 = 0
n_tb = 0
F_tan_tb_0` = (mu_bearing*R_tb*th_tb^3/(4*c_tb^2))*((pi*n_tb)/(1-n_tb^2)^(3/2))

"Seal"
$IF sealtype$='plain'
{L_seal_e = 0.5[in];      L_seal = L_seal_e*convert(in,m)}
n_seal = 0[m]/c_seal
{p_0` =
mu_bearing*R_sh_2^2/c_seal^2*((6*n_seal*sin(theta)*(2+n_seal*cos(theta)))/((2+n_seal^2)*(1+
n_seal*cos(theta))^2))}
F_x_seal_0` ={ integral(p_0`*R_sh_2*L_seal*sin(theta),theta,0,pi)}0
F_y_seal_0` = {integral(p_0`*R_sh_2*L_seal*cos(theta),theta,0,pi)}0
$ENDIF
$IF sealtype$='labyrinth'
F_tan_seal_0` = {(mu_bearing*R_tb*th_tb^3/(4*c_tb^2))*((pi*n_tb[0])/(1-n_tb[0]^2)^(3/2))}0
$ENDIF

"Journal Bearing"
L_jb_tot = 2*L_jb  "total close-clearance length of journal bearings"
n_jb = 0[m]/c_jb
{p_jb_0` =
mu_bearing*R_sh^2/c_jb^2*((6*n_jb*sin(theta)*(2+n_jb*cos(theta)))/((2+n_jb^2)*(1+n_jb*cos(the
ta))^2))}
F_x_jb_0` = 0
F_y_jb_0` = 0

"================================="

"Offset"
DELTAe = e_1 - e_0
e_1 = perc*c_jb
perc = 0.01

{       This method uses pressure distribution about shaft - same result as equations when
small offset
        "Journal Bearing"
        n_jb_1 = e_1/c_jb
        p_jb_1` =
mu_bearing*R_sh^2/c_jb^2*((6*n_jb_1*sin(theta)*(2+n_jb_1*cos(theta)))/((2+n_jb_1^2)*(1+n_jb
_1*cos(theta))^2))
        F_x_jb_1` = 2*integral(p_jb_1`*R_sh*L_jb_tot*sin(theta),theta,0,pi)
        F_y_jb_1` = 2*integral(p_jb_1`*R_sh*L_jb*cos(theta),theta,0,pi)
        DELTAF_jb` = F_x_jb_1` - F_x_jb_0`
        k_tan_jb` = DELTAF_jb`/DELTAe
}
        k_tan_jb = 6*omega*pi*mu_bearing*L_jb_tot*R_sh^3/c_jb^3
```

```
            k_tan_jb` = k_tan_jb/omega

            "Seal"
            n_seal_1 = e_1/c_seal
            $IF sealtype$='plain'
{           This method uses pressure distribution about shaft - same result as equations when
small offset
            p_1` =
mu_bearing*R_sh_2^2/c_seal^2*((6*n_seal_1*sin(theta)*(2+n_seal_1*cos(theta)))/((2+n_seal_1
^2)*(1+n_seal_1*cos(theta))^2))
            F_x_seal_1` = 2*integral(p_1`*R_sh_2*L_seal*sin(theta),theta,0,pi)
            F_y_seal_1` = 2*integral(p_1`*R_sh_2*L_seal*cos(theta),theta,0,pi)
            DELTAF_seal` = F_x_seal_1` - F_x_seal_0`
            k_tan_seal` = DELTAF_seal`/DELTAe
}
            k_tan_seal = 6*omega*pi*mu_bearing*L_seal*R_sh_2^3/c_seal^3
            k_tan_seal = k_tan_seal`*omega
            $ENDIF
            $IF sealtype$='labyrinth'
            {DUPLICATE j=1,N_groove}
            F_tan_seal` = N_land*(mu_bearing*R_sh_2*w_land^3/(4*c_land^2))*((pi*n_seal_1)/(1-
n_seal_1^2)^(3/2))
            k_tan_seal` = F_tan_seal`/DELTAe
            $ENDIF

            "Thrust Bearing"
            n_tb_1 = e_1/c_tb
            F_tan_tb_1` = (mu_bearing*R_tb*th_tb^3/(4*c_tb^2))*((pi*n_tb_1)/(1-n_tb_1^2)^(3/2))
            DELTAF_tb` = F_tan_tb_1` - F_tan_tb_0`
            k_tan_tb` = DELTAF_tb`/DELTAe

C_damp = 12*pi*mu_bearing*L_jb_tot*R_sh^3/c_jb^3

k_r_des = (k_tan_tb` + k_tan_seal`)/k_tot`"ratio of added (non-jb) destabilizing stiffness to total
tangential stiffness"

k_tot` = k_tan_jb`+k_tan_seal`+k_tan_tb`

F_stiff = k_tot`*OMEGA_th*e_1
F_damp = C_damp*omega_n*e_1
F_stiff = F_damp

omega_n = omega_n_Hz*convert(Hz,rad/s)
OMEGA_th_Hz = OMEGA_th*convert(rad/s,Hz)
WFR = omega_n/OMEGA_th

"=========================================================================="
"NATURAL FREQUENCY OF SHAFT AND THRUST BEARING"

"1st bending frequency from table taken from SolidWorks/COSMOS calculations"
N_b = INTERPOLATE2D('Natural Frequency','L_s','a','1st Bending
Frequency','L_s'=L_sh_e,'a'=a_e)

$ENDIF  "ends threshold speed model"
```

```
"=========================================================================="
"FRICTION MODEL"
$IF FRICTIONMODEL$ = 'on'

rho_bearing = density(helium, T=T_bearing,P=P_H)      "density of helium in bearings"
nu_bearing = mu_bearing/rho_bearing                   "kinematic viscosity of helium in
bearings"

"--------------------------------------------------------------------------------------------------------------------------"
"Shaft"
T_f_s = (pi/4)*(mu_bearing*omega*(L_sh-2*L_jb)*D_sh^3)/c_sh   "shaft frictional torque"

"--------------------------------------------------------------------------------------------------------------------------"
"Journal Bearings"

R_He = R/M_He                          "helium gas constant"
M_He = molarmass(Helium)               "helium molecular mass"
R = R#                                 "univeral gas constant"

T_f_jb = (pi/4)*(mu_bearing*omega*2*L_jb*D_sh^3)/c_jb      "frictional torque from journal
bearings"

"--------------------------------------------------------------------------------------------------------------------------"
"Thrust bearing"

N_Re = omega*R_tb^2/nu_bearing   "rotational Reynolds number"
N_Re_crit = 310000               "Reynolds number at transition to turbulent"
s\a = 0.08                       "assumed spacing ratio, axial clearance/bearing radius"

s\a_III_IV = -0.006*ln(N_Re)+0.1206 "Equation for line separating regime III from regime IV (s\a
vs N_Re)"
s\a_II_III = 0.0085*ln(N_Re)-0.0622  "Equation for line separating regime II from regime III (s\a
vs N_Re)"
s\a_I_II = -0.0113*ln(N_Re)+0.1363  "Equation for line separating regime I from regime II (s\a vs
N_Re)"
s\a_I_III = s\a_I_II            "Equation for line separating regime I from regime III (s\a vs
N_Re)"

C_mo_I = pi/(s\a*(omega*a^2/nu_bearing))*IF(s\a,s\a_I_II,1,1,0)          "torque coefficient for
regime I"
C_mo_II =
1.85*(s\a)^0.1/(omega*a^2/nu_bearing)^0.5*IF(N_Re,N_Re_crit,1,1,0)*IF(s\a,s\a_II_III,0,0,1)*IF(
s\a,s\a_I_II,0,0,1)  "torque coefficient for regime II"
C_mo_III =
0.04/(s\a^(1/6)*(omega*a^2/nu_bearing)^0.25)*IF(s\a,s\a_III_IV,1,1,0)*IF(s\a,s\a_II_III,1,1,0)*IF(
s\a,s\a_I_III,0,0,1) "torque coefficient for regime III"
C_mo_IV = 0.051*(s\a^0.1)/(omega*a^2/nu_bearing)^0.2
          *IF(N_Re,N_Re_crit,0,0,1)*IF(s\a,s\a_III_IV,0,0,1)   "torque coefficient for regime IV"

C_mo = C_mo_IV+C_mo_III+C_mo_II+C_mo_I
C_mo = T_f_tb/((rho_bearing/2)*omega^2*a^5)      "moment coefficient to torque relation"

"--------------------------------------------------------------------------------------------------------------------------"
```

```
"Seal"
$IF sealmodel$='on'
$IF massflowrate$ = 'on'
        $IF sealtype$='labyrinth'
        duplicate i = 1,N_groove
        T_f_seal[i] =  (pi/4)*(mu_land[i]*omega*w_land*D_sh^3)/c_seal
        end
        T_f_seal = SUM(T_f_seal[i],i=1,N_groove)
        $ENDIF
        $IF sealtype$='plain'
                $IF thermal$='on'
                mm = 200
                DUPLICATE i=1,mm
                T_f_seal[i] = (pi/4)*(mu_seal[i]*omega*DELTAx*D_sh^3)/c_seal
                END
                T_f_seal = SUM(T_f_seal[i],i=1,mm)
                $ELSEIF
                T_f_seal = (pi/4)*(mu_seal_avg*omega*L_seal*D_sh^3)/c_seal
                $ENDIF
        $ENDIF
$ENDIF
$ENDIF

$IFNOT massflowrate$ = 'on'
T_f_seal = (pi/4)*(mu_seal_avg*omega*2*L_seal*D_sh^3)/c_seal
$ENDIF


"-----------------------------------------------------------------------------------------------------------------------------------------"
"Overall torques & power dissipated"
T_f = T_f_jb + T_f_tb + T_f_s + T_f_seal   "total frictional torque"
{T_tot = T_f + T_alt                       "total torque, T_alt = torque from alternator"}
W_dot_f_jb = T_f_jb*omega                        "frictional power disipated at journal bearings"
W_dot_f_tb = T_f_tb*omega                        "frictional power disipated at thrust bearing"
W_dot_f_seal = omega*T_f_seal              "frictional power disipated at seal"
W_dot_f = T_f*omega                   "total frictional power disipated"
{W_dot_alt = T_alt*omega                   "power dissipated by turboalternator"}
W_dot = W_dot_alt + W_dot_f

$ENDIF              "Ends Friction Model"

$ENDIF          "Ends Rotor Dynamic Analysis"
```

Appendix B: Turboalternator Model EES Code

```
"!*****************************************************************************************************************"
"-----------------------------------------------------------------------------------------------------------------"
"!<<<<<<<<<<<<<<<<<<<<<<<<<<TURBOALTERNATOR MODEL>>>>>>>>>>>>>>>>>>>>>>>>"
"-----------------------------------------------------------------------------------------------------------------"
"!*****************************************************************************************************************"

A_c_st = pi*D_st^2/4    "radial cross-sectional area of stator pole"
Per_st = pi*D_st        "perimeter of stator pole"

L_shl = L_shl_e*convert(in,m)
A_c_lip = pi*D_st_lip^2/4                   "radial cross-sectional area of stator pole lip"
L_shl = D_st                                "axial lenght of stator shell"

c_bar_g_2 = (R_shl_i^2/D_st_lip)*arcsin(D_st_lip/(2*R_shl_i))-(1/2)*sqrt(R_shl_i^2-
(D_st_lip/2)^2)  "average air gap length between shell and pole"
c_g_2 = R_shl_i - sqrt(R_shl_i^2-(D_st_lip/2)^2)        "maximum clearance between shell and
pole (at center of pole)"
A_shl = arcsin(D_st_lip/D_shl_i)*D_shl_i*L_shl

LTSHL = arcsin(D_st_lip/D_shl_i)*D_shl_i
LCHECK = R_shl_i - (c_g_2+L_st_lip+L_st_rad+c_g_1+R_rot)

"//////////////"
"Air gap between rotor and stator"

th_sh_e = (D_sh_e/2-D_rot_e/2)
D_sh_e = 2*R_sh_e

c_bar_g_1 = {R_rot*(1-pi/4)+c_g_1}   c_g_1                  "average rotor/stator air gap,
assumes shaft material equal permeability as free space"
c_g_1 = R_shl_i - (c_g_2 + L_st_lip + L_st_rad + R_rot)

D_bar_rot = pi*D_rot/4          "average flux path length through magnet"

"Maximum number of windings"
gamma = 0.7                     "packing factor"
N_max = gamma*L_st_rad/D_wire
N_winds = {TRUNC(N_max)}35      "number of turns of wire per layer stator pole"
m = 4                           "number of layers of windings per stator pole"

"Magnet properties"
$IF magnet$ = 'N2880'
B_max = 1 [T]                   "maximum flux density"
H_max = 10000[Oe]*convert(Oe,A/m)           "maximum magnetic field intensity"
$ENDIF
$IF magnet$ = 'N4065'
B_max = 1.3 [T]                 "maximum flux density"
H_max = 11500[Oe]*convert(Oe,A/m)           "maximum magnetic field intensity"
$ENDIF
$IF magnet$ = 'N5064'
```

```
B_max = 1.5 [T]                 "maximum flux density"
H_max = 14000[Oe]*convert(Oe,A/m)
$ENDIF
$IF magnet$ = 'Cryo'
B_max = 13450[Gauss]*convert(Gauss,Tesla) "maximum flux density"
H_max = 14050[Oe]*convert(Oe,A/m)         "maximum magnetic field intensity"
$ENDIF

B_m = B_max - H*B_max/H_max     "flux density - magnetic field intensity relation"
phi_m = B_m*A_m                 "flux from magnet"
F_m = D_bar_rot*H               "magnetomotive force from magnet"
phi_m = F_m/Rel_eq              "flux from magnet"
A_m = L_rot*D_rot               "axial cross-section area of magnet"

phi_st = phi_m*Rel_eq/Rel_eq_st         "flux through stator"
V_rms = (2*N_winds*m)*omega*phi_st/sqrt(2)   "rms voltage output"

"Reluctance Calculations"
Rel_rod = L_st_rad/(mu_ferrite*A_c_st)          "reluctance of stator rod"
Rel_shl_half = (pi*D_shl_i+0.5*th_shl)/(2*mu_ferrite*L_shl*th_shl)"reluctance of half of stator
shell"
Rel_g_1 = c_bar_g_1/(mu_0*(A_c_st+A_c_st)/2)          "reluctance of rotor-stator air gap"
Rel_g_2 = c_bar_g_2/(mu_0*(A_shl+A_c_st)/2)           "reluctance of shell-pole air gap"
Rel_loss_half = (D_rot+c_g_1)/(mu_0*L_rot*c_g_1)      "reluctance of half of bypass path"
Rel_eq_shl = Rel_shl_half/2                 "equivalent reluctance of shell halves in parallel"
Rel_eq_loss = Rel_loss_half/2               "equivalent reluctance of loss paths in parallel"
Rel_eq_st = 2*(Rel_rod + Rel_g_1 + Rel_g_2) + Rel_eq_shl  "equivalent reluctance of stator
assembly"

Rel_eq = (1/Rel_eq_st + 1/Rel_eq_loss)^(-1)         "equivalent reluctance seen by magnet"

"From experiment"
duplicate i = 1,18
V_rms[i] = lookup('7_29 data',i, 'V_out_amp')*convert(millivolt,Volt)/sqrt(2)   "rms voltage for a
given speed"
Speed[i] = lookup( '7_29 data',i,'shaft speed')
END

"!Power calculations"

"Inductance"
L = (2*N_winds*m)^2/Rel_eq          "inductance of a magnetic circuit"
Z_L = omega*L                       "inductive impedance"

"Resistance"
rho_Tref = 1.68e-6[ohm]*0.01[m]     "resistivity of copper at reference temperature"
alpha = 0.0039 [C^-1]               "temperature coefficient"
T_ref = converttemp(C,K,20)         "reference temperature"

rho_e = rho_Tref*(1+alpha*(T_room^2-T_bearing^2)/(2*(T_room-T_bearing))-
alpha*T_ref)"resistivity of copper wire leads between Tc and Tw"
rho_c = rho_Tref*(1+alpha*(T_bearing-T_ref))  "resistivity at cold temperature (60K)"
rho_w = rho_Tref*(1+alpha*(T_room-T_ref))     "resistivity at room temperature (295K)"
```

```
R_lead_dc = 2*rho_e*l_lead/(pi*D_wire^2/4)          "resistance of lead (2 poles)"
R_winding_dc = (2*N_winds*m)*Per_st*rho_c/(pi*D_wire^2/4)      "resistance of windings (2 poles)"


"Winding eddy current loss (proximity effect only)"
R_winding_ac/R_winding_dc = xi/2*((sinh(xi)+sin(xi))/(cosh(xi)-cos(xi)))
xi = sqrt(pi)/2*d_wire/delta
delta = 1/sqrt(pi*N_Hz*mu_cu*sigma_cu)
sigma_cu = 1/rho_e
mu_cu = mu_0*(1+chi_m_cu)
chi_m_cu = -0.98e-5

R_winding_ac_layers = R_winding_dc*xi|star*((sinh(2*xi|star)+sin(2*xi|star))/(cosh(2*xi|star)-cos(2*xi|star))+2/3*(m^2-1)*((sinh(2*xi|star)-sin(2*xi|star))/(cosh(2*xi|star)+cos(2*xi|star))))
xi|star = xi*sqrt(eta)
eta = N_winds

R_eq  = R_lead_dc +R_load+R_winding_ac_layers "equivalent resistance of potentiometer, leads, and windings (2 poles)"
Z = sqrt(R_eq^2+(Z_L)^2)          "total impedance (2 poles)"

V_rms = Z*I_rms               "single phase rms current"
W_dot_alt_2 = 3*I_rms*V_rms
W_dot_load = 3*I_rms^2*R_load             "total work dissipated by resistor (6 poles) "
W_dot_alt = W_dot_load + W_dot_loss     "total power dissipated by turboalternator (6 poles)"

"Losses "
W_dot_gen = 3*I_rms^2*(R_lead_dc+R_winding_ac_layers)        "power lost to heat generation in windings and leads"
W_dot_heatleak =(T_0-T_bearing)*k_('Copper', T_bearing)*pi*D_wire^2/(4*L_lead)"power lost to heat leak through windings"

"Core loss"
B_st = phi_st/A_c_st          "flux density in stator poles"
B_st_kgauss = B_st*convert(Tesla,gauss)/1000      "pole flux density in kgauss"
V_st = 6*(A_c_st*L_st_rad)        "combined volume of stator poles"

A_c_shl = L_shl*th_shl        "cross sectional area of stator shell"
B_shl = phi_st/A_c_shl        "flux density in stator shell"
B_shl_kgauss = B_shl*convert(Tesla,gauss)/1000   "stator shell flux density in kgauss"
V_shl = pi*((D_shl_i+th_shl)^2-D_shl_i^2)/4*L_shl   "volume of stator shell"

V_st_total = V_st + V_shl          "total volume of stator"

$IF ferrite$ = '5000'             "Power loss if using 5000 series ferrite"
P_c_st_mW\cc = (0.08*N_kHz^1.39*B_st_kgauss^2.91)
P_c_shl_mW\cc = (0.08*N_kHz^1.39*B_shl_kgauss^2.91)
$ENDIF

$IF ferrite$ = '7000'             "Power loss if using 7000 series ferrite"
P_c_st_mW\cc = (0.147*N_kHz^1.34*B_st_kgauss^2.54)
P_c_shl_mW\cc = (0.147*N_kHz^1.34*B_shl_kgauss^2.54)
$ENDIF
```

```
P_c_st = P_c_st_mW\cc*convert(milliW/cm3,W/m3)       "Power loss conversion to W per m3"
P_c_shl = P_c_shl_mW\cc*convert(milliW/cm3,W/m3)


W_dot_st = P_c_st*V_st                  "power loss in stator poles"
W_dot_shl = P_c_shl*V_shl               "power loss in stator shell"

W_dot_core = W_dot_shl + W_dot_st                   "total core power loss"

V_shl_cc = V_shl*convert(m3,cm3)

W_dot_loss = W_dot_gen + W_dot_heatleak + W_dot_core   "total power loss"
efficiency = (W_dot_alt-W_dot_loss)/W_dot_alt              "efficiency of turboalternator"

flux_efficiency = phi_st/phi_m
efficiency_inc_lstflux = flux_efficiency*efficiency
```

Appendix C: Seal Model EES Code

```
"!*****************************************************************************************************************"
"-----------------------------------------------------------------------------------------------------------------"
"!<<<<<<<<<<<<<<<<<<<<<<<<<<<<<<SEAL MODEL>>>>>>>>>>>>>>>>>>>>>>>>>>>>>"
"-----------------------------------------------------------------------------------------------------------------"
"!*****************************************************************************************************************"

$IF setMassflowrate$ = 'on'
leak = mset
m_dot_leak = mset
$ELSE
m_dot_leak = m_dot
$ENDIF

$IF sealtype$='labyrinth'
L\D_seal = w_land/D_sh
$ENDIF

$IF sealtype$='plain'
L\D_seal = L_seal/D_sh
$ENDIF

$IF SealModel$ = 'on'
m_dot_r = m_dot_leak/m_dot_turb

"Constants"
DP_total = DELTAP

"determine seal thickness depending on pressure vessel stresses"
sigma_hoop = P_seal_avg*(R_sh_2+c_seal+h_t)/h_c     "hoop stress in seal"
sigma_hoop = strain*E                               "determine strain in seal"
E = 110E9[Pa]                                       "modulus of elasticity"
DELTAc_seal = (R_sh_2+c_seal+h_t)*strain            "change in seal clearance due to pressure"
{sigma_y = 9.1E8[Pa]
SF = sigma_y/sigma_hoop}
Perc_cseal = DELTAc_seal/c_seal*100                 "percent change from nominal seal
clearance"

A_t = pi*((R_sh_2+c_seal+h_t+h_c)^2-(R_sh_2+c_seal)^2)          "solid cross sectional area of
toothed section"
A_g = pi*((R_sh_2+c_seal+h_t+h_c)^2-(R_sh_2+c_seal+h_t)^2)  "solid cross sectional area of
grooved section"
A_sh = pi*R_sh_2^2                                          "solid cross sectional area of shaft"
DELTAx = L_seal/m                                           "length between grid points"

m_dot_g\s = m_dot_leak*convert(kg/s,g/s)

"-----------------------------------------------------------------------------------------------------------------"
"!Helium leakage rate through seal"
"-----------------------------------------------------------------------------------------------------------------"
$IF MassFlowRate$ = 'on'
```

```
P=P_seal_avg            "nominal pressure (Pa)"

Ac_land=pi*D_shaft*c_land       "cross-sectional area for flow in the land(s)"
Dh_land=2*c_land                "hydraulic diameter of the land(s)"
m_dot=m_dot_gps*convert(g/s,kg/s)
m_dot_mgs = m_dot*convert(kg/s,mg/s)

$IF sealtype$='labyrinth'

"Calculations"

A_c_seal_avg = (A_t*N_land*w_land + A_g*N_groove*w_groove)/L_seal

"Average temperature and position of the grooves and the lands"
duplicate i=1,N_groove
        x_groove[i]=L_seal*i/(N_groove+1)
        x_groove2[i] = w_groove/2+(i-1)*w_groove+i*w_land
end
x_land[1]=w_land/2
duplicate i=2,N_land
        x_land[i]=x_land[i-1]+w_land+w_groove
        x_land2[i] = w_land/2 + (i-1)*(w_land+w_groove)
end

duplicate i=1,N_land
        xx[i] = ROUND((x_land[i]/L_seal)*m)
end


CALL
LABSEALTEMP(N_groove,N_land,w_groove,w_land,L_seal,T[0..200]:T_groove[1..N_groove],T
_land[1..N_land])


"Average properties within each groove and land"
duplicate i=1,N_groove
        mu_groove[i]=viscosity(f$,T=T_groove[i],P=P)
        rho_groove[i]=density(f$,T=T_groove[i],P=P)
end
duplicate i=1,N_land
        mu_land[i]=viscosity(f$,T=T_land[i],P=P)
        rho_land[i]=density(f$,T=T_land[i],P=P)
end

"viscous pressure drop"
duplicate i=1,N_land
        v_land[i]=m_dot/(Ac_land*rho_land[i])
        Re_land[i]=v_land[i]*Dh_land*rho_land[i]/mu_land[i]
        w_land_plus[i]=w_land/(Dh_land*Re_land[i])
        f_land[i]=3.44/(Re_land[i]*sqrt(w_land_plus[i]))+(24+0.674/(4*w_land_plus[i])-
3.44/sqrt(w_land_plus[i]))/(Re_land[i]*(1+0.00029/w_land_plus[i]^2))
        DP_land[i]=rho_land[i]*v_land[i]^2*f_land[i]*w_land/(Dh_land*2)
end
```

```
"inertial pressure drop"
K_c_inlet=K_c(0)
rho_inlet=density(f$,T=T_turb_out,P=P_c)
v_inlet=m_dot/(Ac_land*rho_inlet)
DP_inlet=K_c_inlet*rho_inlet*v_inlet^2/2
Dh_groove=2*((D_shaft/2+c_land+d_groove)^2-
(D_shaft/2)^2)/((D_shaft/2+c_land+d_groove)+(D_shaft/2))
K_c_groove=K_c(Dh_land/Dh_groove)
K_e_groove=K_e(Dh_land/Dh_groove)
duplicate i=1,N_groove
        v_groove[i]=m_dot/(Ac_land*rho_groove[i])
        DP_groove[i]=(K_c_groove+K_e_groove)*rho_groove[i]*v_groove[i]^2/2
end
K_e_exit=K_e(0)
rho_exit=density(f$,T=T_bearing,P=P_w)
v_exit=m_dot/(Ac_land*rho_exit)
DP_exit=K_e_exit*rho_exit*v_exit^2/2

DP_total=DP_inlet+sum(DP_land[1..N_land])+sum(DP_groove[1..N_groove])+DP_exit

$ENDIF  "ends grooved seal mass flow model"

$IF sealtype$='plain'
A_c_seal_avg = pi*((R_sh_2+c_seal+h_c)^2-(R_sh_2+c_seal)^2)/2
"viscous pressure drop"
{w_land = L_seal}
v_land = m_dot/(Ac_land*rho_seal_avg)
Re_land=v_land*Dh_land*rho_seal_avg/mu_seal_avg
w_land_plus=L_seal/(Dh_land*Re_land)
f_land=3.44/(Re_land*sqrt(w_land_plus))+(24+0.674/(4*w_land_plus)-
3.44/sqrt(w_land_plus))/(Re_land*(1+0.00029/w_land_plus^2))
DP_land =rho_seal_avg*v_land^2*f_land*L_seal/(Dh_land*2)
"inertial pressure drop"
K_c_inlet=K_c(0)
rho_inlet=density(f$,T=T_turb_out,P=P)
v_inlet=m_dot/(Ac_land*rho_inlet)
DP_inlet=K_c_inlet*rho_inlet*v_inlet^2/2
{Dh_groove=2*((D_shaft/2+c_land+d_groove)^2-
(D_shaft/2)^2)/((D_shaft/2+c_land+d_groove)+(D_shaft/2))
K_c_groove=K_c(Dh_land/Dh_groove)}
{K_e_groove=K_e(Dh_land/Dh_groove)}
{duplicate i=1,N_groove
        v_groove[i]=m_dot/(Ac_land*rho_groove[i])
        DP_groove[i]=(K_c_groove+K_e_groove)*rho_groove[i]*v_groove[i]^2/2
end}
K_e_exit=K_e(0)
rho_exit=density(f$,T=T_bearing,P=P)
v_exit=m_dot/(Ac_land*rho_exit)
DP_exit=K_e_exit*rho_exit*v_exit^2/2

DP_total=DP_inlet+DP_land+DP_exit

{cP=cP(f$,T=(T_turb_out+T_bearing)/2,P=P)
q_dot=m_dot*cP*(T_bearing-T_turb_out}
```

```
$ENDIF  "ends plain seal mass flow model"

$ENDIF  "ends mass flow rate calculation"

"-----------------------------------------------------------------------------------------------------------------------"
"!Heat Transfer Through Seal"
"-----------------------------------------------------------------------------------------------------------------------"
$IF thermal$ = 'on'

$IF turbinemodel$ = 'off'
{T_turb_in = 10[K]}
$ENDIF

"Calculations"

"Generation from seal friction (g_dot)"
$IF sealtype$ = 'labyrinth'
mx = m/N_groove
DUPLICATE i = 1,N_groove
        gx[i] = T_f_seal[i]*omega/mx
        sx[i] = ROUND(1+(i-1)*mx)
        ex[i] = ROUND(i*mx)
        DUPLICATE j=sx[i],ex[i]
                g_dot[j] = gx[i]
        END
END
$ENDIF

$IF sealtype$ = 'plain'
DUPLICATE i = 1,m
g_dot[i] = T_f_seal[i]*omega
END
$ENDIF

"Boundary Conditions"
"At cold end"
P_seal[0] = P_L
T[0] = T_turb_in
x[0] = 0
rho[0] = density(helium,P=P_L,T=T[0])
C_p[0] = specheat(helium,P=P_L,T=T[0])

x[1] = DELTAx
k_shaft[1] =k_(ShaftMaterial$,T[1])
k_case[1] = k_(CaseMaterial$,T[1])

q_RHS[1] = (k_shaft[1]*A_sh+k_case[1]*A_c_seal_avg)*((T[2]+T[1])/2-(T[1]+T[0])/2)/DELTAx
q_LHS[1] = (k_shaft[1]*A_sh+k_case[1]*A_c_seal_avg)*(T[0]-(T[1]+T[0])/2)/(DELTAx/2)
q_He[1] = m_dot_leak*C_p[0]*(T[0]-T[1])
q_RHS[1] + q_LHS[1] + q_He[1] + g_dot[1]= 0
P_seal[1] = P_seal[0]
rho[1] = density(helium,T=T[1],P=P_seal[1])

"At warm end"
```

```
P_seal[m] = P_Bearing
T[m] = T_bearing
x[m] = L_seal
rho[m] = density(helium,P=P_bearing,T=T_bearing)
C_p[m] = specheat(helium,P=P_bearing,T=T[m])
k_shaft[m] =k_(ShaftMaterial$,T[m])
k_case[m] = k_(CaseMaterial$,T[m])
q_LHS[m] = -q_RHS[m-1]
q_He[m] =  m_dot_leak*C_p[m]*(T[m-1]-T[m])
q_RHS[m] + q_LHS[m] + q_He[m] + g_dot[m]= 0

"Internal Nodes"
DUPLICATE i=2,m-1
        x[i] = DELTAx*i
        k_shaft[i] =k_(ShaftMaterial$,T[i])
        k_case[i] = k_(CaseMaterial$,T[i])
        C_p[i] = specheat(helium,T=T[i],P=P_seal[i])
        q_He[i] = m_dot_leak*C_p[i]*(T[i-1]-T[i])
        P_seal[i] = P_L- (P_L-P_bearing)*i/m        "assume linear pressure distribution"
        q_RHS[i] = (k_shaft[i]*A_sh+k_case[i]*A_c_seal_avg)*((T[i]+T[i+1])/2-(T[i]+T[i-
1])/2)/DELTAx
        q_LHS[i] = -q_RHS[i-1]
        q_LHS[i] + q_RHS[i] + q_He[i] +g_dot[i]= 0
END

Q_He_RHS = m_dot_leak*enthalpy(helium,T=T[m],P=P_seal[m])
Q_He_LHS = m_dot_leak*enthalpy(helium,T=T[0],P=P_seal[0])

Q_He = abs(sum(q_He[i],i=1,m))                  "sum of change in energy of helium of nodes"
Q_He2 = {abs(Q_He_LHS - Q_He_RHS)}abs(m_dot_leak*(C_p[0]*T[0]-C_p[m]*T[m]))    "overall
change in energy of helium"
Q_cond = abs(q_LHS[1]+q_RHS[m] )            "overall change in conductive energy"

heatleak = -q_LHS[1]        "!heat leak to turbine side - important variable"

DUPLICATE i = 0,m
        x_cm[i] = x[i]*convert(m,cm)
        mu_seal[i] = viscosity(f$,T=T[i],P=P_seal[i])
        rho_seal[i] =density(f$,T=T[i],P=P_seal[i])
END

mu_seal_avg = average(mu_seal[0..m])
rho_seal_avg =average(rho_seal[0..m])
P_seal_avg =  average(P_seal[0..m])

$ENDIF          "Ends Seal Thermal Model"
$ENDIF          "Ends Overall Seal Model"
```

Appendix D: Supplementary Models EES Code

```
"!*****************************************************************************************************************"
"-----------------------------------------------------------------------------------------------------------------"
"!<<<<<<<<<<<<<<<<<<<<<<<<<<RECUPERATOR  MODEL>>>>>>>>>>>>>>>>>>>>>>>>>>"
"-----------------------------------------------------------------------------------------------------------------"
"!*****************************************************************************************************************"

$IF Recuperator$ = 'on'

"Use UA from constant Cp and break apart into control volumes"
N = 250  “number of control volumes”

"Set guess values of variables in the heat exchanger by estimating a linear temperature distribution"
"Running SETGUESS$ as 'on' first may help convergence, but does not garauntee it"
$IF SETGUESS$='on'
{T_c_in = 10[K]
T_w_out = T_c_in + 0.5
DUPLICATE i = 0,N
T_c[i] = T_c_in + i/N*(T_w_in-T_c_in)
T_w[i] = T_c[i] + 0.5[K]
cp_c[i] = specheat(F$,T=T_c[i],P=P_L)
cp_w[i] = specheat(F$,T=T_w[i],P=P_H)
C_c[i] = m_dot_c*cp_c[i]
C_w[i] = m_dot_w*cp_w[i]
C_min[i] = min(C_c[i],C_w[i])
C_max[i] = max(C_c[i],C_w[i])
C_r[i] = C_min[i]/C_max[i]-0.1
END
$UPDATEGUESS}
$ENDIF

$IF SETGUESS$ = 'off'

m_dot_c = m_dot_w - m_dot_leak
m_dot_w = m_dot_turb
T_w_in = T_bearing

"Find UA, q_dot  from constant property, temperature averaged model"

        P_avg = average(P_L,P_H)
        T_avg = average(T_c_in,T_w_in)
        Cpc = specheat(f$,T=T_avg,P=P_L)
        Cpw = specheat(f$,T=T_avg,P=P_H)
        C =  m_dot_w*MIN(Cpc,Cpw)
        C_r = MIN(Cpc,Cpw)/MAX(Cpc,Cpw)
        CALL plainHX(T_w_in,T_c_in,P_H,P_L,m_dot_w:epsilon_hx,R_ac)
        NTU = NTUi(epsilon_hx,C_r,log)
        NTU = UA_constcp/C
        q_dot = epsilon_hx*C*(T_w_in-T_c_in)
```

```
        epsilon2 = q_dot/(m_dot_w*(enthalpy(f$,T=T_w_in,P=P_H)-
enthalpy(f$,T=T_c_in,P=P_L)))
        log = (abs(epsilon_hx-1)/MAX(0.000001,abs(epsilon_hx*C_r-1)))



T_c_in = {T_turb_out}T_afterload      "T_afterload accounts for load, T_turb_out does not"

T_w[N] = T_w_in
T_c[0] = T_c_in

duplicate i = 1,N
q_dot[i] = q_dothx/N                          "equal heat transfer in each control volume (CV)"
cp_c[i] = specheat(F$,T=T_c[i-1],P=P_L)  "specific heat of cold stream entering CV"
cp_w[i] = specheat(F$,T=T_w[i],P=P_H)    "specific heat of warm stream entering CV"
C_c[i] = m_dot_c*cp_c[i]                      "cold stream capacitance rate enterine CV"
C_w[i] = m_dot_w*cp_w[i]                      "warm stream capacitance rate enterine CV"
C_min[i] = min(C_c[i],C_w[i])                 "minimum capacitance rate"
C_max[i] = max(C_c[i],C_w[i])                 "maximum capacitance rate"
C_r[i] = C_min[i]/C_max[i]                    "capacitance ratio"
NTU[i] = UA[i]/C_min[i]                       "NTU as function of UA and C_min"
NTU[i] = NTUi(C_r[i],epsilon_hx[i],log[i])    "NTU as a function of epsilon and Cr - determine
epsilon"
log[i] = (abs(epsilon_hx[i]-1)/MAX(0.0001,abs(epsilon_hx[i]*C_r[i]-1)))"variable given to NTU
function for quicker convergence"
q_dot[i] = epsilon_hx[i]*C_min[i]*(T_w[i]-T_c[i-1])
q_dot[i] = c_c[i]*(T_c[i]-T_c[i-1])           "determine node cold stream exit temperature"
q_dot[i] = c_w[i]*(T_w[i]-T_w[i-1])           "determine node warm stream exit temperature"
q_dot_max[i] = C_min[i]*(T_w[i] - T_c[i-1]) "max heat transfer for CV"
node[i] = i/N                                 "CV number"
DELTAT[i] = T_w[i]-T_c[i]
end

UA_constcp = sum(UA[i],i=1,N)                 "constrain total UA to be same as plain model"
DELTAT[0] = T_w[0] - T_c[0]
node[0] = 0

DELTAT_pinch = min(DELTAT[0..N])         "Pinchpoint temperature difference"

"Minimum and maximum epsilon and C_r values to facilitate guess values and limits, not
significant output variables"
epsilon_min = min(epsilon_hx[1..N])
epsilon_max = max(epsilon_hx[1..N])
epsilon_avg = average(epsilon_hx[1..N])
C_r_min = min(C_r[1..N])
C_r_max = max(C_r[1..N])
C_r_avg = average(C_r[1..N])

T_c_out = T_c[N]
T_w_out= T_w[0]
UA_check = sum(UA[i],i=1,N)

$UPDATEGUESS
```

```
m_dot_c*(h_out_hx-h_in_hx) = q_dot_ch
h_in_hx = enthalpy(helium,T=T_c[0],P=P_L)
h_out_hx = enthalpy(helium,T=T_c[N],P=P_L)

q_dot_max = m_dot_turb*(enthalpy(f$,T=T_w_in,P=P_H)-enthalpy(f$,T=T_c_in,P=P_L))
q_dot_max2 = SUM(q_dot_max[i],i=1,N)
epsilon_overall = q_dothx/q_dot_max

q_dot_ac = (T_c_out - T_c_in)/R_ac
h_c_in_ac = h_c_in + q_dot_ac/m_dot_c
h_c_in = enthalpy(f$,T=T_c_in,P=P_L)
T_c_in_ac =  temperature(f$,P=P_L,h=h_c_in_ac)
DT = T_c_in_ac - T_c_in

h_w_out = enthalpy(f$,T=T_w_out,P=P_H)
h_w_out_ac = h_w_out + q_dot_ac/m_dot_w
h_w_out_ac = enthalpy(f$,P=P_H,T=T_w_out_ac)

h_c[0] = enthalpy(f$,T=T_w[0],P=P_L)
h_w[0] = enthalpy(f$,T=T_c[0],P=P_H)
h_c[N] = enthalpy(f$,T=T_c[N],P=P_L)
h_w[N] = enthalpy(f$,T=T_w[N],P=P_H)

 $ENDIF
$ENDIF

"!*****************************************************************************************************************"
"-----------------------------------------------------------------------------------------------------------------"
"!<<<<<<<<<<<<<<<<<<<<<<<<<TURBINE & LOAD MODEL>>>>>>>>>>>>>>>>>>>>>>>>>"
"-----------------------------------------------------------------------------------------------------------------"
"!*****************************************************************************************************************"
$IF TurbineModel$ = 'on'

P_turb_in = P_H - (P_H-P_L)*x_turb
P_turb_out = P_L
x_turb = 0

"Turbine Equations"
h_in = enthalpy(helium,T=T_turb_in,P=P_turb_in)              "inlet enthalpy"
s_in = entropy(helium,T=T_turb_in,P=P_turb_in)               "inlet entropy"
s_guess = entropy(helium,P=P_turb_out ,h=h_in)               "used to set a guess of entropy
value"
T_out_s = temperature(f$,P=P_turb_out,s=s_in)
{h_out_s = enthalpy(helium,P=P_turb_out,s=s_in)              "isentropic outlet enthalpy"}
h_out_s = enthalpy(helium,T=T_out_s,P=P_turb_out)            "isentropic outlet enthalpy"

eta_s = (h_in - h_out)/(DELTAh_s)                            "isentropic efficiency of turbine"

h_min = -1.6E6[J/kg]                                         "minimum enthalpy - for purpose of
limits"
T_turb_out_1 = temperature(helium,P=P_turb_out ,h=h_out)     "outlet temperature of turbine
without heatleak"
```

```
DELTAh = h_in - h_out                    "change in enthalpy of helium through turbine"
DELTAh_s = h_in - h_out_s                "isentropic enthalpy change"

W_dot = m_dot_turb*DELTAh                    "Shaft power"
eta_s = INTERPOLATE('Turbine Efficiency','Velocity Ratio', 'Efficiency', 'Velocity Ratio'=lambda)

u_t = R_sh_2*omega                       "turbine tip velocity, equal to shaft edge velocity"
lambda = u_t/sqrt(2*MAX(1e-4,DELTAh_s))"velocity ratio"
W_dot = omega*T_tot                      "torque produced from turbine"

"Account for heat and mass leakage"

"assuming heatleak is absorbed entirely by helium before leakage flow exits"
m_dot_turb*h_out + heatleak= (m_dot_turb - m_dot_leak)*h_out_new + m_dot_leak*h_out_new
{T_turb_out = temperature(f$,P=P_L,h=h_out_new)      "temperature out with heat leak"}
h_out_new = enthalpy(f$,P=P_turb_out,T=T_turb_out)   "determine temperature out w/ heatleak
- more stable"

"load"
m_dot_load = m_dot_turb-m_dot_leak
m_dot_load*h_out_new + q_dot_load = m_dot_load*h_afterload
h_afterload = enthalpy(f$,T=T_afterload,P=P_turb_out)

$ENDIF
```

Appendix E: Subprograms and Functions

```
"=========================================================="
"!-----------------------------SUBPROGRAMS-----------------------------------"
"=========================================================="

"Recuperator performance for constant fluid properties"

SUBPROGRAM plainHX(T_h_in,T_c_in,P_high,P_low,m_dot_total:eff_HX_nac,Raxial)

"Operating Conditions"

gas$ = 'helium'                    "fluid"
plate$ = 'copper'                  "Plate material"
spacer$ = 'Stainless_AISI304'      "Spacer material"

"Geometry"
w_f_e = 0.0088[in];     w_f = w_f_e*convert(in,m)        "width of copper between slots"
w_s_e = 0.0072[in];     w_s = w_s_e*convert(in,m)        "width of slot"
w_bf_e = 0.11[in]; w_bf = w_bf_e*convert(in,m)           "width of material between fin rows"
L_f_e = 0.11[in];       L_f = L_f_e*convert(in,m)        "length of slots"
t_p_e = 0.008[in];  t_p = t_p_e*convert(in,m)            "thickness of plat"
t_sp_e = 0.014[in];     t_sp = t_sp_e*convert(in,m)      "thickness of spacer"
w_sp_e = 0.04[in];w_sp = w_sp_e*convert(in,m)            "width of spacer"
w_p_e = 0.04[in];  w_p = w_p_e*convert(in,m)             "width of plate material around spacers"
N_f = 32                                                 "number of fins in each row"
N_fr = 30                                                "rumber of fin rows"
N_p = 1000                                               "number of plates"
N_module = 1                                             "number of HX modules"

AR_slot = MAX(t_p,w_s)/MIN(t_p,w_s)                      "aspect ratio of slot through metal"
AR_fin = MAX(t_p,w_f)/MIN(t_p,w_f)                       "aspect ratio of fin material"
AR_slot_l = MAX(L_f,w_s)/MIN(L_f,w_s)                    "slot aspect ratio length-wise"
AR_spacer = MAX(w_sp,t_sp)/MIN(w_sp,t_sp)                "aspect ratio of spacer"
AR_HX = MAX(A_HX,B_HX)/MIN(A_HX,B_HX)                    "aspect ratio of heat exchanger"

"Braze Geometry"
L_fillet_e = 0.005[in];    L_fillet = L_fillet_e*convert(in,m)  "length scale of the fillet (along spacer
wall)"

"Calculations"
T_avg = (T_h_in+T_c_in)/2
P_avg = (P_high+P_low)/2
A_HX = 2*N_f*(w_s+w_f)+3*w_sp+4*w_p
B_HX = 2*w_sp+2*w_p+N_fr*L_f+(N_fr-1)*w_bf
H_HX = (N_p+1)*t_sp+N_p*t_p
Aplate = A_HX*B_HX-2*N_f*N_fr*L_f*w_s
Vplate = Aplate*t_p
rhoplate = rho_(plate$,T_avg)
Mplate = rhoplate*Vplate
Aspacer = A_HX*B_HX-(A_HX-3*w_sp)*(B_HX-2*w_sp)
Abraze = 2*(A_HX+B_HX)*L_fillet/2+4*(B_HX-2*w_sp)*L_fillet/2+2*(A_HX-4*w_sp)*L_fillet/2
```

```
Vspacer = Aspacer*t_sp
rhospacer = rho_(spacer$,T_avg)
Mspacer = rhospacer*Vspacer
M_HX = N_p*Mplate+(N_p+1)*Mspacer
M_HX_total = M_HX*N_module
Dhyd = L_f*w_s/(2*(L_f+w_s))
mu_g = viscosity(gas$,T=T_avg,P=P_avg)
k_g = conductivity(gas$,T=T_avg,P=P_avg)
rho_g = density(gas$,T=T_avg,P=P_avg)
cP_g = specheat(gas$,T=T_avg,P=P_avg)
Prandtl = mu_g*cP_g/k_g
k_p = k_(plate$,T_avg){kOFHCCu(T_avg)}
k_sp = k_(spacer$,T_avg){k304SS(T_avg)}
k_br = 150[W/m-K]
gamma = {cP_g/(cP_g-get_Rg(gas,T_c_in,T_h_in))}1.667
m_dot = m_dot_total/N_module
m_dot_f = m_dot/(N_f*N_fr*2)
Ac_f = N_f*N_fr*w_s*L_f
u_g = m_dot/(Ac_f*rho_g)
Re = u_g*Dhyd*rho_g/mu_g
invGz = (t_p/Dhyd)/(Re*Prandtl)
alpha = MIN(w_s,L_f)/MAX(w_s,L_f)
KNus = 1
NusNum = {Nusselt(alpha)}6.4
htc = NusNum*k_g/Dhyd
NTU_f=2*(L_f/2)*(t_p+w_f*KNus)*htc/(m_dot_f*cP_g)
beta_f = L_f*SQRT(2*htc*(t_p+KNus*w_f)/(k_p*w_f*t_p))/2
eff_f = {eff_fin(NTU_f,beta_f)}0.65
R_f =1/(eff_f*m_dot_f*cP_g)+w_bf/(2*k_p*t_p*(w_s+w_f))
mrow = SQRT(2/(R_f*(w_s+w_f)*w_bf*t_p*k_p))
Rplate =
1/(k_p*t_p*w_bf*mrow*TANH(mrow*N_f*(w_s+w_f))*N_fr)+(w_p+w_sp/2)/(N_fr*w_bf*t_p*k_p)
Rspwbr = ((L_fillet/(k_br*Abraze))^(-1)+(L_fillet/(k_sp*Aspacer))^(-1))^(-1)
Rspacer = 2*Rspwbr+(t_sp-2*L_fillet)/(k_sp*Aspacer)
NTUplate = 1/(Rplate*m_dot*cP_g)
eff_plate = 1/(2*Rplate*m_dot*cP_g)
Raxial = Rspacer*(N_p+1)
eff_HX = 1-1/(1+N_p*eff_plate/(1-eff_plate))-1/(Raxial*m_dot*cP_g)
eff_HX_nac = 1-1/(1+N_p*eff_plate/(1-eff_plate))
xplux = t_p/(Dhyd*Re)
fapp = {3.44/(Re*SQRT(xplus))+(friction(Re,alpha)*Re+0.674/(4*xplus)-
3.44/SQRT(xplus))/(Re*(1+0.000029/xplus^2))}0.67
Dp_v = 0.5*rho_g*u_g^2*fapp*t_p/Dhyd
sigma = 2*N_f*N_fr*w_s*L_f/((A_HX-3*w_sp)*(B_HX-2*w_sp))
Kc = 0.79352+0.060341*sigma-0.44822*sigma^2
Ke = 1-2.35386*sigma+0.96156*sigma^2
Dp_i = 0.5*rho_g*u_g^2*(Kc+Ke)
Dp = N_p*(Dp_i+Dp_v)
DT_rec = (T_h_in-T_c_in)*(1-eff_HX)
joint_length = 2*N_p*(3*B_HX+2*A_HX)

END
```

```
"-------------------------------------------------------------------------------------------------"
"Program to calculate journal bearing stiffness and mass flow parameters"


SUBPROGRAM jbconst(T_gas,DELTAP,Pse_gage,c_e,r_se:C_k,C_m)
"Input inlet temperature (T_gas [K]) and pressure (Pse_gage [psi]), pressure drop through
bearings (DELTAP [psi]), and bearing clearance (c_e [in])"

"! INPUT VARIABLES FOR PARAMETRIC TABLES"
"gas characteristics"
gas$='helium'                    "working fluid"
Pee_gage=Pse_gage-DELTAP  "exhaust gage pressure"

p_atm=14.7
Pse=p_atm+Pse_gage"supply pressure of gas in psi"
Pee=p_atm+Pee_gage"exhaust pressure of gas in psi"

"bearing geometry"

N=6       "number of supply holes in each row"
b_e=0.3 "bearing length in inches"
x=0.5     "location of supply holes along bearing length (ratio of position/total length, L/b) "
Epsilon=0.001      "shaft offset distance expressed as a ratio of offset distance to centered
clearance"
r_he=.004          "radius of supply holes in inches"

"! CALCULATIONS FOR MODEL"
"housing, bearing, and shaft geometry conversions to SI for model"
r_s=r_se*CONVERT(inch,m)      "shaft radius in meters"
b=b_e*CONVERT(inch,m)         "width of bearing in meters"
L=(x)*b                       "axial location of supply holes in meters"
c=c_e*CONVERT(inch,m)         "centered clearance in meters"
r_h=r_he*CONVERT(inch,m)      "supply hole radius in meters"
Pe=Pee*CONVERT(psi,Pa)        "exhaust gas pressure in Pa"
Ps=Pse*CONVERT(psi,Pa)        "supply gas pressure in Pa"
pr=Ps/Pe                      "overall pressure ratio"

L_e=(x)*b_e                   "axial location of supply holes in english units"
a_s=(2*2*PI*r_s)/N            "effective bearing pad width-rectangular for duplicate equations"
check_2=50                    "cross over point value for discharge coefficient correlation"
L_orifice=(0.02 [in])*convert(in,m)      "length of orifice (based on bearing geometry)"
D=2*r_h                       "diameter of orifice"
CD=1                          "unadjusted discharge coefficient"

"! PROPERTY CALCULATIONS"
CP=CP(gas$,T=T_gas,P=Pe)
CV=CV(gas$,T=T_gas,P=Pe)
gamma=CP/CV
mu=VISCOSITY(gas$,T=T_gas,P=Ps)
rho_gas_inlet=DENSITY(gas$,T=T_gas,P=Ps)
MM=MOLARMASS(gas$)            "molecular weight of gas"
R_gas=(R#/MM)                 "gas constant"
rcrit=(2/(gamma+1))^(gamma/(gamma-1))
```

```
"! DETERMINE MASS FLOW, STIFFNESS, AND SCALING FACTORS"
DUPLICATE i=1,N
A_h[i]={PI*r_h^2} 2*PI*r_h*h[i]              "effective area for plain jets"
theta[i]=((2*i-1)*PI)/N                      "angle between jet and line connecting bearing and
shaft centers"
theta_deg[i]=theta[i]*CONVERT(rad,degree)    "converts radians to degrees"
h[i]=c*(1-Epsilon*COS(theta[i]))             "bearing pad height"

rp[i]=pc[i]/ps
F1[i]=SQRT((gamma/(gamma-1))*((rp[i])^(2/gamma)-(rp[i])^((gamma+1)/gamma)))
m_dot_inertial_unchoked[i]=CD*(ps/(R_gas*T_gas))*A_h[i]*SQRT(2*R_gas*T_gas)*F1[i]
        "unchoked mass flow rate thru orifice"

F2[i]=SQRT((gamma/(gamma-1))*((rcrit)^(2/gamma)-(rcrit)^((gamma+1)/gamma)))
m_dot_inertial_choked[i]=CD*(ps/(R_gas*T_gas))*A_h[i]*SQRT(2*R_gas*T_gas)*F2[i]
        "choked mass flow rate thru orifice"
m_dot_inertial[i]=IF(rp[i],rcrit,m_dot_inertial_choked[i],m_dot_inertial_choked[i],m_dot_inertial_u
nchoked[i])"mass flow rate thru orifice based on rp"
m_dot_inertial[i]=m_dot_viscous[i]                                    "conservation
of mass at steady state conditions"
m_dot_viscous[i]=a_s*h[i]^3*(pc[i]^2-pe^2)/(24*mu*R_gas*T_gas*L)      "mass flow rate
in bearing bad"

pmeanv[i]=(a_s*h[i]^3*(pc[i]^3-pe^3)/(36*mu*m_dot_viscous[i]*R_gas*T_gas*L))"mean viscous
pressure in bearing pad"
pbar[i]=(L*(pmeanv[i]-pe)+(pc[i]-pe)*((b/2)-L))/(b/2)    "mean pressure elevation in bearing"
Fn[i]=pbar[i]*b*r_s*(SIN(theta[i]+PI/N)-SIN(theta[i]-PI/N))"normal restoring force"
END

corfac=1{0.8}{0.315*(((COSH((6.36*L)/(2*r_s))-1)/(SINH((6.36*L)/(2*r_s))))+(TANH(6.36*(b-
2*L)/(2*r_s))))/((b-L)/(2*r_s))    "correction factor for normal force"}
Fn_tot=corfac*SUM(Fn[i],i=1,N)
k\bearing=Fn_tot/(Epsilon*c)                  "! stiffness/bearing corrected for non
axial effects"
k\bearing_kNpm=k\bearing*CONVERT(N,kN)
m_dot\bearing=SUM(m_dot_viscous[i],i=1,N)     "! mass flow rate/bearing"
m_dot\bearing_gps=m_dot\bearing*CONVERT(kg/s,g/s)

C_m=(m_dot\bearing*mu)/(rho_gas_inlet*c^3*(Ps-Pe))   "! nondimensional mass constant"
C_k=(k\bearing)*c/((Ps-Pe)*(2*r_s)^2)                "! nondimensional stiffness constant"

END

"========================================================="
"!------------------------------FUNCTIONS-----------------------------------------"
"========================================================="
$tabstops 0.5,1
"Calculate epsilon from NTU, Cr "
Procedure eps(NTU,C_r,ex:epsilon)
        "ex = (-UA/C_min*(1-C_r))"
        If C_r < 0.99999 THEN
        ex1 = SIGN(ex)*MIN(abs(ex),1e4)
        epsilon = (1-exp(ex1))/(1-C_r*exp(ex1))
```

```
        Else
        epsilon = NTU/(1+NTU)
        Endif
END

"Calculate NTU from epsilon, Cr, log variable"
Function ntui(epsilon, C_r,log)
        If C_r > 0.999 THEN
                If (epsilon=1) THEN
                NTUi = 999    "note that this is not a realistic situation, it is meant for program
stability"
                ELSE
                NTUi = epsilon/(1-epsilon)
                ENDIF
        ELSE
        NTUi = 1/(C_r-1)*ln(MAX(1e-5,log))
        Endif
END

"Factor for sudden contraction pressure drop"
function K_c(Dr)
        if (Dr<=0.76) then
        K_c=0.42*(1-Dr^2)
        else
        K_c=(1-Dr^2)^2
        endif
end

"Factor for sudden expansion pressure drop"
function K_e(Dr)
        K_e=(1-Dr^2)^2
end

FUNCTION NEAREST(N,D)
"Round to nearest D
(ie D = 0.5 rounds to nearest half, D = 10 rounds to nearest 10)"
a = N/D
b = ROUND(a)
NEAREST = D*b
END

FUNCTION BALANCE(L_sp2)
        IF (L_sp2<=0.1) THEN
        BALANCE = 0.1
        ENDIF

        IF (L_sp2>0.1) THEN
        BALANCE = 0
        ENDIF
END

PROCEDURE SEAL(N_groove:SEALTYPE$)
        IF (N_groove=0) THEN
        SEALTYPE$ = 'plain'
```

```
        ELSE
        SEALTYPE$ = 'labyrinth'
        ENDIF
END

PROCEDURE
LABSEALTEMP(N_groove,N_land,w_groove,w_land,L_seal,T[0..200]:T_groove[1..N_groove],T
_land[1..N_land])
        m = 200
        i = 0
        REPEAT
                i = i+1
                xgroove = w_groove/2+(i-1)*w_groove+i*w_land
                xxgroove = ROUND(m*xgroove/L_seal)
                T_groove[i] = T[xxgroove]
        UNTIL (i=N_groove)
        i = 0
        REPEAT
                i = i+1
                xland = w_land/2 + (i-1)*(w_land+w_groove)
                xxland = ROUND(m*xland/L_seal)
                T_land[i] = T[xxland]
        UNTIL (i=N_land)
END

FUNCTION k304SS(T)
        "This function returns the thermal conductivity of 304 stainless steel "
        " T = temperature in Kelvin"
        "http://cryogenics.nist.gov/NewFiles/material_properties.html"
        a  =    -1.4087
        b  =    1.3982
        c =     0.2543
        d =     -0.6260
        e =     0.2334
        f =     0.4256
        g =     -0.4658
        h =     0.1650
        i =     -0.0199
        k304SS =
10^(a+b*(log10(T))+c*(log10(T))^2+d*(log10(T))^3+e*(log10(T))^4+f*(log10(T))^5+g*(log10(T))^6
+h*(log10(T))^7+i*(log10(T))^8)
END

FUNCTION kOFHCCu(T)
        "This function returns the thermal conductivity of OFHC copper"
        " T = temperature in Kelvin"
        "http://cryogenics.nist.gov/NewFiles/material_properties.html"
        a = 2.2154E0
        b = -4.746E-1
        c = -8.8068E-1
        d = 1.3871E-1
        e = 2.9505E-1
        f = -2.0430E-2
        g = -4.831E-2
```

```
        h = 1.281E-3
        i = 3.207E-3
        kOFHCCu = 10^((a+c*T^0.5+e*T+g*T^1.5+i*T^2)/(1+b*T^0.5+d*T+f*T^1.5+h*T^2))
END
```

Appendix F: Input Parameters EES Code

```
"!<><><><><><><><><><><><><><><><><><><><><><><><><><><><><><><><><><><><<"

"STRING CONSTANTS - turn on/off different models"

TURBINEMODEL$ =    'on'              {'off'}              "run turbine efficiency/load model"

ROTORDYNAMICS$ =       'on'          {'off'}              "run overall rotor dynamics model"
THRESHOLDSPEED$ =      'on'          {'off'}              "run threshold speed model"
FRICTIONMODEL$ =   'on'              {'off'}              "run friction model"
AXIALBALANCE$ =    'on'              {'off'}              "forces spacing to be such that shaft is
axially balanced on bearings"
SETSPEED$ =        'on'              {'off'}              "if on, sets shaft speed to 80% of
threshold speed"
STEPPEDSHAFT$ =    {'on'}            'off'                “different turbine radius”

SEALMODEL$ =       'on'              {'off'}              "turns overall seal model 'on' or 'off' "
SEALTYPE$ =        'labyrinth'{'plain'}                   "seal type, either 'plain' or 'labyrinth' "
MASSFLOWRATE$ =    'on'              {'off'}
THERMAL$ =         'on'              {'off'}              "turns seal thermal model 'on' or 'off' "
SETMASSFLOWRATE$ =  {'on'}           'off'

RECUPERATOR$ =     'on'              {'off'}              "turns recuperator model 'on' or 'off' "
SETGUESS$ =        {'on'}            'off'                "sets a linear temperature profile within
recuperator, helps for convergance"

TURBOALTERNATOR$ =  {'on'}           'off'
SETR$ =            {'on'}            'off'

SETLOAD$ =          'on'             {'off'}              "if 'on', sets load to specified value"


"!<><><><><><><><><><><><><><><><><><><><><><><><><><><><><><><><><><><><<"

"DEPENDENCIES, given values for when models are not run"
$IF THRESHOLDSPEED$ = 'off'
m_dot_tot = 0.0011
$ENDIF

$IF SEALMODEL$ = 'off'
m_dot_leak = 0
$ENDIF

$IF SEALMODEL$ = 'on'
$IF MASSFLOWRATE$ = 'off'
m_dot_leak = 0
$ENDIF
$ENDIF

$IFNOT thermal$='on'
rho_seal_avg = density(f$,T=T_bearing,P=P_bearing)
```

```
P_seal_avg =  P_bearing
mu_seal_avg = viscosity(f$,T=T_bearing,P=P_L)
$ENDIF

$IF ROTORDYNAMICS$ = 'off'
W_dot_f = 0.5[W]
$ENDIF

$IF setng$='on'
N_groove=ngset                          "# grooves installed in the seal (m), ngset set in diagram"
$ENDIF

$IF SealModel$='off'
DELTAc_seal = 0
$ENDIF

$IF AXIALBALANCE$ = 'on'
N_f_jb1 = N_f_jb2
$ELSE
L_sp2_e = L_sp2_e_XX
$ENDIF

$IF Recuperator$ = 'off'
T_turb_in = 12[K]                       "temperature entering nozzle"
$ELSE
{T_turb_in = 20{T_w_out}}
T_turb_in = T_w_out_ac
$ENDIF

$IF SETSPEED$ = 'on'
N_Hz = 0.80*OMEGA_th_Hz
$ELSE
N_Hz = N_Hz_XX
$ENDIF

$IF thermal$ = 'off'
heatleak = 0
$ENDIF

$IF SETR$ = 'on'
R_load = 2[ohm]
$ENDIF

$IF TurbineModel$ = 'off'
T_turb_out = 12[K]
T_tot = 0.00025[N-m]
{W_dot = 1[W]}
$ENDIF

$IF STEPPEDSHAFT$ = 'on'
R_sh_e_2 = R_sh_e_2XX;
$ELSE
R_sh_e_2 = R_sh_e
$ENDIF
```

```
$IF setload$='on'
q_dot_load = setload    "cooling load applied, setload set in diagram"
$ELSE
q_dot_load = 0[W]
$ENDIF

"-----------------------------------------------------------------------------------------------------------------------"
"!<<<<<<<<<<<<<<<<<<<<<<<<<<<<<<INPUT PARAMETERS>>>>>>>>>>>>>>>>>>>>>>>>>>>"
"-----------------------------------------------------------------------------------------------------------------------"
"HIGHLIGHT DENOTES IMPORTANT VARIABLE, IF COMMENTED THEN LIKELY SET IN
DIAGRAM WINDOW OR PARAMETRIC TABLE"

"Overall limits - used in variable limits"
"-----------------------------------------------------------------------------------------------------------------------"
P_limit_h = 350[psia]*convert(psia,Pa)      “upper limit on pressures”
T_up = T_bearing +1[K]                      “upper limit on cycle temperatures”

"Outside turbine assembly"
"-----------------------------------------------------------------------------------------------------------------------"
{P_H_e = 250[psi];}                    P_H = P_H_e*convert(psi,Pa)      "pressure in high
pressure buffer volume"
{P_L_e = 150[psi]}                     P_L = P_L_e*convert(psi,Pa)      "pressure in low
pressure volume"
P_L_e = P_H_e - DELTAP_tot_e”total pressure difference”
P_R = P_H/P_L                  "definition of pressure ratio"
{P_R= 1.2}                     "pressure ratio"
P_bearing_in = P_H             "pressure in bearing assumed to be at pressure of high P
bufffer volume"
P_bearing_out = P_L+(P_H-P_L)*beta
{T_bearing = 70 [K];}          "temperature in high temp space - bearings"
T_room = 295 [K];              "assumed room temperature"
T_comp = 200 [K];              "assumed temperature at piston in compressor"
T_0 = 295 [K];                 "room temperature"
f = 45 [1/s];                  "compressor frequency"
V_comp = 400[cm3]*convert(cm3,m3)      "swept volume of compressor"
f$ = 'helium'                  "working fluid"
m_dot_tot = m_dot_turb + m_dot_jb  "total mass flow to turbine and journal bearings"
m_dot_turb = 0.001[kg/s]       “mass flow to the turbine”

"-----------------------------------------------------------------------------------------------------------------------"
"Shaft and bearings"

"shaft"
 L_sh = L_sh_e*convert(in,m)           "Length of shaft"
L_sh = L_turb + L_seal + L_sp1 + L_jb1 + L_stsp + L_jb2 + L_sp2
{R_sh_e = 0.1[in];}                    R_sh = R_sh_e*convert(in,m)     "Radius of shaft"
{R_sh_e_2XX = 0.08105[in];}            R_sh_2 = R_sh_e_2*convert(in,m)"radius of stepped-down
shaft"
D_sh = 2*R_sh;                 D_sh = D_sh_e*convert(in,m)     "shaft diameter"
D_sh_e_2 = 2*R_sh_e_2;         D_sh_2 = D_sh_e_2*convert(in,m)
c_sh_e   = 0.01[in];           c_sh = c_sh_e*convert(in,m)             "clearance of shaft and
case"
L_turb_e = (1/4)[in];          L_turb = L_turb_e*convert(in,m)  "length of turbine on shaft"
```

```
{s = s_e*convert(in,m)                                    "axial clearance of thrust bearing"}
{N_Hz_XX = 2500 [Hz];}          omega = N_Hz*convert(rev/s,rad/s)"operating speed"

N_kHz = N_Hz/1000[Hz]

"Journal bearings"
L_jb_e = 0.3[in];               L_jb = L_jb_e*convert(in,m)       "lenght of EACH journal bearing"
L_stsp_e = 0.4[in];                 L_stsp = L_stsp_e*convert(in,m) "length of stator space
between journal bearings"
{c_jb_e = 0.0005[in];}          c_jb = c_jb_e*convert(in,m)       "Radial clearance of journal
bearings"
L_jb1_e = L_jb_e;               L_jb1 = L_jb1_e*convert(in,m)     "length of for journal bearing"
L_jb2_e = L_jb_e;               L_jb2 = L_jb2_e*convert(in,m)     "length of aft journal bearing"

"Thrust bearing "
th_tb_e = 0.1{25}[in];          th_tb = th_tb_e*convert(in,m)     "thrust bearing thickness (axial
length)"
c_tb_e = 0.001[in];             c_tb = c_tb_e*convert(in,m)       "thrust bearing radial clearance"
a_e = 0.25[in];                 a = R_tb                          "thrust bearing radius"
R_tb_e = 0.3[in];               R_tb = R_tb_e*convert(in,m)
D_tb = 2*R_tb                                                     "diameter of thrust bearing"

"spacing"
L_sp1_e = 0.16[in];             L_sp1 = L_sp1_e*convert(in,m)     "space between seal and journal
bearing cartridge"
L_sp2_e_XX = (1/4)[in];         L_sp2 = L_sp2_e*convert(in,m)     "space between journal bearing
cartridge and thrust bearing"
L_bore2_e = 0.5[in];            L_bore2 = L_bore2_e*convert(in,m)    "length of extended bore (past
magnet)"
phi_bore2_e = 0.1[in];          phi_bore2 = phi_bore2_e*convert(in,m)       "diamter of extended
bore"

"material properties"
rho_m = 7.4[g/cm3]*convert(g/cm3,kg/m3)       "density of magnet"
rho_Ti = 4.42[g/cm3]*convert(g/cm3,kg/m3)     "density of titanium alloy"
sigma_yield_Ti = 910E6[Pa]

"-------------------------------------------------------------------------------------------------------------------------"
"SEAL"

L_t_e = 0.02[in];               L_t = L_t_e*convert(in,m)         "length of each 'tooth' "
L_g_e = 0.1[in];                L_g = L_g_e*convert(in,m)         "length of each groove"
{n_t = 5                                                          "number of teeth"}
{c_seal_e = 0.00075[in];}       c_seal = c_seal_e*convert(in,m) + DELTAc_seal   "seal tooth tip
clearance"
h_c_e = 0.025[in];              h_c = h_c_e*convert(in,m)         "thickness of seal shell"
h_t_e = 0.03[in];               h_t = h_t_e*convert(in,m)         "height of teeth"
L_seal_e = 0.5[in];                 L_seal = L_seal_e*convert(in,m) "length of seal"

DELTAP_inH2O = DELTAP_e*convert(psi,inH2O)
DELTAP = DELTAP_e*convert(psi,Pa)
DELTAP_inH2O = 3 [inH2O]
P_bearing = P_L - DELTAP
```

```
"Materials "
ShaftMaterial$='TitaniumAlloy'          "Shaft material : titanium or macor"
CaseMaterial$='TitaniumAlloy'           "Seal material : titanium or macor"

"Geometry"
D_shaft=D_sh                            "shaft diameter (m)"
c_land=c_land_inch*convert(inch,m)      "radial clearance between the shaft and the seal in the
lands (m)"

{Ngset = 4}
N_groove = 10
N_land=N_groove+1                                                   "number of lands"
w_groove_e = 0.01[in]; w_groove=w_groove_e*convert(inch,m)   "width of each groove (m)"
w_land = w_land_e*convert(in,m)
d_groove=0.02*convert(inch,m)                                       "depth of each groove
(m)"
w_land=(L_seal-N_groove*w_groove)/(N_groove+1)                      "width of each land"
c_land_inch = c_seal_e                                              "land clearance is
overall seal clearance"
R_groove = w_groove/w_land

m = 200                                                         "number of grid points"

"-----------------------------------------------------------------------------------------------------------------------"
"TURBOALTERNATOR"

"Rotor"
D_rot_e = 0.12 [in];     D_rot = D_rot_e*convert(in,m)    "diamter of rotor magnet"
L_rot_e = 0.3 [in];  L_rot = L_rot_e*convert(in,m)        "length of the rotor magnet"

"Stator poles"
D_st_e = 0.125[in];      D_st = D_st_e*convert(in,m)"diameter of stator pole"
L_st_rad_e = {0.24[in]}0.26; L_st_rad = L_st_rad_e*convert(in,m)  "radial length of stator pole"
D_st_lip_e = 0.2563 [in];     D_st_lip = D_st_lip_e*convert(in,m)    "diameter of stator lip"
L_st_lip_e = 0.03 [in];   L_st_lip = L_st_lip_e*convert(in,m)     "length of stator lip"

"Stator shell"
th_shl_e = 0.125 [in];    th_shl = th_shl_e*convert(in,m)   "thickness of ferrite shell"
D_shl_o_e = 1.25[in];                                       "outer diameter of ferrite shell"
D_shl_i_e = D_shl_o_e - 2*th_shl_e; D_shl_i = D_shl_i_e*convert(in,m) "inner diameter of ferrite
shell"
R_shl_i_e = D_shl_i_e/2;     R_shl_i = R_shl_i_e*convert(in,m)"inner radius of ferrite shell"

mu_0 = pi*4E-7                          "permeability of free space"
mu_ferrite = mu_ferrite_rel*mu_0        "estimate of ferrite permeablility (mu_r = 400 at LN temp) "
mu_ferrite_rel = 400                    “relative permeability of ferrite at LN2 temperature”
"Wires"
l_lead = 1 [m]                                              "length of the lead wires"
D_wire_e = 0.005 [in];  D_wire = D_wire_e*convert(in,m)"wire diameter, 0.01 -> 30 AWG"

R_rot = D_rot/2

magnet$ = 'cryo'                "magnet grade"
```

```
ferrite$='5000'                    "ferrite grade"

"-------------------------------------------------------------------------------------------------------------------------------------------"
"OTHER PROPERTIES"

mu_bearing = viscosity(helium, T=T_bearing,P=P_H)      "viscosity of helium in bearings"

"-------------------------------------------------------------------------------------------------------------------------------------------"
```